CANINE OSTEON FORMATION (MODELING) AND REMODELING DURING DEVELOPMENT AND MECHANICAL LOADING

A Dissertation

by

KE WANG

Submitted to the Office of Graduate and Professional Studies of
Texas A&M University
in partial fulfillment of the requirements for the degree of

DOCTOR OF PHILOSOPHY

Chair of Committee,	Jian Q. Feng
Committee Members,	Kathy Svoboda
	Yongbo Lu
	Hu Zhao
	Yan Jing
Head of Department,	Larry Bellinger

August 2019

Major Subject: Oral Biology

ABSTRACT

The osteon (Haversian system) is the basic structural and functional unit of cortical bones in human and many other large mammals like dogs and cows. Different from mouse cortical bones consisting of uniform lamellar bones, osteons consist of multiple concentric lamellae surrounding a central vascular canal named Haversian canal. Osteon structures are significant for the function of skeletal system in providing both sufficient blood supply and mechanical support. Osteons also display striking changes under pathological conditions, such as osteoporosis. Despite their importance, there is limited research on osteons using large mammals, in contrast to the relatively exhaustive bone research using rodents. Therefore, there are many knowledge gaps in osteon biology, including the modeling and remodeling of osteons during early development and in response to mechanical loading.

Here, by examining the cross sections of the tibia midshaft of young beagle dogs at postnatal day 1, day 14, day 28, and 4 months using different approaches, we demonstrated that periosteum had a major contribution to osteonal bone formation by giving rise to abundant “preosteon” structures – the unique semicircular canals that were highly cellular and would develop into future osteons. The endosteum, on the other hand, served as a location where bone resorption took place allowing the bone marrow cavity to enlarge.

Furthermore, we investigated the effects of enhanced mechanical loading on the formation of new osteons and the remodeling of existing osteons by applying a novel

loading model to the tibia midshafts of adult beagle dogs. Compared to the contralateral tibia without a loading device, the loaded tibia exhibited a preferential role of periosteum in new bone formation, with many details recapitulating the periosteal osteon formation process during early development. In addition, the remodeling activity of the existing bone area of loaded bone was also increased.

In summary, our study was the first one to provide detailed information on the osteon modeling and remodeling during early development and under mechanical loading. Furthermore, this work lays a solid foundation for understanding the human bone responses under various physiological and pathological conditions, as well as in response to force-delivering medical devices.

DEDICATION

To all the dogs sacrificed for this study. Though any area of research, including the osteon biology, is like a huge iceberg, hopefully this study may serve as the tip of the iceberg, and lay a foundation for further exploration.

ACKNOWLEDGEMENTS

It once seemed almost impossible for me to get through this PhD study, but today, here I am. During this four-year journey, I received tremendous help and support from so many people. I sincerely thank them, for giving me the courage to move on, despite how frustrated I was at the moment.

I would like to thank my mentor, Dr. Jian Q (Jerry) Feng, for keeping pushing me forward on the way of exploring truth in the darkness. As energetic as he is in life, he is also so courageous and innovative in research field. Although we sometimes had differing opinions on research questions, I have to admit that for most of the time, he was right. I couldn't see it then, but I see it later. I thank him for giving me space to think deeply and independently, and for tolerating any mistakes I made. Apart from research, I also thank him for constant support and caring of my career development.

I also would like to thank all my other committee members, Dr. Kathy Svoboda, Dr. Bob Lu, Dr. Hu Zhao, and Dr. Yan Jing, for their valuable suggestions throughout the course of this study. For the loaded dog experiment, I also thank Dr. Buschang for generously providing the implants and springs, and sharing the dogs used for research projects in Department of Orthodontics.

I also thank Gerald, Priscilla and Connie for their help with this study. This study could not have been done without Gerald, who took very good care of the puppies and adult dogs, performed the surgeries to place loading devices, and helped with fluorescence dye injection and euthanasia of the dogs.

My thanks also go to Dr. Lynn Opperman, Dr. Larry Bellinger, Dr. Xiaohua Liu, Dr. Xiaofang Wang and all the other faculty in the Department of Biomedical Sciences, as well as the adjunctive faculty from other departments, including Dr. Peter Buschang and Dr. Hongjiao Ouyang. Their joint efforts create a good learning environment for us graduate students. Our staff, including Nancy, Marge, Meghann, Darla, and Jeanne, makes our student life easier and more diverse.

I also sincerely thank all the members in Dr. Feng's lab, including the current members Yan, Jun, Xudong, Mary, Chunmei, Zheng, Hui, and Xiaolin, and previous members Rene, Min, Yuan, Chaoyuan, Ying, Pavani, Ning, et al. They are like my brothers and sisters, and offered me tremendous help and support. I am really going to miss this big and loving family.

Special thanks go to my roommate and friend, Bei, who accompanied me at every moment during the past four years, and generously offered comfort and support whenever I was frustrated. I also thank all the graduate students, Mickey, Wenjing, Yongxi, Bikash, and many others, for their help and company.

My family has always been my strongest backup. I thank my parents and my brother for their love and support. My parents-in-law, treat me as their own daughter, rather than just daughter-in-law. My husband, whom I have already known for 12 years by now, always encourages me and comforts me, and I could not have made it this far without him. I am truly blessed to have them as my family.

CONTRIBUTORS AND FUNDING SOURCES

Contributors

This work was supervised by a dissertation committee consisting of Dr. Jian Q. Feng, Dr. Kathy Svoboda, Dr. Yongbo Lu of the Department of Biomedical Sciences, Dr. Hu Zhao of the Department of Restorative Sciences, and Dr. Yan Jing of the Department of Orthodontics.

The surgery of placing the loading device in Chapter III was performed by Ernest Gerald Hill. The paraffin sections of loading bone in Chapter III was provided by Yuan Hui. All other work conducted for the dissertation was completed by the student independently.

Funding Sources

This study was supported by Grants DE025014 to Dr. Jian Q. Feng from the National Institutes of Dental and Craniofacial Research.

NOMENCLATURE

3D	Three dimensional
Ar	Area
BFR	Bone formation rate
Bma	Bone marrow
BMD	Bone mineral density
BS	Bone surface
BSP	Bone sialoprotein
Ct	Cortical
Ctsk	Cathepsin K
DMP1	Dentin matrix acid phosphoprotein
DXA	Dual energy x-ray absorptiometry
EC	Endothelial cell
EdU	5-ethynyl-2’-deoxyuridine
EDX	Energy dispersive X-ray spectroscopy
Es	Endosteum, endosteal surface
EtOH	Ethonal
FITC	Fluorescein isothiocyanate
HUVEC	Human umbilical vein endothelial cell
IACUC	Institutional Animal Care and Use Committee
ICL	Inner circumferential lamellae

IOn	Immature osteon
M	Month
Ma	Marrow
MEPE	Matrux extracellular phosphoglycoprotein
MMA	Methyl-methacrylate
N.Oc	Osteoclast number
O	Osteoid
OC	Osteoclast
OCL	Outer circumferential lamellae
On	Osteon
OPN	Osteoponin
OS	Osteoid surface
OSX	Osterix
P	Postnatal
PHEX	Phosphate Regulating Endopeptidase Homolog X-Linked
Po	Porosity
POn	Primary osteon
Postn	Periostin
PreOn	Preosteon
Ps	Periosteum, periosteal surface
qBEI	Quantitative backscattered electron imaging
RANKL	Receptor activator of nuclear factor kappa-B ligand

SEM	Scanning electron microscopy
SOn	Secondary osteon
TRAP	Tartrate-resistant acid phosphatase
Tt	Total
VEGF	Vascular endothelial growth factor

TABLE OF CONTENTS

Page

ABSTRACT ii

DEDICATION iv

ACKNOWLEDGEMENTS v

CONTRIBUTORS AND FUNDING SOURCES vii

NOMENCLATURE viii

TABLE OF CONTENTS xi

LIST OF FIGURES xiv

CHAPTER I INTRODUCTION 1

I.1 Haversian System (Osteon) 2
I.1.1 Bone Architecture in Large Mammals 2
I.1.2 Periosteum and Endosteum 4
I.1.3 Primary Osteons and Secondary Osteons 6
I.1.4 Osteon Remodeling 7
I.1.5 Significance of Osteon Structures in Large Mammals 11
I.1.5.1 Osteons and Blood Supply 11
I.1.5.2 Osteons and Mechanical Properties 12
I.1.5.3 The Intimate Association Between Osteons and Bone Microstructure in Disease 13
I.1.6 Osteon Changes in Osteoporosis 13
I.1.6.1 Cortical Porosity 13
I.1.6.2 Bone Mineral Density (BMD) 14
I.1.6.3 Osteocytes in Osteoporosis 16
I.1.6.3.1 Osteocyte Lacunocanalicular Network 16
I.1.6.3.2 Osteocyte Lacuna Size and Morphology 17
I.2 Bone Responses to Mechanical Loading 20
I.2.1 Osteocytes in Mechanosensation and Transduction 20
I.2.2 Anabolic Effects Of Mechanical Loading On Bones 21
I.2.3 Preferential Roles of Periosteum and Endosteum in Bone Responses Under Mechanical Loading 22

CHAPTER II CANINE OSTEON FROMATION (MODELING) AND REMODELING DURING EARLY DEVELOPMENT 25

II. 1 Introduction 25
II. 2 Materials and Methods 26
II.2.1 Dogs Breeding, 5-ethynyl-2'-deoxyuridine (EdU) Injection, and Fluorochrome Labeling 26
II.2.2 Sample Preparation 28
II.2.3 Histomorphometry and Immunohistochemistry 28
II.2.4 Backscattered and Acid-Etched Scanning Electron Microscopy (SEM) 30
II.2.5 Fluorochrome Labeling and FITC Imaging 30
II.2.6 Radiograph and μCT 31
II.2.7 Statistical Analysis 32
II. 3 Results 32
II.3.1 An Overview of Rapid Growth at Early Postnatal Stage 32
II.3.1.1 Tibia Midshaft of Young Adult Dogs were Dense with Minimal Porosity 32
II.3.1.2 Bone Mass of Young Dog Tibias Increased Rapidly at Early Postnatal Stage 33
II.3.1.3 Periosteum-Derived Preosteons and Large Haversian Canals Resulted in a High Cortical Porosity 34
II.3.1.4 Periosteal Bone Showed a Higher Cortical Porosity and Lower Bone Mineral Density than Endosteal Bone 35
II.3.2 Periosteum as the Major Contributor to the Apposition Bone Growth by Giving Rise to New Osteons 35
II.3.2.1 Periosteal Bone Was More Immature than Endocortical Bone 35
II.3.2.2 Periosteal Bone Was Formed More Rapidly than Endocortical Bone 37
II.3.3 The Regulation Mechanisms on Molecular Level Differed in Periosteal and Endosteal Bone Growth 39
II.3.4 Active Osteoclast Activities in Endosteal Bone 41
II. 4 Discussion 42

CHAPTER III CANINE OSTEON FROMATION (MODELING) AND REMODELING IN RESPONSE TO MECHANICAL LOADING 45

III. 1 Introduction 45
III. 2 Materials and Methods 46
III.2.1 Dogs, Mechanical Loading Model, and Fluorochrome Labeling 46
III.2.2 Sample Preparation 48
III.2.3 Histology and Immunohistochemistry 48
III.2.4 Backscattered and Acid-Etched Scanning Electron Microscopy (SEM), and Energy Dispersive X-ray (EDX) Microanalysis 48
III.2.5 Fluorochrome Labeling and FITC Imaging 49
III.2.6 Radiograph 49

III.2.7 Statistical Analysis 49
III. 3 Results 50
III.3.1 A Preferential Role of Periosteum in Loading-Induced New Bone Formation, Recapitulating Early Developmental Processes 50
III.3.1.1 The Establishment of Mechanical Loading Model on Dog Tibias 50
III.3.1.2 More Robust Preosteon Formation from the Periosteum than from the Endosteum 50
III.3.2 Loading-Induced New Osteonal Bone Was Immature and Undergoing Active Mineral Apposition 52
III.3.3 The Molecular Mechanisms that Regulated Periosteal New Bone Formation in Response to Mechanical Loading 53
III.3.4 Bone Remodeling of Existing Cortical Bone Was Enhanced under Mechanical Loading 54
III.3.5 Enhanced Osteoclastic Activity Was Critical for the Remodeling of the Transition Zone between Preosteons and Existing Bone 55
III. 4 Discussion 57

CHAPTER IV CONCLUSION 60

REFERENCES 65

APPENDIX A FIGURES 85

LIST OF FIGURES

Page

Figure 1 Plain X-ray Radiographs and Toluidine Blue Staining of the Cross Section of the Tibia Midshafts in Adult Dogs. 85

Figure 2 Plain X-ray Radiographs and Toluidine Blue Staining of the Cross Sections of the Tibia Midshafts in Puppies. 86

Figure 3 μCT Analyses of Young Dog Tibia Midshafts. 88

Figure 4 Masson-Goldner Trichrome Staining of Young Dog Tibia Midshafts. 90

Figure 5 SEM Assays and FITC Staining of Nondecalcified Young Dog Bones. 91

Figure 6 Fluorochrome Labeling Assay of Young Dog Bone. 94

Figure 7 Immunohistochemistry of Young Dog Bones. 97

Figure 8 Cell Proliferation Assays of Young Dog Bones. 99

Figure 9 Osteoclast Activities on the Endosteal Surface. 100

Figure 10 Plain X-Ray Radiographs and Toluidine Blue Staining of the Loaded Tibias and Control Tibias 101

Figure 11 Backscattered SEM/EDX Assays and Corresponding Fluorochrome Labeling Images of Loaded Bone and Control Bone. 104

Figure 12 Immunohistochemistry of Loaded Bone and Control Bone. 106

Figure 13 Backscattered SEM Images and TRAP Staining for the Existing Bone Area of Loaded Bone and the Counterpart of Control Bone. 108

Figure 14 TRAP Staining of Transition Zone in Loaded Tibias and the Corresponding Toluidine Blue Staining. 109

CHAPTER I

INTRODUCTION

The skeletal system serves a variety of functions, such as mechanical support, protection, mediating mineral ion homeostasis, and producing endocrine signals to regulate other organs[1-4]. The adult human skeleton is composed of 80% cortical bone and 20% trabecular bone[5]. Cortical bone is dense and takes on most of the responsibilities of load bearing, while trabecular bone is more porous and functions to redirect stresses to the stronger cortical shell[1].

Currently, most bone biology studies are using rodents as animal models, despite the fact their bones do not have osteons-the basic structural and functional unit in the cortical bones of humans and other large mammals (e.g. rabbits, dogs and horses)[6]. Osteons consist of a central vascular canal called Haversian canal, and multiple concentric lamellae with bone cells[1].

Since the molecular biology era, studies on osteonal bone have fallen out of favor and scholarship on osteons is limited. Therefore, this study will focus on the knowledge gaps in osteon formation and remodeling during early bone development, as well as under mechanical loading.

This dissertation is comprised of three parts. First, we will review the current knowledge on osteon structure, modeling, remodeling, and changes in osteons during pathological conditions such as osteoporosis. The knowledge on bone responses to mechanical loading (mainly from studies on rodents) will also be reviewed. Second, we

will investigate in depth osteon formation (modeling) and remodeling processes during early development in canines, including the roles of periosteum, endosteum, osteocytes, critical transcription factors and proteins, etc. We will then propose mechanisms for the initiation of osteon formation and maturation. Third, we will establish a loading model on the tibia of adult dogs, and explore the effects of mechanical loading on new osteon formation together with remodeling of existing osteons.

I.1 Haversian System (Osteon)

I.1.1 Bone Architecture in Large Mammals

To begin, the overall structure of bone must be understood to contextualize obstacles in animal osteon studies. Bone is currently known to be organized in a hierarchical manner with multiscale structures, which work in concert to achieve diverse functions. These functions range from mechanical support, protection, mediating mineral ion homeostasis, to producing endocrine signals, which regulate other organs[1-4]. There are four levels and structures: (1) the macrostructure- made from cortical and trabecular bone; (2) the microstructure and sub-microstructure contain osteons, lamellae, and trabeculae. (3) Furthermore, the nanostructure is composed of collagen fibers and interspersed mineral; (4) the sub-nanostructure is the molecular structure of constituent elements, such as collagen, non-collagenous proteins, and minerals[1, 2].

In return to the macrostructure level, four distinct surfaces of bone exist defined by their location in bone envelopes: periosteal, endocortical, intracortical, and trabecular. These surfaces are morphologically discrete, and consequently play differing roles in bone biology health and disease. They also vary in response to mechanical loading[1, 7].

However, when bone microstructure level was examined next, key parts of its content were found to change depending on the type of species. Cortical bone of mice consists of uniform lamellar bones[8]. In contrast to mice which are commonly used in bone studies, a striking characteristic of bones in humans and other large mammals (e.g. rabbits, dogs and horses) is the presence of osteons (i.e. Haversian system)— the basic structural and functional unit of their cortical bones[6]. Specifically, osteons are composed of a central vascular canal called the Haversian canal and multiple concentric lamellae with bone cells. These abundant osteons located between the outer circumferential lamellae and inner circumferential lamellae. These lamellae are then covered by periosteum and endosteum, located at the respective outer and inner surfaces of cortical bone[5, 6].

The classic model of osteonal bone organization is a system of Haversian (longitudinal) canals connected by Volkmann's (transverse) canals, along with a blood flow path within these components[9]. Besides the classic model, studies in the recent decade have been able to reveal more detailed and accurate three-dimensional structures of osteons and the canals using advanced techniques (e.g. synchrotron radiation-based micro-CT, phase retrieval tomography) and software[10-14]. For instance, the incline of Haversian canals from the long axis of bone is from 5° to 20° [12, 15]. Likewise, osteons are subject to frequent and complex branching. This shape leads to various patterns including: 1) lateral and dichotomous branching, 2) intraosteonal remodeling (defined as a Haversian system growing within the boundaries of another Haversian system), and 3) transverse connections, et cetera[10].

I.1.2 Periosteum and Endosteum

In addition to osteon structures, another important feature of bone is periosteum, defined as a composite connective tissue developed from mesodermal cells during embryonic development. It is firmly anchored to the underlying bone surfaces via Sharpey's fibers, and plays a determinant role in bone formation and fracture healing under both physiological and pathological conditions[16, 17]. Histologically, periosteum composition includes two distinct layers: an outer fibrous layer and an inner cambial layer. The outer fibrous layer is composed of fibroblasts, collagen, and elastin fibers[18], along with a rich vascular and neural network[19, 20]. The inner cambium layer is highly cellular, containing mesenchymal stem cells, differentiated osteogenic progenitor cells, osteoblasts, fibroblasts, as well as microvessels and nerves[3, 19, 21, 22]. Periosteal vessels are connected to vessels in Haversian canals within the bone cortex[23].

In contrast, endosteum is a connective tissue containing osteoprogenitor cells that line the interior surfaces of bones, including the inner surface of the cortex, trabeculae, and Haversian canals[24]. Though the endosteum lining shows that the inner surface of cortex and the trabeculae are bathed in the bone marrow, studies have identified some characteristics of endosteum regions that are distinct from bone marrow. For example, a few areas hold different capillary subtypes, such as the type H subtype (containing a high level of endomucin, CD31 expressions, and an association of Osterix+ osteoprogenitors) are present in the metaphysis and endosteum regions. In addition, the type L subtype has been found (with low level of endomucin and CD31 expression and

no association pertaining to Osterix+ osteoprogenitors). Likewise, the type L subtype was identified to make up the sinusoidal capillaries in the bone marrow cavity[25]. Moreover, Ishikawa et al. applying a xenogeneic transplantation model, presented that the human leukemic stem cells primarily homed to and were retained in greater numbers in the endosteum region of the femur than in bone marrow[26]. Hemopoietic stem cells (HSC) isolated from the endosteal region also exhibited significantly increased in vitro (proliferation) and in vivo (homing, lodgement, and reconstituting) hemopoietic potential compared with their central marrow counterparts[27].

Although both periosteum and endosteum contain osteoprogenitor cells, they are located in different physical and hormonal environments, leading to differing gene expression profiles and sensitivities to mechanical and hormonal stimuli. With ligaments and tendon-muscle attachments on the periosteal surface, periosteal bone exhibits a greater mechanosensitivity to strain compared to endosteal bone[28]. Certainly, multiple studies of mechanical loading models in rodents have revealed robust new bone formation on periosteal surface rather than on the endosteal surface[29, 30]. In actuality, periosteum and periosteal bone express a high level of periostin (Postn), a matricellular protein secreted by osteocytes and osteoblasts[31]. The expression of periostin is essential for sost inhibition and the periosteal bone formation in response to mechanical loading and parathyroid hormone (PTH) stimuli[32-34].

Periosteum and endosteum also exhibit different osteogenic potential during development, remodeling, and fracture healing. Immersed in a bone marrow cavity, endosteum and the inner layers of the cortex in rodents accumulate bounteous

osteoclasts during embryonic and early postnatal stages, which leads to the rapid resorption of endosteal bone surfaces and therefore the enlargement of the bone marrow cavity, whereas preferential periosteal growth makes a major contribution to rapid bone mass increase[35]. Moreover, throughout all phases of the bonosteoe healing process, periosteum plays a central role. Depending on the biomechanics of the fracture site, periosteum gives rise to chondrocytes and/or osteoblasts, contributing to bone repair by endochondral and intramembranous ossifications, while endosteum contributes only via intramembranous ossification[24, 36, 37]. Indeed, experimental removal of periosteum has shown a severe effect on bone repair[38].

I.1.3 Primary Osteons and Secondary Osteons

Osteons can be divided into primary osteons and secondary osteons according to their formation mechanisms and structural characteristics. Primary osteons are a type of primary bone, and secondary osteons are a type of secondary bone[1]. Primary bone is defined as new bone formed in a space where there is no preexisting bone or formed on the surfaces of an existing bone or mineralized cartilage[1, 7]. Whereas secondary bone is produced by the resorption of previously deposited bone followed by new bone formation in its place, a process called remodeling. Thus, primary bone requires only bone formation, while secondary bone requires the coupling of bone formation and resorption[1, 7]. Likewise, primary osteons are formed by filling large vascular canals with the deposition of concentric lamellae until only a small canal remains, and secondary osteons are formed by removal of primary bones and replacement with new osteons[1].

Primary osteons are small in size (only about 50-100 um in diameter or smaller), typically have fewer than ten lamellae, and no well-defined outer boundary. It has been suggested that the existence of primary osteons is related to body size and rapid growth[1].

In contrast, secondary osteons are larger (100-250 um in diameter in human bone), have more concentric lamellae (about 20-25), and a cement line at their outer boundary to separate them from the interstitial lamellae[1, 39]. Additionally, the cement line (known as a reversal line), is often scalloped, representing a remnant of the reversal phase in bone remodeling, i.e. the point where osteoclastic bone resorption stops and bone formation begins[1, 7]. As for when the secondary osteons start to form during development, a study of the human fetus by P. Burton et al. found the presence of secondary osteons in long bones and 6th and 7th ribs as soon as the twenty-fourth week of gestation[40]. Another study by Goret-Nicaise et al. identified the secondary osteons in the mandibular body during the 20th week of gestation[41].

I.1.4 Osteon Remodeling

Bone modeling is the process of either bone formation by osteoblasts (formation modeling) or the bone resorption by osteoclasts (resorption modeling) on separate surfaces[42]. The primary function of bone modeling is to increase bone mass, alter bone shape, or adapt it to a change in mechanical loading. Modeling activity takes place on periosteal, endocortical, and trabecular bone surfaces and occurs primarily during skeletal growth but continues throughout adulthood to a lesser extent. Therefore, bone modeling is critical for the proper functioning of longitudinal and radial growth, as well

as and cortical and trabecular bone drifts[7, 42]. Furthermore, the principal signal for bone modeling is local tissue strain[42].

Conversely, bone remodeling involves osteoclastic bone resorption and osteoblastic bone formation occurring sequentially on the same surfaces in a coupled manner[7, 42]. Bone remodeling can occur at any of the four envelopes: periosteal, endocortical, intracortical, and trabecular[43].

The process is constant and lengthy, occurring throughout an organism`s entire life. In contrast to non-Haversian rodent bone which is rarely remodeled, Haversian bone (osteonal bone) in large mammals undergo much more dynamic remodeling throughout their life[44]. Remodeling rates change with age and in response to physical activity. In human adults, about 5% of cortical bone and 25% of trabecular bone is removed and replaced each year[45]. In particular, the iliac crest exhibits a higher turnover rate of about 0.1% per day[45], and each remodeling cycle takes six to nine months to complete[46]. A better understanding of bone remodeling is necessary for studying various aspects of bone activity physiologically and pathologically, including osteoporosis.

Although there remains much to discover on the topic, it is known that bone remoldeling is performed by the so-called basic multicellular unit (BMU)[7, 47]. The BMUs in trabecular and cortical bone differ in their structures and how they remove or replace the bone. In trabecular bone, the BMU is located on the surface and becomes covered by a canopy in which the osteoblasts resorb the bone, followed by osteoblasts depositing new bone matrix. In the cortical bone of osteonal bone, the BMU works

through a mechanism described as cutting cone theory, resulting in secondary osteons; namely, the BMU encompasses a cutting cone of osteoclasts in front, followed by a closing cone lined by osteoblasts, connective tissue, blood vessels, and nerves filling the cavity[48].

Specifically, the recruit of osteoclasts to certain bone surfaces initiates the cutting cone, and the process of bone resorption lasts twenty-one days on average in humans. The resorption phase is followed by the reversal phase, (which lasts approximately five days for humans) and is characterized by the cessation of bone resorption and initiation of bone formation[7].

Moreover, the cement line (reverse line), visible as a scalloped edge in transverse sections, represents a remnant of the reversal phase in bone remodeling[1, 10]. Cement lines are important for the mechanical property of the bone because they serve as fiber reinforcements to bone tissue. They are collagen deficient, yet contain high levels of certain kinds of non-collagenous proteins including osteoponin (OPN)[1, 49]. The OPN component is logical in two ways; first, OPN plays a role in osteoclast adhesion during the resorption phase and the cement line is where the osteoclasts stop resorption; secondly, OPN makes an important contribution to enhance the mechanical property by providing fiber matrix bonding [1, 7].

Once the aforementioned cement line has formed, a cavity is successively refilled with lamellae by a team of osteoblasts, most likely originating from precursors that reside within local connective tissue[7, 48]. In humans, the resulting synthesis of osteoid lasts approximately ninety days, and primarily consists of type I collagen fibers

while serving as a template for mineralization. The subsequent mineralization is comprised of two phases: rapid primary and secondary. Rapid primary mineralization takes approximately two to three weeks and accounts for roughly 70% of the mineral deposition; in contrast, the slower secondary mineralization may take up to one year or more and involves the maturation of mineral crystals to reach the final mineral content[7, 50].

Whereas there are some steps uncovered such as the ones above, a recent study by Lassen et al. has shed new light on more details of human osteon remodeling using human femur or fibular longitudinal sections combined with specific markers for osteoblasts and osteoclasts[49]. At the front of cutting cones, besides the initial resorption events that are responsible for extending erosion in a given resorption (elongating the Haversian canals), there are also secondary resorption events which cause erosion to expand in other directions (widening the Haversian canals)[49]. The secondary resorption events make the most contribution to the overall resorption and interrupts the reversal phase. Further, this integrated resorption and reversal phase (RvRs) is made up of osteoclast and osteoblast lineage cells —and goes along with a gradual increase in the density of osteoprogenitor cells. When the resulting density of osteoprogenitor cells reaches a certain threshold, secondary resorption stops and bone formation starts. This action indicates that the rate of osteoprogenitor recruitment influences the length of the RvRs phase and the persistence of bone removal through secondary resorption.

Furthermore, bone remodeling can be classified as targeted or stochastic based

on events which signal remodeling[42]. For example, targeted remodeling requires a specific local signaling event that directs osteoblasts to a given surface to initiate the remodeling. Microdamage and osteocyte apoptosis are the two most accepted signaling events, although they two may not be independent. In contrast, stochastic remodeling is a random process, during which osteoclasts resorb bone without a specific local signaling event. Targeted remodeling serves to repair mechanically compromised bone matrix and permit mechanical adaptation, whereas stochastic remodeling is considered to play more of a role in calcium homeostasis[42, 51-53]. These processes would not be possible without ample blood supply to other parts of bone, an issue expounded upon in the following section.

I.1.5 Significance of Osteon Structures in Large Mammals

I.1.5.1 Osteons and Blood Supply

The function of any vertebrate organ relies on sufficient and efficient blood circulation[54]. Bone has an extensive vascular network that consumes almost 10-15% of resting cardiac output[55-57]. However, considering the fact that bone cells must reside within about 250 μm of their blood supply and dense calcified tissue limits the material which rapidly diffuses their nourishment, the efficient spatial arrangement of blood vessels within the skeletal system becomes extremely pivotal, especially in humans and larger animals (e.g. rabbits, dogs, and horses) with thicker bones[1, 7]. This issue may be one important reason that bones in humans and these larger animals are internally structured with osteons, as otherwise, bones with a cortex thicker than 500 μm would not be able to support healthy osteocytes in the center of the cortex; thus, it makes

sense in that the secondary osteons are as large as 100 – 250 μm in diameter. Moreover, the structure of concentric lamellae surrounding vascular bundles provides a geometrically efficient system which supplies the maximum amount of bone tissue with the minimum number of vessels[1]. Therefore, the osteon structure serves as an ideal geometric system to ensure sufficient and efficient blood supply to the bone cells.

I.1.5.2 Osteons and Mechanical Properties

Dense cortical bone makes up a majority of bone mass and takes on most responsibilities of load bearing[1]. Enhanced mechanical properties with age partly develop from expanded bone size, increased mineralization, and improved organization[8, 58]. In mice, highly organized lamellar bones are added during normal growth, likely contributing to improved strength, stiffness, and mineralization[8]; moreover, the intracortical canal network is important for mouse bone mechanics[44]. Similarly, the formation, maturation and mineralization of osteon structures significantly enhance the bone mechanical properties in humans and larger animals.

Specifically, cement lines in osteons are of mechanical importance by serving as fiber reinforcements to the bone tissue[1]. This function lies in their ability to control fatigue and fracture processes. They create point-specific stiffness variations in bone and increase static toughness by preventing deleterious crack growth, thereby improving fatigue properties.

I.1.5.3 The Intimate Association Between Osteons and Bone Microstructure in Disease

Lastly but perhaps most importantly, osteons serve as a structural and functional unit in cortical bones of large mammals. The changes in their properties are intimately associated with changes in the bone microstructural properties, which can be revealed most distinctly under pathological conditions, especially during osteoporosis. This concept will be elaborated in detail in the following section.

I.1.6 Osteon Changes in Osteoporosis

I.1.6.1 Cortical Porosity

Much of osteoporosis research has focused on vertebral fractures and trabecular bone loss. However, approximately 80% of all fractures in old age are non-vertebral, predominantly at cortical sites, and occur after the age of sixty when the rate of trabecular bone loss has decreased[59-62]. Moreover, present treatments reduce non-vertebral fractures by only 20-30%[59]. Therefore, in-depth investigation of intracortical remodeling, chiefly osteon remodeling, is essential for understanding the mechanism causing fragility of cortical bone, therefore preventing and treating osteoporosis in a more targeted and effective way.

Further, increased remodeling of osteons resulting from aging or postmenopausal estrogen deficiency has led to increased cortical porosity[63, 64]. “Giant” Haversian canals (large pores) are commonly observed in transverse sections of cortical bones in patients with osteoporotic fractures, particularly in the inner third of the cortical structure. Subsequently, these large pores coalesce to generate large-sized defects referred to as

super-osteons, eventually leading to trabecularization of the endocortical surface and cortical thinning. By comparison, the cortex adjacent to periosteum appears compact with enlarged pores, but without trabecularization[59, 62, 65-67].

Recognizing the intracortical porosity from enlargement and coalescence of Haversian canals is significant for studying and correctly evaluating osteoporosis. For instance, aging-related and postmenopausal cortical bone loss is underestimated if trabecularized cortical fragments are erroneously allocated to the “medullary” trabecular mass and are not quantified as a part of the original cortical bone. Similarly, the decline in trabecular number and thickness is also underestimated for the same reason[62].

In fact, clinical evidence shows that patients with fractures have more clustered super-osteons than age/gender-matched controls, suggesting the substantial contribution of super-osteons to cortical porosity and consequent eventual osteoporotic fractures [65, 67]. However, the underlying mechanisms of super-osteon generation at cellular and molecular levels require further in-depth investigation rather than obscurely owing them to enhanced resorption or increased remodeling[59].

I.1.6.2 Bone Mineral Density (BMD)

Apart from increased porosity, change of bone mineral density (BMD) is also a focus of osteoporosis studies. Current clinical diagnosis of osteoporosis includes bone mineral density testing, which is usually measured with dual energy x-ray absorptiometry (DXA) in clinical practice[68-70]. BMD is considered to have a strong correlation with fracture risk. This discovery is enforced even greater by the statistic that the risk of osteoporotic fractures increases by approximately 1.5 times per SD decrease

in BMD[71, 72]. In addition, approximately 45% of the women who are diagnosed with osteoporosis based on BMD at the age of fifty will fracture their hip, spine, forearm or proximal humerus in the next ten years[69]. Unfortunately, BMD testing does have limitations— sensitivity is low when used alone for osteoporosis screening; most fractures occur in individuals with a BMD T-score better than -2.5 (the conventional definition for osteoporosis)[71, 73-76]. A combination of clinical risk factors (such as age, sex, previous fractures) and BMD can better aid in fracture risk prediction[69, 70, 77]. Hence, several fracture risk assessment tools have been developed and independently validated[78].

However, studies on human bone samples obtained from biopsy or autopsy reveal more details regarding bone mineral density in osteoporosis using backscattered electron microscopy. In a study by Busse et al., compared with non-osteoporotic younger females (forty-nine years of age on average), osteoporotic rod-like trabeculae in transiliac bordier bone cores and T12 vertebrae in osteoporotic aged females (seventy-eight years of age on average) showed a significant increase in the mean calcium content and calcium width. Meanwhile, there was a sharp decrease in mechanical properties, including fracture load, yield strength, ultimate stress, bending stiffness, and work to failure[79]. Using quantitative backscattered electron imaging (qBEI) combined with energy dispersive X-ray spectroscopy (EDX) microanalysis, a higher calcium weight percentage was identified in aged osteons (estimated tissue age reflected by the calcium-to-phosphorus ratio) in femoral mid-shaft cross sections[80]. Moreover, calcium content in the external cortical bone from the superolateral femoral neck was also found

at higher rates and a more homogenous distribution in fracture patients than age/gender-matched healthy controls[81]. Within the continuing unknowns of osteoporosis, emerging information on osteocytes may provide more answers.

I.1.6.3 Osteocytes in Osteoporosis

I.1.6.3.1 Osteocyte Lacunocanalicular Network

Osteocytes, comprising 90% to 95% of all bone cells in adult bone yet once thought to be passive, have now been found to play multiple essential roles during bone modeling and remodeling, including mediating bone formation and resorption, mineral homeostasis, and adaptation to changes in mechanical loading.

Several studies have focused on the roles of osteocytes during age-related osteoporosis. For instance, researchers have found that an altered lacunocanalicular network is the most striking change in aged human bone, including (1) a reduction in osteocyte lacunar density (the lacunar number per unit of bone area) and an osteocyte density of approximately 20-30%[80-88]. (2) Furthermore, during osteoporosis there was also an increase in the number of hypermineralized (micropetrotic) lacunae, especially in endocortical bone, where they reach 10% of the total amount at eighty years of age compared with 10% at twenty years of age[83, 89-91]. (3) Likewise, a dramatic decline in the canalicular number per osteocyte occurs (at a rate of approximately 30%), as well as compromised osteocyte network connectivity [80].

The overall loss in the connectivity of the entire osteocyte network during aging may be as high as approximately 50%, which could be inferred based on the aforementioned losses of lacunar/osteocyte density and dendrite number per

osteocyte[92]. These discoveries could have profound implications for skeletal health in many aspects due to the osteocytes' multifunction, as their dendrites are critical for mechanotransduciton[93-95]. Evidently, a sharp reduction in dendrite number and connectivity may be partially responsible for attenuated bone anabolic response to mechanical loading during aging [96, 97]. A decrease in osteocyte density may also contribute to compromised biomechanical quality[98, 99]. Likewise, a reduced number of osteocytes may compromise bone remodeling, which results from decreases of important factors secreted by osteocytes, including sclerostin, a natural inhibitor of Wnt/β-catenin signaling[30, 100, 101] and RANKL, an essential regulator of osteoclast activity[102].

In spite of these advances, the underlying mechanisms responsible for age-related changes in osteocyte lacunocanalicular network and connectivity are still not fully understood, although osteocyte osteoporosis and cellular senescence are proposed to play a possible role in age-related bone loss[103-105].

I.1.6.3.2 Osteocyte Lacuna Size and Morphology

Besides changes in osteocyte lacunocanalicular network, the morphology, alignment, size of osteocytes, and their lacunae are also subject to change under different physical and pathological conditions.

Osteocytes can contribute to mineral homeostasis through osteocytic perilacunar/canalicular remodeling during conditions where high calcium is demanded, such as lactation [106, 107]. As early as the 1960s and 1970s, osteocytes have been proposed to be able to remove their perilacunar matrix, a concept called "osteocytic

osteolysis" [108], upon observations of enlarged osteocyte lacunae in response to PTH treatment or low calcium diet [109-111]. Though this concept was overlooked or denied afterwards, studies in the past decade using advanced technology have shed light on this idea once again. During lactation, enlarged osteocyte lacunae were observed, along with increased expressions of osteoclast-specific genes in osteocytes, including tartrate-resistant acid phosphatase (TRAP) and cathepsin K (Ctsk). Osteocytes were also shown to directly deposit minerals, as lacunae returned to virgin morphology after lactation ceased [106]. This action suggests that osteocytes can not only remove the perilacunar/canalicular matrix, but also can replace it.

Several studies also observed an increase in the size of osteocyte lacunae/canaliculi during osteoporosis. In an ovariectomized (OVX) rat model, effective canalicular size was larger than in control rats, and the collagen surrounding osteocyte canaliculi was loose[112]. In humans, Van Hove et al. examined the morphology and alignment of osteocytes plus their lacunae in the proximal tibia, and found the osteocytes in osteopenic patients to be relatively large and round. Meanwhile, osteopetrotic osteocytes were small and discoid shaped, with osteoarthritic osteocytes described by as large and elongated. These results indicate a complex relationship between osteocyte morphology and bone architecture[113].

In contrast, there are studies where the osteocyte lacunae volumes were found to be unchanged or even smaller during osteoporosis. For example, Bach-Gansmo showed that osteocyte lacunae volumes were unaffected by both age and sex in human iliac crest cortical bone, though osteocyte lacunar density significantly decreased with age in both

sexes and didn't differ between women and men[88]. Further, in a study of the femoral shaft from females by Carter et al., a reduction in osteocyte lacunae volume with age was reported; the lacunae in the older group (>50 years of age) were found ~30% smaller, less flat, and more equant (spherical) compared to the younger group (<50 years of age)[114].

In summary, we have gained some knowledge on the major changes in osteonal bone during aging, which are comprised of the following: an increase in cortical porosity due to the enlargement and coalescence of Haversian canals, an escalation in bone mineral density, as well as some knowledge on changes in the osteocyte lacunocanalicular network and osteocyte lacunae during osteopenic or osteoporotic conditions. It will be highly important and intriguing to explore if these changes in osteocytes are related or contribute to major changes in osteonal bone during aging. To answer this dual inquiry, a more meticulous examination of osteocyte changes during osteoporosis is required, which may include careful evaluation of lacunar size and morphology together with a test regarding osteoclast-related gene expressions in osteocytes, etc. As previously mentioned, osteolysis refers to a kind of perilacunar/canalicular remodeling which mediates mineral homeostasis and is associated with lacunar enlargement. Future research should aim to investigate if osteocytic osteolysis is involved in the increases of cortical porosity and bone mineral density or other possible changes in aged osteonal bone.

I.2.1 Osteocytes in Mechanosensation and Transduction

I.2 Bone Responses to Mechanical Loading

I.2.1 Osteocytes in Mechanosensation and Transduction

While osteons participate in formation and bone remodeling within current literature, they prove crucial in mechanical loading. Osteocytes make up 90-95% of bone cells and are thought to be the dominant cell type responsible for sensing and transducing mechanical strain due to their distribution throughout the bone matrix and extensive interconnectivity to neighboring osteocytes and osteoblasts via gap junctions[115, 116]. Mechanical loading induces the flow of canalicular fluid through the lacunocanalicular network, resulting in fluid flow shear stress, which induces the mechanosensation in osteocytes through perturbation of integrin[4, 94, 117]. In an study by Tatsumi et al., mice with specific ablation of osteocytes through targeted expression of the diphtheria toxin receptor exhibited fragile bone with increased intracortical porosity, microfractures, and trabecular bone loss. Strikingly, these mice failed to show bone loss in response to unloading, indicating a compromised mechanosensation in absence of osteocytes[118].

On the other hand, osteocyte processes are found to be extremely responsive to piconewton-level mechanical loading, whereas the osteocyte cell body and processes without local attachment sites are not[80, 93, 94]. Connexin 43 (Cx43), the gap junction protein most abundantly expressed in bone, plays an important role in mechaniosensing of osteocytes; a bone-specific deletion of Cx43 resulted in an osteopenic phenotype in mice and a failure to exhibit suppression of bone formation in response to unloading[119, 120]. Mechanical loading and unloading also has other implications for humans, as shown below.

I.2.2 Anabolic Effects Of Mechanical Loading On Bones

Mechanical loading has a major functional influence on bone mass and architecture, therefore facilitating the ability of the skeleton to withstand loads of everyday activity without fractures[121]. It is well established that bone is capable of adapting to changes in loading[122]. Reduced mechanical loading leads to bone loss, as experienced by bedridden patients and astronauts[101, 120, 123, 124], whereas increased mechanical loading results in anabolic bone responses. For instance, professional tennis players possess up to 35% more bone in the dominant arm than the other arm that tosses the ball[125].

Moreover, there are many features which impact this process of bone adaptation. Wnt/β-catenin signaling is one of the most important pathways in bone cell activation in response to mechanical loading[30, 96, 115, 126]. Deletion of various components of the Wnt/β-catenin pathways demonstrated impact on bone responses to loading and unloading. For example, mice without LRP5, a major component of the co-receptor for Wnt signaling, exhibit compromised osteogenic responses to mechanical loading[127]. Furthermore, conditional knockout of β-catenin using *Dmp1*-cre promoter caused a dramatic bone loss[128], while a heterozygote exhibited a normal skeleton but a complete abrogation of anabolic responses to mechanical loading[129]. Conversely, down regulation of Sost/sclerostin in mature osteocytes was an obligatory step in the mechanotransduction cascade that activated Wnt signaling and directed osteogenesis to where bone was structurally needed[29, 30, 101]. Anabolic loading reduceed sclerostin expression in bone[29], whereas hind limb unloading increased sclerostin level[101].

Another aspect connected to bone adaptation is periostin (Postn), a matricellular protein predominantly expressed in periosteum and osteocytes. This component was essential for periosteal bone formation mediated by Wnt/β-catenin signaling in response to mechanical loading [31, 32, 34, 130, 131]. Additionally, PGE_2 released during mechanical loading acts through the Wnt/β-catenin pathway to enhance connexin 43 expression, gap junction function, and protected osteocytes from glucocorticoid-induced apoptosis[132, 133].

Other genes regulated by loading and unloading included E11, a marker for early osteocytes and important for their dendrite elongation, which was up-regulated in response to mechanical loading[134], along with regulators of mineralizaton and phosphate homeostasis such as DMP1, MEPE, or PHEX[135-138]. Finally, unloading increased RANKL expression in osteocytes, which was responsible for the bone loss associated with unloading[139].

However, the effects of mechanical loading on osteon formation in large mammals are still unclear. Studies are required to address questions, including the form of new bone, how it remodels into a resulting osteon structure, the roles of periosteum and endosteum during this process, and whether these aforementioned signals and proteins will be involved in a bone response, etc.

I.2.3 Preferential Roles of Periosteum and Endosteum in Bone Responses Under Mechanical Loading

To start, periosteum and endosteum differ by their location within a physical environment and in response to mechanical loading. With ligaments and tendon-muscle

attachments on the periosteal surface, periosteal bone exhibits a greater mechanosensitivity to strain compared to endosteal bone[28]. Studies in mice and rats using various mechanical loading models have shown that mechanical loading promotes more prominent new bone formation on the periosteal surface rather than endosteal areas[29, 30]. In a study by Robling et al., an increase in fluorochrome incorporation on the periosteal surface revealed robust osteogenesis as a result of cyclic axial loading on rat ulna[29]. In another study where compression was applied on the longitudinal axes of mouse tibia, the increase in periosteum bone formation rate (BFR) was more prominent than endosteum BFR[31].

In contrast to robust studies on the effects of mechanical loading on rodent bone, it is still not fully understood how mechanical loading affects osteonal bone in large mammals, specifically primary osteon formation and secondary osteon remodeling. Some research has attempted to conceptualize various loads on bone in general, such as Wolff`s 1892 study which reported that trabeculae within the femoral neck align in the direction of principal stress.

In addition, early studies using ink have found that osteons align themselves parallel to the loading direction, indicating that the organization of the osteonal bone is a functional adaptation to the mechanical loading[15, 140, 141]. As for the effect of loading on osteon geometry, Young et al. reported that increased strain resulted in a decreased osteon size in monkeys[142]. Similarly, Britz et al. found that osteon diameter in heavier people tended to be smaller[39]. However, even fewer or no studies focus on the effects of loading on the newly formed osteon—namely, primary osteon modeling

and remodeling. Therefore, more in-depth studies are required to delineate the changes in secondary osteon remodeling under mechanical loading, and fill in knowledge gaps of loading-induced primary osteon formation, as well as its relationship with primary osteon formation process during early development.

CHAPTER II

CANINE OSTEON FROMATION (MODELING) AND REMODELING DURING EARLY DEVELOPMENT

II. 1 Introduction

Skeletal development begins during embryonic stage and continues into the postnatal years[143]. Two distinct mechanisms are responsible for the bone development – intramembranous and endochondral ossification. Intramembranous ossification is responsible for most of the craniofacial bones and parts of the clavicles and scapulae. Endochondral ossification is responsible for the formation of all long bones of the appendicular skeleton (limbs) and the axial skeleton (vertebrae and ribs)[42, 143]. Both processes start with mesenchymal progenitor cells aggregating and forming condensations in the areas where bones will be formed. In intramembranous ossification, the cells in these condensations directly differentiate into osteoblasts; whereas in endochondral ossification, these cells differentiate into chondrocytes[42, 143]. For decades, it is widely accepted that these chondrocytes would eventually undergo apoptosis, and be replaced by osteoblasts. However, in recent years, cell lineage tracing techniques in transgenic mice has shown a transition; the hypertrophic chondrocytes directly transdifferentiate into bone cells in metaphysis, trabecular bone and cortical bone in long bones[144-147]. This transdifferentiation was also observed in the mandibular condyle, where the chondrocytes in the fibrocartilaginous condylar cartilage transdifferentiate into bone cells in the subchondral bone[148].

Studies in rodents also demonstrated differing roles of periosteum and endosteum during early bone development. Preferential periosteal growth makes a major contribution to the rapid bone mass increase; whereas endosteum and the inner layers of the cortex accumulate abundant osteoclasts during embryonic and early postnatal stages, which leads to the rapid resorption of endosteal bone surfaces and therefore the enlargement of the bone marrow cavity[35]. With ligaments and tendon-muscle attachments on the periosteal surface, periosteal bone also exhibited a greater mechanosensitivity to strain compared the endosteal bone, which may partly contribute to the preferential periosteal growth during development[28].

However, in contrast to the relatively exhaustive research on bone development in rodents, our knowledge on osteonal bone development is very limited, despite the fact that osteon is the structural and functional unit in cortical bones in human and many other large mammals such as dogs and cows.

In the present study using long bone samples from young beagle dogs, we investigated in depth the osteon formation (modeling) and remodeling processes during early development, including the roles and periosteum and endosteum, and critical transcription factors and proteins, etc.

II. 2 Materials and Methods

II.2.1 Dogs Breeding, 5-ethynyl-2'-deoxyuridine (EdU) Injection, and Fluorochrome Labeling

Two pregnant beagle dogs were purchased and gave birth to 18 puppies. These young dogs were divided into 4 groups according to their ages by the time of sacrifice,

including postnatal day 1 (P1), day 14 (P14), day 28 (P28), and 4 months (4M), with at least 4 young dogs in each group, and their body weight and food intake were monitored daily. The average body weights were approximately 237 g at P1, 636 g at P14, 1039 g at P28, and 5804 g at 4 months. Breast milk from the female dogs was their major source of food until they were weaned from the female dogs at 6 weeks of age, after which regular dog food was supplied. The young dogs started to walk at about 3 weeks old (P21). The P1 and P14 dogs had limited movement. The 4-month-old dogs were able to actively exercise on their own.

The anesthesia of the puppies were induced and maintained with Isoflurane at 3% in a mask over the faces. Depth of anesthesia was confirmed by lack of reflex to toe pinch and lack of muscle tone in the jaw. The chest was opened and the pericardium was removed from the heart. The right atrium was cut and an 18-gage needle was inserted into the apex of the left ventricle to inject saline using a 20cc syringe. Once the dog had expired from exsanguination and all the blood was removed, 4% paraformaldehyde was injected throughout the body to fix the tissues.

The housing, care, and experimental protocols for this study were reviewed and approved by the Institutional Animal Care and Use Committee (IACUC) at Texas A&M University College of Dentistry.

For cell proliferation assays, the three younger groups (P1, P14 and P28) were given EdU injections intraperitoneally (Carbosynth, NE08701, 20mg/kg body weight) 4 hours prior to euthanasia.

To determine new bone formation, fluorochrome labeling was administered intraperitoneally as described previously[149]. The dose of calcein (Fluka, 21030) was 10 mg/kg body weight and alizarin red (Sigma, A3882) was 20 mg/kg body weight. For P1 group, calcein was given on P0 (24 hours prior to euthanasia); For P14 group, the 1st injection of calcein was given on P1, 2nd injection of alizarin red on P13, and 3rd injection of calcein was given 4 hours prior to euthanasia on P14; For P28 group, the 1st injection of alizarin red was given on P7, 2nd injection of calcein on P27, 3rd injection of alizarin was given 4 hours prior to euthanasia on P28.

II.2.2 Sample Preparation

Tibia samples of these young dogs were collected and fixed in 4% paraformaldehyde in phosphate-buffered saline (PBS, pH = 7.4) at 4°C for 2-4 days, followed by trimming the mid-shaft portions into several 1-2 mm cross-sectional slices. Nondecalcified tibia mid-shaft slices were dehydrated in ascending graded ethanol (EtOH) (75%, 95%, and 100% for twice, 2-4 days each) followed by xylene, and embedded in methyl-methacrylate (MMA, Buehler, Lake Bluff, IL) as previously describes[150]. Other bone slices were decalcified in 15% EDTA at 4°C, embedded in paraffin and cut into 4 μm-thick sections[151].

II.2.3 Histomorphometry and Immunohistochemistry

Nondecalcified MMA-embedded blocks were cut into 5 μm-thick sections (Leica Polycut S microtome) for Masson-Goldner trichrome [152] and tartrate-resistant acid phosphatase (TRAP) staining. All histomorphometric analyses were performed with

Image J software (National Institutes of Health, Bethesda, MD) and reported following the ASBMR guideline[153].

Decalcified paraffin sections were used for Sirius red, toluidine blue, and H&E staining as previously described[154, 155]. Toluidine blue was performed to reveal the cement lines of osteons. Sections were immersed in the toluidine blue solution comprised of 1% toluidine blue (Sigma 198161) and 1% sodium tetraborate decahydrate (Sigma S9640) in distilled water (pH = 9.5) for 3 min, followed by rinse with distilled water, dehydration with ascending concentration of ethanol and mounting. The following antibodies were used for immunohistochemistry: rabbit polyclonal anti-OSX (1:400, Abcam, ab22552), mouse monoclonal anti-BSP and rabbit polyclonal anti-DMP1 (1:400 for both, generously provided by Dr. Chunlin Qin, Texas A&M university College of Dentistry), rabbit polyclonal anti-MEPE (1:100, LF-155, a gift from Dr. Larry W. Fisher, NIDCR/NIH), mouse monoclonal anti-β-catenin (1:5, DSHB, PY489), goat polyclonal anti-sclerosin (1:100, R&D Systems, AF1598), goat polyclonal anti-periostin (1:100, R&D Systems, AF2955), rabbit polyclonal anti-Ki67 (1:100, Invitrogen, PA5-19462). For immunofluorescence, corresponding Alexa Fluor 488 secondary antibodies were applied (1:200, Thermo Fisher). EdU staining was performed as previously reported to detect cell proliferation for P1, P14, and P28 groups[156].

Histology and immunohistochemistry sections were photographed using an Olympus VS120 virtual slide microscope. Immunofluorescence images were captured using a Leica TCS SP5 confocal laser scanning microscope[157].

II.2.4 Backscattered and Acid-Etched Scanning Electron Microscopy (SEM)

The surfaces of MMA-embedded blocks were polished using 800 grit and 1200 grit sandpaper sheet (Buehler), followed by 1-, 0.3-, and 0.05 μm MicroPolish II alumina solution (Buehler) on a rotating wheel covered with soft cloth. The blocks were cleaned in an ultrasonic bath, and air-dried with vacuum for 48 hours. The dehydrated samples were sputter-coated with gold/palladium and imaged with backscattered SEM (JEOL JSM-6010LA, Japan)[164].

For acid-etched SEM, surfaces of the blocks for backscattered SEM were re-polished and acid-etched with 15% phosphoric acid for 10 seconds, followed by two 20-minute washes with 5% sodium hypochlorite. Subsequently, the blocks were washed, dried, coated with gold prior to SEM imaging.

II.2.5 Fluorochrome Labeling and FITC Imaging

Nondecalcified MMA-embedded blocks of P1, P14, and P28 groups were cut into 10 μm-thick sections (Leica Polycut S microtome) to examine the fluorochrome labeling using the SP5 Leica confocal microscope. For the 4M group, thick sections (300-400 μm) were cut from the MMA-embedded blocks with a diamond bladed saw (Buehler, Lake Bluff, IL), ground down to a final thickness of 30-50 μm, and polished for confocal imaging[150].

Fluorescein isothiocyanate (FITC) is a low molecular weight dye that fills in the spaces with no or little mineral content but does not enter the mineralized matrix. Thus, the dye provides a visual representation of porous structures in bone, including the lacunocanalicular system[158]. To prepare the 1% FITC solution, FITC powder (Sigma,

F7250) was diluted in 100% EtOH, gently mixed in a magnetic induction stirrer for overnight at room temperature until clear, and then filtered. After dehydration in ascending graded EtOH, the nondecalcified bone slices were placed in freshly prepared FITC solution for 1-3 days (depending on the sample size) at room temperature. The samples were washed in 100% EtOH for 24 hours, followed by subsequent steps of MMA-embedding process. These FITC-stained plastic blocks were cut and ground down to thin sections of 30-50 μm for confocal imaging, following the method described above.

II.2.6 Radiograph and μCT

Thin plastic sections for FITC were taken X-ray images prior to being mounted (Faxitron MX-20 Cabinet X-ray System, Faxitron X-Ray LLC, Lincolnshire, IL, USA).

μCT analyses of the tibia midshafts were performed using a Scanco μCT35 (Scanco Medical, Bassersdorf, Switzerland). X-ray tube potential of 55 kV and intensity of 145 μA were applied when scanning all the samples. The voxel size was 6 μm and integration time was 800 ms for the scanning of P1, P14, and P28 tibia midshafts. The voxel size was 10 μm and integration time was 600 ms for the scanning of 4 mos tibia midshafts. 200 slices (total of 1.2 mm) were selected from the center of each tibia midshaft, and analyzed at a threshold of 260 mg/cm^3. Assessment of the bone microstructure was reported following the guideline[159]. For the analyses of full-thickness tibia midshafts, variables were measured including cortical bone area (Ct.Ar), total cross-sectional area (Tt.Ar), cortical area fraction (Ct.Ar/Tt.Ar), bone marrow area (Ma.Ar), cortical porosity (Ct.Po), and bone mineral density (BMD), and compared

among different age groups. Furthermore, within each sample, the full thickness of the tibia midshaft was equally divided into three compartments: periosteal 1/3, middle 1/3, and endosteal 1/3. The Ct.Po and BMD of periosteal bone and endosteal bone were quantified and compared.

II.2.7 Statistical Analysis

Data were analyzed with SPSS software (version 16.0; SPSS, Chicago, IL). All results were expressed as mean ± standard deviation. One-way ANOVA with Bonferroni post-hoc test was used for comparing the bone microstructure of full-thickness tibia midshafts at different ages. Paired *t* test was used to compare the Ct.Po and BMD of periosteal bone and endosteal bone in each age group. The significance level was set at $P < 0.05$.

II. 3 Results

II.3.1 An Overview of Rapid Growth at Early Postnatal Stage

II.3.1.1 Tibia Midshaft of Young Adult Dogs were Dense with Minimal Porosity

To better understand the bone microstructure during early development, cross sections of the tibia midshaft from young adult dogs (~1.5 years, samples obtained from the experiment in Chapter III) were examined with X-ray imaging (Fig. 1a) and toluidine blue staining (Fig.1b). Both assays revealed dense cortical bone with minimal areas of pores. Covered by periosteum (Ps) and endosteum (Es), the bone was composed of lamellar bone in different formats; the outer circumferential lamellae (OCL, Fig. 1b1, above white dashed outline) and inner circumferential lamellae (ICL, Fig. 1b3, below white dashed outline) constituted the outer and inner zone of the cross section,

respectively; the osteons, composed of concentric lamellae surrounding a central canal (Haversian canal), located between OCL and ICL and made up the majority of the bone (Fig. 1b, between two white dashed outlines); lastly, the interstitial lamellae (IL, Fig. 1b2, yellow dashed outline) filled in the space among adjacent osteons, and represented the remnants of preexisting bone that were left over during remodeling[1].

In particular, most osteons in adult tibia midshaft were secondary osteons (SOn), which had cement lines (Fig. 1b1, orange arrows) at their outer boundaries to separate them from the interstitial lamellae; whereas there were also smaller primary osteons (POn, black dashed outline) with less layers of lamellae located next to the outer circumferential lamellae. The Haversian canals of both SOn and POn were very small in young adult dogs, leading to the minimal cortical porosity and a dense cortical bone appearance.

II.3.1.2 Bone Mass of Young Dog Tibias Increased Rapidly at Early Postnatal Stage

The cross sections of young dog tibias exhibited rapid bone mass increase with age, as revealed by X-ray images (Fig. 2a) and toluidine blue staining (Fig. 2b and c). This bone mass increase resulted from a robust periosteal appositional growth (laydown of new bone on the periosteal surface), as well as a decrease in the cortical porosity within the bone, despite an enlargement of bone marrow cavity with age (Fig. 2a, b, and c).

Three-dimensional (3D) reconstruction of the bones by μCT further confirmed the dramatic increase in total intracortical volume and bone masses with age (Fig. 3a). Quantitative analyses showed the following changes with age: increases in cortical bone

area (Ct.Ar), total cross-sectional area (Tt.Ar), cortical area fraction (Ct.Ar/Tt.Ar), bone marrow area (Ma.Ar), and bone mineral density (BMD), along with a decrease in cortical porosity (Ct.Po) (Fig. 3b, n=4/group, one-way ANOVA with Bonferroni post-hoc test, *P<0.05, **P<0.01, ***P<0.001).

II.3.1.3 Periosteum-Derived Preosteons and Large Haversian Canals Resulted in a High Cortical Porosity

At early postnatal stages (P1, P14, P28, and 4 mos.), the dense periosteum (Ps) covered the outer surface of the bone and gave rise to numerous semicircular canals that would develop into future osteons; therefore, we name these structures "preosteons" (PreOn) (Fig. 2b and c, yellow arrows). The preosteons were highly cellular with cuboid osteoblast-like cells lining the boundary, and vessel(s) and fibrous tissue filled in the center.

In sharp contrast to the young adult dog (Fig. 1), bones of early postnatal stages exhibited a much higher porosity due to the presence of numerous large pores, including the preosteons and large Haversian canals (Fig.2 b and c). The osteons in P1, P14 and P28 groups were almost exclusively primary osteons with giant Haversian canals (Fig. 2b, red asterisk), as no cement lines were identified. At 4 months, the majority of intracortical osteons were secondary osteons (Fig. 2c2, orange arrows indicating cement lines), with only a few primary osteons interspersed among them (Fig. 2c2, black dashed outlines), whereas most primary osteons constituted a thin layer in periosteal bone next to periosteum-derived preosteons (Fig. 2c, between black dashed outlines, and c1, black dashed outline). Another striking difference of 4-month bone was the formation of inner

circumferential lamellae on the endosteal surface (Es, Fig. 2c3), though the periosteum (Ps) was still responsible for osteon formation as in earlier stages (Fig. 2c1).

II.3.1.4 Periosteal Bone Showed a Higher Cortical Porosity and Lower Bone Mineral Density than Endosteal Bone

Interestingly, we also found the periosteal bone to be more porous than the endosteal bone both on X-ray (Fig. 2a) and histology (Fig. 2b and c). By dividing the μCT images of tibia midshaft into three equal parts, we compared the periosteal 1/3 and endosteal 1/3 bones, and confirmed a higher cortical porosity and lower bone mineral density in periosteal bone at P1, P14, and P28 (Fig. 3c, n=4/group, paired *t* test, *P<0.05, **P<0.01, ***P<0.001). This indicated that the periosteal bone was newly formed, while the endosteal bone was more mature. At 4 months, with the formation of inner circumferential lamellae, the cortical porosity of endosteal bone continued to be than that of periosteal bone, however, the bone mineral density did not show significant difference (Fig. 3c).

II.3.2 Periosteum as the Major Contributor to the Apposition Bone Growth by Giving Rise to New Osteons

II.3.2.1 Periosteal Bone Was More Immature than Endocortical Bone

Although the μCT data qualitatively and quantitatively revealed the periosteal bone to be less mineralized and less mature, it cannot distinguish detailed differences in bone matrix on periosteal and endosteal sides. Therefore, we analyzed the bone matrix with multiple other approaches. As P14 bone and P28 bone shared many similarities in

histology and bone microstructures revealed by μCT, P14 data would not be shown in most of the following analyses.

Masson-Goldner trichrome staining showed that periosteal bone comprised abundant osteoid, which mainly located surrounding the boundaries of the periosteum-derived preosteons (yellow arrows), and surrounding the boundaries of the large central canals (orange arrows) in periosteal 1/3 to 2/3 of the bone depending on the ages (Fig. 4). In contrast, very few osteoid were identified on the endosteal bone at P1 and P28 (Fig. 4a and b, white arrows), whereas at 4 months, more osteoid were found to on the boundary between inner circumferential lamellae and the bone marrow cavity (Fig. 4c, white arrows). Quantitative histomorphometry measurement of osteoid surface confirmed a much higher content of osteoid in periosteal bone surface (outer boundaries of preosteons) than in endosteal surface at P1, P14, and P28 (Fig. 4d, n=4/group, paired *t* test, ***P<0.001), whereas this difference were not statistically significant at age of 4 months (Fig. 4d).

These finding were further confirmed by backscattered SEM (Fig. 5a-c), confocal microscopic images of FITC-stained bones (Fig. 5d-f), and SEM of acid-etched resin-casted bones (Fig. 5g-i). Fluorescein isothiocyanate (FITC) is a low molecular weight dye that fills in the spaces with no or little mineral content but does not enter the mineralized matrix. Thus, the dye provides a visual representation of porous structures in bone[158]. At the ages of P1 and P28, periosteal bone displayed a lower mineral content than endosteal bone, as shown by a less radio-opacity in backscattered SEM (Fig. 5a and b) and more filling of FITC (Fig. 5d and e). SEM images of acid-etched resin-casted

blocks revealed typical spindle-shaped osteocyte morphology in endosteal bone, along with numerous elongated osteocyte dendrites (Fig. 5g'' and h''), whereas the osteocytes in periosteal bone were less mature as they were more cuboid with much fewer dendrites and less complex lacunocanalicular systems (Fig. 5 g' and h'). At age of 4 months, periosteal bone and endosteal bone composed of similar levels of mineral content (Fig. 5c and f). Accordingly, the osteocytes on both sides shared similar morphologies and complexity of lacunocanalicular system (Fig. 5I and I''). Of note, at 4 months, the bone matrix was not fully mineralized as there was much FITC dye filled in both periosteal and endosteal bones (Fig. 5f and f'), indicating the ongoing process of new bone formation on both surfaces.

II.3.2.2 Periosteal Bone Was Formed More Rapidly than Endocortical Bone

Calcein and alizarin red were administrated in dogs in order to mark new bone formation. For P1 group, calcein was given on P0, namely, 24 hours before euthanasia. Confocal microscopic images revealed that the calcein label was much stronger in periosteal bone than in endosteal bone (Fig. 6a1 and a2, white arrows), indicating that periosteum side is the mineralization front.

For P14 group, the first calcein was administrated on P1, followed by alizarin red on P13 and another calcein on P14 (4 hours before euthanasia). Interestingly, in the endosteal bone, we found that the alizarin red label lined the boundaries of the osteon central canals, and the strong calcein label in the bone matrix surrounding the alizarin red label (Fig. 6b2, white arrows). As the new bones were added on bone surfaces with time, we could infer that the strong green label in the endosteal bone was from the first

calcein injection. The third injection of calcein (20 hours after the alizarin red, and 4 hours before euthanasia) was only captured by very few locations, leading to a yellow label due to its incorporation with the alizarin red label (Fig. 6b1 and b2, yellow arrows). Therefore, the distance between the first calcein label and the second alizarin red label indicated the mineral apposition within 12 days in endosteal bone (Fig. 6b2, white double-headed arrow). Mineral apposition rate of endosteal bone can thereby be achieved (distance between the corresponding edges of two consecutive labels, divided by the time between the midpoints of the labeling periods[153]).

In sharp contrast, since the first calcein should have labeled the entire bone matrix at P1 and displayed strongest labeling in periosteal bone (based on data from P1 group, Fig. 6a), and the second alizarin red label lined the boundaries of osteon central canals throughout all bone matrixes (Fig. 6b and b1), we could infer that the bone between periostal surface and the endocortical calcein label was laid down within 12 days (Fig. 6b, white doubleheaded arrow). Therefore, the mineral appositional rate of periosteal bone was much higher than that of endosteal bone.

For the P28 group, sequential fluorochrome labels were administrated in the order of calcen, alizarin red, and calcein at P7, P27, and P28, respectively. Similar with P14 group, the mineral apposition rate was much higher in periosteal bone than in endosteal bone. Taken together, the fluorochrome labeling assays of P1, P14, and P28 groups suggest that at these time points, periosteal bone was formed much more rapidly than endosteal bone, and periosteum served as the major contributor to appositional growth of the bone.

For 4 months group, fluorochrome labeling were given in the order of alizarin red, calcein, and alizarin red 2 weeks, 1 day, and 4 hours before euthanasia, respectively. The red labeling in these confocal microscopic images came from the first alizarin red injection (Fig. 6d, d1-d4, white arrows), whereas the last two injections were only 20 hours apart and could not to be distinguished under confocal microscope, leading to a mixed labeling in yellow color (Fig. 6d, d1-d4, yellow arrows). One of the most striking characteristics at 4 months was the linear pattern of mineral apposition in the inner circumferential lamellae (Fig. 6d4, white and yellow arrows), in contrast to the circular pattern of mineral apposition surrounding the preosteons and the osteons (Fig. 6d and d3, white and yellow arrows). The directions of mineral apposition could also be inferred from the sequential labels; new mineral was added on the periosteal surface (Fig. 6d3, white and yellow arrows) and on the endosteal surface (towards to bone marrow cavity) (Fig. 6d4, white and yellow arrows); in osteons, mineral was added in the direction towards Haversian canals, leading to smaller canals and thicker osteonal lamellae (Fig. 6d, white and yellow arrows).

II.3.3 The Regulation Mechanisms on Molecular Level Differed in Periosteal and Endosteal Bone Growth

Supporting the theory that periosteal bone was more immature and formed more rapidly, we found a high expression of an early bone transcription factor, osterix, in periosteum and periosteum-derived preosteons (Fig. 7a-c, upper right panels, arrows). Osterix+ osteoprogenitors were also occasionally found in the endosteum and endosteal bone, especially at the age of 4 months (Fig. 7a-c, lower right panels, arrows).

Accordingly, endosteal bone displayed higher expression of matrix proteins that regulate mineralization than periosteal bone at P1 and P28, including DMP1 and MEPE (Fig. 7d, e, g, and h, lower right panels, arrows), while this difference was minimal at 4 months (Fig. 7f, and i). At all stages, sclerostin, a marker for mature bone, was rich in endosteal bone matrix (Fig. 7j, k, and l, lower right panels, arrows) (but not in the matrix where the endosteum lined, Fig. 7j, k, and l, asterisks). Immunohistochemistry also demonstrated a robust expression of β-catenin in periosteum and periosteum-derived preosteons (Fig. 7m-r, upper right panels, arrows), suggesting a critical role of wnt/β-catenin signaling in periosteal new bone formation. The matricellular protein periostin was expressed in periosteum, perioteum-derived preosteons, as well as in the Haversian canals and bone matrixes throughout the entire bone at P1 and P28, and continued to be highly expressed in the periosteum and preosteons at 4 months.

On the other hand, periosteum and peroiosteum-derived preosteons displayed a high level of cell proliferation activity, as revealed by the 24 hours of EdU labeling for P1, P14, and P28 groups (Fig. 8a-c, red arrows), along with the Ki67 immunofluorescence staining for the 4 months group (Fig. 8d, red arrows). In the endocortical bone, the osteons close to endosteum were infiltrated with bone marrow cells and therefore showed a high level of EdU incorporation, though many of these EdU (+) cell did not necessarily differentiate into osteoblast lineage and contribute to endosteal bone formation (Fig. 8a-d, white arrows). Similarly, at 4 months, EdU (+) cells were also identified in the bone marrow cavity close to inner circumferential lamellae (ICL).

Taken together, using multiple approaches including μCT, histomorphometry, SEM, and immunohistochemistry, we demonstrated that (1) the periosteal bone was more immature in both mineralization and matrix protein production, and was formed more rapidly than the endosteal bone until the age of 4 months, when the endosteum served to generate the inner circumferential lamellae; (2) the periosteum produced numerous preosteon structures, thereby making a major contribution to the appositional bone expansion; (3) mechanistic investigation revealed a significant role of wnt/β-catenin signaling in periosteal new bone formation; periostin, a matricellular protein that is essential for sost inhibition and associated with wnt/β-catenin signaling, also contributed to periosteal bone formation.

II.3.4 Active Osteoclast Activities in Endosteal Bone

TRAP staining revealed that many TRAP (+) osteoclasts lined on the endosteum surface throughout all the ages, in sharp contrast to the periosteum where osteoclasts were rarely detected (Fig. 9a-d, a1-d1, black arrows). Quantitation analyses of osteoclast number per unit of bone surface (N.OC/BS) showed that endosteal osteoclasts number were the highest at P14 and P28, and declined sharply at 4 months (Fig. 9e). Masson-Goldner trichome staining showed osteoid formation along the endosteum (Fig. 9f-i, asterisks) in close proximity to active osteoclast activities (Fig. 9f-i, black arrows), especially at P1 and 4 months, suggesting the coupling of bone formation and bone resorption on the endosteum. Therefore, endosteal surfaces were undergoing active bone remodeling, when the periosteal surface was almost exclusively comprised of bone formation.

In addition to the endosteum surface, TRAP (+) osteoclasts were also found in some Haversian canals close to endosteum at P14 and P28 (Fig. 9b1 and c1, blue arrows). At 4 months, TRAP (+) osteoclasts were present in Haversian canals in endosteal bone, the central part of the cortical bone, as well as the periosteal bone (Fig. 9d and d1, blue arrows). TRAP (+) monocytes were also identified in periosteum and periosteum-derived preosteons at 4 months (Fig. 9d and d2, white arrows).

II. 4 Discussion

Osteon, also called Haversian system, is the basic structural and functional unit of cortical bones in human and many other large mammals like dogs, and cows. Composed of multiple concentric lamellae surrounding a vascular central canal, osteon structure is meaningful for the function of skeletal system in providing both blood supply and mechanical support. Studies in recent years also showed striking changes in osteons in patients with osteoporosis, indicating that osteon modeling and remodeling is intimately associated with bone health. However, there is very limited research that investigated osteons using large animals, in contrast to the relatively exhaustive bone research using rodents. Therefore, knowledge gaps exist in our understanding of osteons, including the modeling and remodeling of osteons during early development.

In this study, using young beagle dogs as the animal model, we showed that during early postnatal development, periosteum gave rise to abundant “preosteon” structures, the highly cellular semicircular canals that develop into future osteons. The fluorochrome labeling proved that the periosteal bone was formed much more rapid than the endosteal bone. Along with a much higher expression of early bone markers, we data

suggested that periosteum was the major contributor to the appositional expansion during early bone development.

On the other hand, our study revealed an active osteoclast activity on the endosteum surface, apart from a mild activity of bone formation. Therefore, the endosteum side, rather than the periosteum side, was where bone remodeling first took place.

These preferential roles of periosteum and endosteum in osteonal bone development were similar to their roles in rodent bone development[35]. These differing roles could be associated with the differing physical and hormonal environments where the periosteum and endosteum locate. With ligaments and tendon-muscle attachments on the periosteal surface, periosteal bone also exhibits a greater mechanosensitivity to strain compared the endosteal bone[28]. Bathed in the bone marrow cavity, the endosteum accumulated more osteoclasts and monocytes than the periosteum. As the bone marrow cells could infiltrate into the Haversian canals in endocortical bone, osteoclasts could also be found in these canals.

Apart from the roles of periosteum and endosteum, our study also revealed the microstructure changes with age in dog bones. Tibia midshafts in P1, P14, and P28 dogs all displayed large Haversian canals throughout the entire bone, and for most of these immature osteons, the osteocytes surrounding Haversian canals were not arranged in the typical pattern of concentric lamellae. Moreover, the outer and inner circumferential lamellae were not yet formed at these three stages. In contrast, by the age of 4 months, most of these large Haversian canals were filled with bone matrixes, leaving only a small

central canal; typical concentric lamellae were formed in many of the osteons, especially in endocortical osteons; the inner circumferential lamellae had been formed on the endosteum side, whereas the periosteum continued to give rise to preosteons.

There are still many other questions that need to be answered. Among these questions, one of the most intriguing one would be, how do newly formed osteons become mature and form typical concentric lamellae. We observed abundant osteocytes in the interstitial bone matrix surrounding the preosteons and immature osteons. We hypothesize that these osteocytes play a role in the maturation of osteons. Coupling of angiogenesis and osteogenesis during osteon formation is also a topic worthy of further investigation, since the osteon itself is an exquisite combination of bone cells and vasculature, and the osteon is essential for sufficient blood supply and mechanical support.

In summary, this study filled the knowledge gap in osteon modeling and remodeling during early development, and demonstrated differing roles of periosteum and endosteum in these processes. A thorough understanding of osteon biology in development is essential, as it gives us a solid foundation in understanding osteon turnover in adulthood under both physiological and pathological conditions, such as under enhanced mechanical loading and osteoporosis, respectively.

CHAPTER III

CANINE OSTEON FROMATION (MODELING) AND REMODELING IN RESPONSE TO MECHANICAL LOADING

III. 1 Introduction

Mechanical loading is the major functional influence on bone mass, architecture, and thus the ability of the skeleton to withstand the loads of everyday activity without fracture. Reduced mechanical loading leads to bone loss, as experienced by bedridden patients and astronauts[101, 120, 123, 124]. Studies in mice and rats have shown that mechanical loading promotes more prominent new bone formation on periosteal surface rather than on endosteal surface. In a study by Robling et al., increased fluorochrome incorporation on the periosteal surface revealed a robust increase in osteogenesis as a result of cyclic axial loading on the rat ulna[29]. In another study where compression was applied on the longitudinal axes of mouse tibia, the increase in periosteum bone formation rate (BFR) was more prominent than endosteum BFR[31].

Several signaling pathways and proteins were significant for bone response to mechanical loading. Wnt- β-catenin signaling in bone cells was activated by mechanical stimulation[30, 96]. Downregulation of Sost/sclerostin in osteocytes was an obligatory step in the mechanotransduction cascade that activated Wnt signaling and directed osteogenesis to where bone was structurally needed [29, 30, 101]. Periostin (Postn), a matricellular protein predominantly expressed in periosteum and osteocytes that has an

essential role for periosteal bone formation mediated by Wnt/β-catenin signaling in response to mechanical loading [31, 32, 34, 130, 131].

However, in contrast to abundant studies on the effects of mechanical loading on rodent bone, it is still not fully understood how mechanical loading affects the osteonal bone in large mammals, specifically, how it affects both primary osteon formation and secondary osteon remodeling.

In the present study, we established a novel loading model on the tibias of beagle dogs, and investigated in depth the impact of mechanical loading on osteonal bone. Several important questions were proposed and addressed, including whether new primary osteons would be formed, the roles of periosteum and endosteum in new bone formation, how the remodeling of secondary osteons would be affected, whether these aforementioned signals and proteins would be involved in bone responses, etc. To the best of our knowledge, this is the first study to reveal the effects of mechanical loading on the osteonal bone on histologically and protein levels, and will shed light on the future studies.

III. 2 Materials and Methods

III.2.1 Dogs, Mechanical Loading Model, and Fluorochrome Labeling

8 adult male beagle dogs, between 1 to 2 years of age and weighing 21-29 lbs., were used in this study. For each dog, we randomly chose one tibia to set up the mechanical loading model (“loaded side”), and used the other tibia as control (“control side”). For the loaded side, two mini-screw implants were surgically placed in the midshaft of the tibia and penetrated the full-length of the cortical bone. The NiTi spring

connecting these two implants constantly delivered compressive force of approximately 200 grams on the bone compartment between two implants.

To determine new bone formation and trace the bone turnover, fluorochrome labeling was administered intraperitoneally as described previously[149]. The first injection of calcein was given one day after the surgery (5 weeks before euthanasia), followed by the second injection of alizarin red two weeks later (3 weeks before euthanasia), and the third injection of calcein another two weeks later (1 weeks before euthanasia). The dose of calcein (Fluka, 21030) was 10 mg/kg body weight and alizarin red (Sigma, A3882) was 20 mg/kg body weight.

One week after the last injection, the dogs were euthanized. Specifically, surgical plane anesthesia was induced and maintained using Ketamine (2.2mg/kg, intramuscular) and Xylazine (0.22 mg/kg, intramuscular). Depth of anesthesia was confirmed by lack of reflex to toe pinch and lack of muscle tone in the jaw. Anesthesia was supplemented as needed. The femoral artery and vein were isolated and a cannula was placed in the artery. The dogs was euthanized with Beuthanasia-D (2cc, intracardiac). Asystole was confirmed by stethoscope. The vein was cut and saline was injected into the artery until the saline ran clear coming from the vein. Then 4% paraformaldehyde was injected into the artery to fix the tissues.

The animal protocol for this study was approved by the Institutional Animal Care and Use Committee (IACUC) at Texas A&M University College of Dentistry.

III.2.2 Sample Preparation

The tibia bones between two implants were harvested, as well as the counterpart of bones in the control tibias. These bone samples were fixed in 4% paraformaldehyde in phosphate-buffered saline (PBS, pH = 7.4) at 4°C for 2 days, followed by trimming the middle portions into several 1-2 mm thick cross-sectional slices. Nondecalcified tibia mid-shaft slices were dehydrated in ascending graded ethanol (EtOH) (75%, 95%, and 100% for twice, 2-4 days each) followed by xylene, and embedded in methyl-methacrylate (MMA, Buehler, Lake Bluff, IL) as previously describes[150]. Other bone slices were decalcified in 15% EDTA at 4°C, embedded in paraffin and cut into 4 μm-thick sections[151].

III.2.3 Histology and Immunohistochemistry

Decalcified paraffin sections were used for Sirius red, toluidine blue, and H&E staining as previously described[154, 155]. Immunohistochemistry of OSX, DMP1. Sclerostin, BSP, β-catenin, and periostin were performed using the antibodies described in Chapter II, Section II.2.3.

Histology and immunohistochemistry sections were photographed using an Olympus VS120 virtual slide microscope. Immunofluorescence images were captured using a Leica TCS SP5 confocal laser scanning microscope[157].

III.2.4 Backscattered and Acid-Etched Scanning Electron Microscopy (SEM), and Energy Dispersive X-ray (EDX) Microanalysis

The MMA-embedded blocks were processed for scanning electron microscopy with or without acid etching the surface, as previously described in Chapter II, Section

II.2.4. EDX microanalysis is a technique for spectral analysis of individual elements such as calcium, oxygen, and phosphate. A total of 4 loaded tibia blocks and 4 control tibia blocks were imaged by backscattered electrons and analyzed with EDX to determine the relative atomic percentages of calcium in different areas of the samples. The percentage of calcium atom number to the total number of calcium, oxygen, and carbon atoms were defined as Ca%. 10 spots were picked out for each area, and the average Ca% of the these 10 spots was used for statistical analysis[160].

III.2.5 Fluorochrome Labeling and FITC Imaging

Nondecalcified MMA-embedded blocks with or without FITC dye were cut into thick sections (300-400 μm) with a diamond bladed saw (Buehler, Lake Bluff, IL). These sections were then ground down to a final thickness of 30-50 μm, and polished for confocal imaging, as described in Chapter II, Section II.2.5.

III.2.6 Radiograph

Thin plastic sections were taken X-ray images prior to being mounted (Faxitron MX-20 Cabinet X-ray System, Faxitron X-Ray LLC, Lincolnshire, IL, USA) for confocal imaging.

III.2.7 Statistical Analysis

Data were analyzed with SPSS software (version 16.0; SPSS, Chicago, IL). All results were expressed as mean ± standard deviation. Paired *t* test was used to compare the calcium contents in different areas within the same loaded bone, or within the same control bone. The significance level was set at $P < 0.05$.

III. 3 Results

III.3.1 A Preferential Role of Periosteum in Loading-Induced New Bone Formation, Recapitulating Early Developmental Processes

III.3.1.1 The Establishment of Mechanical Loading Model on Dog Tibias

X-ray showed that two mini-screw implants with a NiTi spring in between were placed in the midshaft of the loaded tibia and penetrated the full-length of cortical bone, and the contralateral tibia without implants and spring were used as control (Fig. 10a).

III.3.1.2 More Robust Preosteon Formation from the Periosteum than from the Endosteum

After 5-week mechanical loading, there was a thin layer of new bone formed on the periosteal surface, which was less radio-opacity than the existing bone in the X-ray image (Fig. 10b, red arrow). Some of the dogs also had slight new bone formation on the endosteal surface of the loaded tibias (Fig. 10b, white arrow) while some dogs did not. Interestingly, we also found numerous pores in the new bone and existing bone areas of loaded tibia (Fig. 10b, blue arrows). The control side tibias did not display apparent new bone in the X-ray image (Fig. 10b).

Toluidine blue staining revealed more detailed histological changes in the tibia bone in response to mechanical loading (Fig. 10c and d). The control tibia showed typical microstructure of osteonal bone; the periosteum (Ps) and endosteum (Es) covered the outer and inner surfaces of the cross section; the outer circumferential lamellae (OCL, Fig. 10d1, red and black arrows indicating its outer and inner boundaries, respectively) and inner circumferential lamellae (ICL, Fig. 10d3, white dashed outline) constituted the

outer and inner zone of the cross section, respectively. The osteons located between OCL and ICL made up the majority of the bone (Fig. 10d2, orange arrows indicating cement lines of secondary osteons). Compared to the control tibia, the most striking characteristic of the loaded tibia was the formation of preosteon structures on the periosteal surface. Very similar to the preosteons formed during early development, these loading-induced preosteons were also semicircular shaped, highly cellular with cuboid osteoblast-like cells lining the boundary, with vessel(s) and fibrous tissue in the center (Fig. 10c1 and c2, yellow arrows). These preosteons may develop into immature osteons (IOn, Fig. 10c1) in the new bone area. The new bone matrix was laid down on top of the outer circumferential lamellae (OCL, Fig. 10c1 and c2, red arrows indicating the outer boundary of OCL). The existing bone area and inner circumferential lamellae did not show apparent changes in toluidine blue staining (Fig. 10c3 and c4).

As mentioned earlier, some of the loaded tibias also displayed mild new bone formation on the endosteal surface. Toluidine blue staining showed that these new bone matrixes were laid down between the inner circumferential lamellae (ICL, Fig. 10e4, white dashed outline) and the bone marrow cavity. The endosteal new bone close to the ICL contained typical immature osteon structures (IOn, Fig. 10e4, yellow arrows); whereas, the new bone close to bone marrow cavity displayed trabecular bone-like morphology (Fig. 10e4, red arrows). Existing bone area (Fig. 10e3) still failed to show differences from the counterpart in the control dog (Fig. 10d2) using toluidine blue staining. For these loaded tibias with endosteal new bone formation, the periosteal new bone (Fig. 10e1 and e2) was usually thicker than that in loaded tibias without endosteal

new bone formation (Fig. 10c1 and c2). The inner boundary of OCL was distinguishable in most areas (Fig. 10e1, black arrows); however, its outer boundary was usually more obscure (Fig. 10e1, asterisks), indicating a trend of fusion of periosteal new bone and the OCL. In some areas, both the inner and outer boundaries of OCL became difficult to distinguish (Fig. 10e2, white dashed outline and asterisks, respectively), indicating that this transition zone between preosteons and the inner boundary of OCL, might be undergoing active bone remodeling. This will be further investigated in Section III.3.5.

III.3.2 Loading-Induced New Osteonal Bone Was Immature and Undergoing Active Mineral Apposition

The periosteal new bone in loaded tibia (Fig. 11a, blue asterisks) displayed a lower mineral content than the existing bone area (Fig. 11a, red asterisks), as shown by a less radio-opacity in backscattered SEM. Calcium content determined by EDX confirmed this finding. In contrast, control bone did not show apparent new bone formation, and the counterparts of "periosteal bone" (Fig. 11b, green asterisks) and "existing bone" (Fig. 11b, purple asterisks) areas in the control dog tibia did not show significant difference in calcium content.

Enlarged SEM images of perioseal and endosteal new bone revealed preosteon structures (Fig. 11a1 and a2, yellow arrows) and newly formed immature osteons (IOn, Fig. 11a3 and a4, white arrows). Of note, there were also newly formed osteons (Fig. 11a1, white arrow) in the original OCL (Fig. 11a1, between white dashed outlines). Control bone did not show apparent new bone on periosteal and endosteal surfaces (Fig. 11b1-b4).

Interestingly, these loading-induced new bones were undergoing active mineral apposition, as revealed by the fluorochrome labeling. The osteocytes surrounding newly formed central canals and close to bone surfaces were strongly labeled by the calcein and alizarin red, and played a major role in mineralization of the new osteonal bone (Fig. 11c3 and c4, white arrows). Osteocytes also contributed to the mineral apposition of outer and inner circumferential lamellae in the control bone (OCL, ICL, Fig. 11d3 and d4, white arrows).

III.3.3 The Molecular Mechanisms that Regulated Periosteal New Bone Formation in Response to Mechanical Loading

Supporting the theory that the periosteum was the source of robust new bone formation under mechanical loading, immunochemistry revealed abundant OSX (+) cells in periosteum, as well as the boundaries of periosteum-derived preosteons in loaded dog (Fig. 12a, red arrows). OSX was also expressed in some of the immature osteocytes in the new bone area (Fig. 12a, blue arrows). In contrast, much less OSX expression was detected in the periosteum of control bone. BSP was highly expressed in the new bone area of loaded tibia (Fig. 12c, red arrows), but was barely detectable in the control tibia (Fig. 12d).

Similar to the developmental process, immunohistochemistry also revealed high expression of β-catenin in periosteum and periosteum-derived preosteons (Fig. 12e, red arrows) in loaded bone compared to controls, suggesting a critical role of wnt/β-catenin signaling in periosteal new bone formation. The matricellular protein periostin was highly expressed in periosteum, perioteum-derived preosteons, as well as in the

Haversian canals and bone matrixes in the periosteal bone of loaded tibias (Fig. 12g, red arrows) compared to controls(Fig. 12h, red arrows).

In the loaded bone, periosteum and peroiosteum-derived preosteons also displayed a higher level of cell proliferation activity (Fig. 12i, red arrows) than the periosteum in control bone, as revealed by the Ki67 immunofluorescence staining (Fig. 12j, red arrows).

III.3.4 Bone Remodeling of Existing Cortical Bone Was Enhanced under Mechanical Loading

A combined assay of backscattered SEM and fluorochrome labeling on the same MMA-embedded bone samples showed that the existing bone area in loaded bone had more osteons undergoing remodeling, specifically, demineralization (Fig. 13a, orange arrow) and remineralization (Fig. 13c, orange arrow), compared to the counterpart area of control bone (Fig. 13b and d). There were also numerous *de novo* osteons being formed, which displayed pore-like structures in cross sections (Fig. 13a and c, white arrows). Active mineral apposition was taking place surrounding the central canals of these *de novo* osteons (Fig. 13c1, white arrow), resulting in an increased but relatively low mineral content in the concentric lamellae, and therefore these newly formed lamellae were darker than the adjacent interstitial lamellae in backscattered SEM (Fig. 13a1, white arrow). Of note, same with the periosteal and endosteal new bone (Fig. 11c1-c4), osteocyte dendrites surrounding the central canal were also strongly labeled by calcein and alizarin red, demonstrating a contribution to mineral apposition (Fig. 13c1,

white arrow). In contrast, there were fewer *de novo* osteons and remodeling osteons in control bone (Fig. 13b and d).

Osteoclastic resorption was also enhanced in the existing bone area in response to mechanical loading. TRAP (+) osteoclasts were found in the central canals of the *de novo* osteons in the existing bone area (Fig. 13e1, black arrows), along with TRAP (+) osteocytes in adjacent bone matrix (Fig. 13e1, blue arrows). In contrast, the control bone had very few osteons undergoing resorption.

In summary, compared to the control bone, mechanical loading induced more active bone remodeling in the existing bone tibia. Specifically, there were numerous osteons undergoing coupled resorption (TRAP staining) and formation (fluorochrome labeling, white arrows). There were also osteons undergoing active demineralization (backscatttered SEM, orange arrow) and remineralization (fluorochrome labeling, orange arrow). Osteocytes played a role in all these activities.

III.3.5 Enhanced Osteoclastic Activity Was Critical for the Remodeling of the Transition Zone between Preosteons and Existing Bone

As mentioned in Section III.3.1.2, the boundary between the loading-induced new bone and the original OCL (namely, the outer boundary of OCL) became obscure, suggesting that the transition zone between preosteons and the inner boundary of OCL was undergoing active bone remodeling. Therefore, to better understand the remodeling activity of the transition zone, we performed TRAP staining and imaging followed by toluidine blue staining on the same paraffin section.

This combined assay revealed diverse remodeling activities in different areas of the transition zone. TRAP (+) Osteoblasts and monocytes were identified in some of the preosteons (Fig. 14b, black arrows), and the outer boundary of OCL in this area was still well distinguishable (Fig. 14a, asterisks). In another location where the boundary was obscure (Fig. 14c and d, asterisks), there were several immature osteons newly developed from preosteons, and these immature osteons possessed numerous osteoclasts and monocytes in their central canals, suggesting a possible relationship between the osteoclastic resorption in newly formed osteons and the turnover of outer boundary of OCL. In another area where the outer boundary of OCL was already completely missing (Fig. 14 e and f), there were osteons located at the inner boundary of OCL, and these osteon were also undergoing osteoclastic resorption, indicating that the inner boundary of OCL was also subject to remodeling in response to mechanical loading. Importantly, numerous TRAP (+) osteocytes were identified in the bone matrix close to these preosteons and immature osteons (Fig. 14b and d, blue arrows).

Based on these observations, we propose that the osteoclastic resorption in these preosteons and newly formed immature osteons, along with the osteoclastic activity in osteocytes, were critical for the remodeling of the transition zone. Specifically, this activity facilitated the diminishment of OCL boundaries, and the turnover of original OCL into new osteonal bone. In this way, the newly formed osteonal bone was integrated into the existing bone. Furthermore at some point, the periosteum ceased to produce preosteons, and started to generate new OCL.

III. 4 Discussion

The anabolic effect of appropriate mechanical loading on the skeletal system has been well studied using rodents as animal model, which do not have osteon structures[29, 31]. Correspondingly, rodent studies also proved that reduced mechanical loading lead to bone loss[101, 120]. Mechanistic studies using rodents also proposed a number of signaling pathways and proteins that were important for bone responses to mechanical loading, such as Wnt/β-catenin signaling, sclerostin, and periostin [29, 30, 32, 34, 101]. In contrast, it is still not fully understood how mechanical loading affects the osteonal bone in humans and large mammals. Though there are some studies showing a bone loss in humans due to reduced mechanical loading, as experienced by bedridden patients and astronauts[123, 124], no studies have elucidated the detailed changes in bone microarchitecture in response to enhanced or decreased loading, including the changes in osteon structures. Several important questions should be addressed, such as whether the mechanical loading would induce anabolic effect on osteonal bone, and if yes, where the new bone would be formed, whether the existing bone will exhibit an increased remodeling, etc.

In the present study, we established a novel mechanical loading model on dog tibia using two mini-screw implants connected by a NiTi spring. This device was able to constantly deliver compression force with a direction parallel to the long axis of tibia, thereby well mimicking an enhanced physiological loading.

The effects of 5-week loading were examined on histological, electronic microscopic, and molecular levels, meanwhile using the contralateral tibia bone without

implants as control. First, we discovered a preferential role of periosteum in loading-induced new bone formation compared to endosteum, which recapitulated early development in several aspects: (1) the periosteum produced more abundant preosteons, which would further develop into immature osteons; (2) both preosteons and the immature osteons were undergoing active mineral apposition; (3) periosteum and periosteum-derived preosteons expressed high levels of early bone markers, as well as and β-catenin and periostin. Second, we found that the remodeling of the existing bone area in loaded bone was enhanced compared to the counterpart of control bone. Third, we identified an increased osteoclast activity in the transition zone between preosteons and the inner boundary of outer circumferential lamellae (OCL), which contributed to the remodeling of the original OCL and the integration of new bone to the existing bone.

The reconstruction of bone microstructure was worthy of further investigation. We captured the gradual diminishment of the OCL inner boundary and the presence of immature osteons in the original OCL area, indicating that this lamellar bone was remodeled into osteonal bone. We predicted that at some point, the periosteum creased to give rise to preosteons, and started to produce new OCL instead. It is also possible that the periosteum continued to form preosteons, but these preosteons developed into parallel lamellar bone, rather than osteons with concentric lamellae. Therefore, in future experiments we suggest extending the loading period, or interrupt loading for a period of time, and then re-evaluate the microstructure changes. Studies are also needed to determine the differing regulation mechanisms for osteon formation and circumferential lamellae.

In summary, we established a mechanical loading model on large mammals, and investigated detailed bone microstructure changes in response to mechanical loading, including a robust new osteon formation on periosteal surface. This study filled a knowledge gap on the anabolic effects of mechanical loading on osteonal bone, and will provide a foundation for future basic and clinical research regarding human bone responses under diverse physiological loading or medical device-delivered forces.

CHAPTER IV

CONCLUSION

The osteon (Haversian system) is the basic structural and functional unit of cortical bones in human and many other large mammals such as dogs and cows[6]. Different from mouse cortical bones consisting of uniform lamellar bones[8], osteons consist of multiple concentric lamellae surrounding a central vascular canal named Haversian canal. Osteon structures are meaningful for the function of skeletal system in providing both blood supply and mechanical support, and displayed striking changes under pathological conditions, such as osteoporosis. Despite its importance, there is very limited research on osteons using large mammals, in contrast to the relatively exhaustive bone research using rodents. Therefore, there are knowledge gaps in our understanding of osteons, including the modeling and remodeling of osteons during early development and in response to mechanical loading.

Similar to the rodent bone development, there was a preferential role of periosteum in appositional expansion of osteonal bone. Specifically, periosteum produced a unique semicircular canal, called preosteon, which developed into immature osteons. By constantly and rapidly generating abundant preosteons, the periosteum made a major contribution to bone growth in early development. Endosteum, on the other hand, served as a location where bone resorption took place and thereby the bone marrow cavity could enlarge.

Enhanced mechanical loading on adult dog tibias also resulted in a preferential role of periosteum in new bone formation, with many details recapitulating the periosteal

osteon formation process during early development. Specifically, periosteum also produced new bone by forming preosteon structures. These preosteons and preosteon-derived immature osteons were undergoing active mineral apposition and shared similar regulation mechanisms with the developmental process. The endosteum produced less new bone than the periosteum. The remodeling activity of existing bone area of loaded bone was also increased.

In summary, our study was the first that provided valuable information on the osteon modeling and remodeling during early development and under mechanical loading. However, there are still many questions regarding osteon biology that remain to be answered, including:

First, the mechanism of osteon maturation, including the formation of concentric lamellae. In both young dogs and loaded adult dogs, we noticed that there were abundant osteocytes in the bone matrixes surrounding the preosteons and the central canals of immature osteons, and the osteocytes were randomly arranged, rather than being arranged in an organized circular pattern as seen in the concentric lamellae of mature osteons. In mature osteons from the 4-month-old dogs and existing bone area of loaded bone, not only the osteocytes in osteons became well-organized, the osteocyte density in the interstitial bone matrixes also decreased. Therefore, we propose that there may be a link between the randomly arranged osteocytes in the interstitial bone matrixes surrounding preosteons and immature osteons, and the well-organized osteocytes in mature osteons. Specifically, do some of the immature osteocytes remodel and rearrange themselves to become osteocytes in mature concentric lamellae?

The underlying mechanisms for this unique remodeling may include osteocytic osteolysis, which refers to a kind of perilacunar/canalicular remodeling of osteocytes[106, 107]. In osteolysis, osteocytes are able to remove perilacunar/canalicular matrix, and express osteoclast-related genes, such as TRAP, Ctsk, and MMP13. It's also been shown that osteocytes are able be directly deposit mineral as well[106].

Second, the coupling of angiogenesis and osteogenesis during osteon formation. Angiogenesis refers to the growth of new capillaries from preexisting blood vessels either via "sprouting" or "intussusception"[161, 162]. Studies with rodents have shown that bone vasculature growth and osteogenesis may be coupled during both endochondral ossification and intramembranous ossification[163-165], where endothelial cells (ECs) and bone cells interact reciprocally by paracrine signaling; for instance, bone cells produce angiogenic factor to mediate the migration and proliferation of endothelial cells, among which the vascular endothelial growth factor (VEGF) is best understood.

However, to the best of our knowledge, there has not been a study on the coupling of angiogenesis and osteogenesis in osteonal bone, in either human or other large mammals. In this investigation, we have shown that periosteum played a major role in forming new osteons in both early development and during enhanced mechanical loading. Periosteum contained abundant vasculature, and the periosteum-derived preosteons are semicircular canals with vessels in the center and osteoblasts at the boundary. Therefore, we hypothesize that the coupling of angiogenesis and osteogenesis may exist in osteonal bones. Since the osteon itself is an exquisite combination of bone

cells and vasculature, and the osteon is essential for sufficient blood supply and mechanical support, coupling of angiogenesis and osteogenesis in osteon formation and remodeling is worthy of deep investigation.

Third, osteon changes in diseases such as osteoporosis, and the underlying mechanisms. Studies have shown that the changes in osteon remodeling may be associated with increased cortical porosity in aging or postmenopausal osteoporosis[63, 64], in particular, “giant” Haversian canals (large pores) were commonly observed in transverse sections of cortical bones in patients with osteoporotic fractures. However, a meticulous examination of osteon changes in osteoporosis lack information at histological and molecular levels, including the size of osteons, the size of Haversian canals, osteocyte density, etc. The mechanistic investigation should also include the possibility of osteocytic osteolysis.

Forth, the tissue engineering approaches to reconstruct osteons. Several studies have reconstructed osteon-like structures using different materials and tissue engineering approaches[166-171]. For example, in a study by Zuo et al.[169], an osteon-like concentric double-ring structure were developed by seeding human umbilical vein endothelial cells (HUVECs) onto collagen microspheres laden with human osteoblast-like cells (MG63) and collagenase. The inner ring encapsulating HUVECs was designed to imitate blood vessel in Haversian canal, while the outer ring encapsulating MG63s was used to imitate concentric lamellae. Although these osteon-like modules were able to facilitate the growth and differentiation of vasculogenic and osteogenic cells, further and deeper exploration is needed to better recapitulate the complex osteon

microstructure, and imitate the highly cellular microenvironment, and ultimately to achieve the goal of reconstructing functional tissue for therapeutic applications.

Although much more effort is needed, a thorough understanding of osteon modeling and remodeling will lay a solid foundation for understanding the human bone responses under various physiological and pathological conditions, as well as in response to force-delivering medical devices, such as during bone extraction and orthodontic tooth movement. In addition, the understanding of osteon biology will shed light on the reconstruction of human osteonal bone via tissue engineering approaches in order to serve clinical application.

REFERENCES

1. Burr, D.B. and O. Akkus, *Bone Morphology and Organization*, in *Basic and Applied Bone Biology*. 2014. p. 3-25.
2. Rho, J.-Y., L. Kuhn-Spearing, and P. Zioupos, *Mechanical properties and the hierarchical structure of bone.* Medical Engineering & Physics, 1998. **20**(2): p. 92-102.
3. Long, F., *Building strong bones: molecular regulation of the osteoblast lineage.* Nat Rev Mol Cell Biol, 2011. **13**(1): p. 27-38.
4. Dallas, S.L., M. Prideaux, and L.F. Bonewald, *The osteocyte: an endocrine cell ... and more.* Endocr Rev, 2013. **34**(5): p. 658-90.
5. Clarke, B., *Normal bone anatomy and physiology.* Clin J Am Soc Nephrol, 2008. **3 Suppl 3**: p. S131-9.
6. Cvetkovic, V., et al., *A comparison of the microarchitecture of lower limb long bones between some animal models and humans: a review.* Veterinarni Medicina, 2013. **58**(7).
7. Gasser, J.A. and M. Kneissel, *Bone Physiology and Biology*, in *Bone Toxicology*. 2017. p. 27-94.
8. Ferguson, V.L., et al., *Bone development and age-related bone loss in male C57BL/6J mice.* Bone, 2003. **33**(3): p. 387-398.
9. Pazzaglia, U.E., et al., *Anatomy of the intracortical canal system: scanning electron microscopy study in rabbit femur.* Clin Orthop Relat Res, 2009. **467**(9): p. 2446-56.

10. Maggiano, I.S., et al., *Three-dimensional reconstruction of Haversian systems in human cortical bone using synchrotron radiation-based micro-CT: morphology and quantification of branching and transverse connections across age.* J Anat, 2016. **228**(5): p. 719-32.

11. Pratt, I.V. and D.M.L. Cooper, *A method for measuring the three-dimensional orientation of cortical canals with implications for comparative analysis of bone microstructure in vertebrates.* Micron, 2017. **92**: p. 32-38.

12. Hennig, C., et al., *Does 3D orientation account for variation in osteon morphology assessed by 2D histology?* J Anat, 2015. **227**(4): p. 497-505.

13. Kim, J.N., et al., *Haversian system of compact bone and comparison between endosteal and periosteal sides using three-dimensional reconstruction in rat.* Anat Cell Biol, 2015. **48**(4): p. 258-61.

14. Cooper, D.M., et al., *Visualization of 3D osteon morphology by synchrotron radiation micro-CT.* J Anat, 2011. **219**(4): p. 481-9.

15. Hert, J., P. Fiala, and M. Petrtyl, *Osteon orientation of the diaphysis of the long bones in man.* Bone, 1994. **15**(3): p. 269-77.

16. Fan, W., R. Crawford, and Y. Xiao, *Structural and cellular differences between metaphyseal and diaphyseal periosteum in different aged rats.* Bone, 2008. **42**(1): p. 81-9.

17. Chang, H. and M.L.K. Tate, *Concise review: the periosteum: tapping into a reservoir of clinically useful progenitor cells.* Stem cells translational medicine, 2012. **1**(6): p. 480-491.

18. Taylor, J., *The periosteum and bone growth.* Bone, 1992. **6**: p. 21-52.

19. Ellender, G., S.A. Feik, and B. Carach, *Periosteal structure and development in a rat caudal vertebra.* Journal of anatomy, 1988. **158**: p. 173.

20. Hohmann, E.L., et al., *Innervation of periosteum and bone by sympathetic vasoactive intestinal peptide-containing nerve fibers.* Science, 1986. **232**(4752): p. 868-871.

21. Squier, C., S. Ghoneim, and C. Kremenak, *Ultrastructure of the periosteum from membrane bone.* Journal of anatomy, 1990. **171**: p. 233.

22. Allen, M.R., J.M. Hock, and D.B. Burr, *Periosteum: biology, regulation, and response to osteoporosis therapies.* Bone, 2004. **35**(5): p. 1003-1012.

23. Ramasamy, S.K., *Structure and Functions of Blood Vessels and Vascular Niches in Bone.* Stem Cells Int, 2017. **2017**: p. 5046953.

24. Dwek, J.R., *The periosteum: what is it, where is it, and what mimics it in its absence?* Skeletal Radiol, 2010. **39**(4): p. 319-23.

25. Kusumbe, A.P., S.K. Ramasamy, and R.H. Adams, *Coupling of angiogenesis and osteogenesis by a specific vessel subtype in bone.* Nature, 2014. **507**(7492): p. 323-328.

26. Ishikawa, F., et al., *Chemotherapy-resistant human AML stem cells home to and engraft within the bone-marrow endosteal region.* Nat Biotechnol, 2007. **25**(11): p. 1315-21.

27. Haylock, D.N., et al., *Hemopoietic stem cells with higher hemopoietic potential reside at the bone marrow endosteum.* Stem Cells, 2007. **25**(4): p. 1062-9.

28. Jones, D.B., et al., *Biochemical signal transduction of mechanical strain in osteoblast-like cells.* Biomaterials, 1991. **12**(2): p. 101-10.

29. Robling, A.G., et al., *Mechanical stimulation of bone in vivo reduces osteocyte expression of Sost/sclerostin.* J Biol Chem, 2008. **283**(9): p. 5866-75.

30. Tu, X., et al., *Sost downregulation and local Wnt signaling are required for the osteogenic response to mechanical loading.* Bone, 2012. **50**(1): p. 209-17.

31. Bonnet, N., et al., *Cathepsin K Controls Cortical Bone Formation by Degrading Periostin.* J Bone Miner Res, 2017. **32**(7): p. 1432-1441.

32. Bonnet, N., et al., *The matricellular protein periostin is required for sost inhibition and the anabolic response to mechanical loading and physical activity.* J Biol Chem, 2009. **284**(51): p. 35939-50.

33. Gerbaix, M., et al., *Periostin expression contributes to cortical bone loss during unloading.* Bone, 2015. **71**: p. 94-100.

34. Bonnet, N., S.J. Conway, and S.L. Ferrari, *Regulation of beta catenin signaling and parathyroid hormone anabolic effects in bone by the matricellular protein periostin.* Proc Natl Acad Sci U S A, 2012. **109**(37): p. 15048-53.

35. Sharir, A., et al., *Muscle force regulates bone shaping for optimal load-bearing capacity during embryogenesis.* Development, 2011. **138**(15): p. 3247-59.

36. Roberts, S.J., et al., *Uncovering the periosteum for skeletal regeneration: the stem cell that lies beneath.* Bone, 2015. **70**: p. 10-8.

37. He, X., et al., *Sox9 positive periosteal cells in fracture repair of the adult mammalian long bone.* Bone, 2017. **103**: p. 12-19.

38. Ozaki, A., et al., *Role of fracture hematoma and periosteum during fracture healing in rats: interaction of fracture hematoma and the periosteum in the initial step of the healing process.* Journal of orthopaedic science, 2000. **5**(1): p. 64-70.

39. Britz, H.M., et al., *The relation of femoral osteon geometry to age, sex, height and weight.* Bone, 2009. **45**(1): p. 77-83.

40. Burton, P., C. Nyssen-Behets, and A. Dhem, *Haversian bone remodelling in human fetus.* Acta Anat (Basel), 1989. **135**(2): p. 171-5.

41. Goret-Nicaise, M. and A. Dhem, *The mandibular body of the human fetus. Histologic analysis of the basilar part.* Anat Embryol (Berl), 1984. **169**(3): p. 231-6.

42. Allen, M.R. and D.B. Burr, *Bone Modeling and Remodeling,* in *Basic and Applied Bone Biology*. 2014. p. 75-90.

43. Crockett, J.C., et al., *Bone remodelling at a glance.* J Cell Sci, 2011. **124**(7): p. 991-998.

44. Schneider, P., et al., *The importance of the intracortical canal network for murine bone mechanics.* Bone, 2013. **53**(1): p. 120-8.

45. Parfitt, A.M., *Misconceptions (2): turnover is always higher in cancellous than in cortical bone.* Bone (NY), 2002. **30**: p. 807-809.

46. Parfitt, A., et al., *Effects of ethnicity and age or menopause on osteoblast function, bone mineralization, and osteoid accumulation in iliac bone.* Journal of Bone and Mineral Research, 1997. **12**(11): p. 1864-1873.

47. Sims, N.A. and T.J. Martin, *Coupling the activities of bone formation and resorption: a multitude of signals within the basic multicellular unit.* Bonekey Rep, 2014. **3**: p. 481.

48. Parfitt, A.M., *Osteonal and hemi-osteonal remodeling: the spatial and temporal framework for signal traffic in adult human bone.* Journal of cellular biochemistry, 1994. **55**(3): p. 273-286.

49. Lassen, N.E., et al., *Coupling of bone resorption and formation in real time: new knowledge gained from human Haversian BMUs.* Journal of Bone and Mineral Research, 2017. **32**(7): p. 1395-1405.

50. Fuchs, R.K., et al., *In situ examination of the time-course for secondary mineralization of Haversian bone using synchrotron Fourier transform infrared microspectroscopy.* Matrix Biology, 2008. **27**(1): p. 34-41.

51. Martin, R., *Is all cortical bone remodeling initiated by microdamage?* Bone, 2002. **30**(1): p. 8-13.

52. Parfitt, A., *Targeted and nontargeted bone remodeling: relationship to basic multicellular unit origination and progression.* Bone, 2002. **1**(30): p. 5-7.

53. Martin, R.B., *Targeted bone remodeling involves BMU steering as well as activation.* Bone, 2007. **40**(6): p. 1574-80.

54. Grüneboom, A., et al., *A network of trans-cortical capillaries as mainstay for blood circulation in long bones.* Nature Metabolism, 2019. **1**(2): p. 236-250.

55. Gross, P., M. Marcus, and D. Heistad, *Measurement of blood flow to bone and marrow in experimental animals by means of the microsphere technique.* JBJS, 1981. **63**(6): p. 1028-1031.

56. Gross, P.M., D.D. Heistad, and M.L. Marcus, *Neurohumoral regulation of blood flow to bones and marrow.* American Journal of Physiology-Heart and Circulatory Physiology, 1979 **237**(4): p. H440-H448.

57. Kane, W.J. and E. Grim, *Blood flow to canine hind-limb bone, muscle, and skin: a quantitative method and its validation.* JBJS, 1969. **51**(2): p. 309-322.

58. Wang, X., et al., *Age-related changes in the collagen network and toughness of bone.* Bone, 2002. **31**(1): p. 1-7.

59. Zebaze, R.M., et al., *Intracortical remodelling and porosity in the distal radius and post-mortem femurs of women: a cross-sectional study*. Lancet, 2010. **375**(9727): p. 1729-36.

60. Burghardt, A.J., et al., *Age- and gender-related differences in the geometric properties and biomechanical significance of intracortical porosity in the distal radius and tibia.* J Bone Miner Res, 2010. **25**(5): p. 983-93.

61. Kanis, J.A., et al., *Ten year probabilities of osteoporotic fractures according to BMD and diagnostic thresholds.* Osteoporos Int, 2001. **12**(12): p. 989-95.

62. Zebaze, R. and E. Seeman, *Cortical bone: a challenging geography.* Journal of Bone and Mineral Research, 2015. **30**(1): p. 24-29.

63. Brockstedt, H., et al., *Age- and sex-related changes in iliac cortical bone mass and remodeling.* Bone, 1993. **14**(4): p. 681-91.

64. Yeni, Y.N., et al., *The influence of bone morphology on fracture toughness of the human femur and tibia.* Bone, 1997. **21**(5): p. 453-9.

65. Bell, K.L., et al., *A novel mechanism for induction of increased cortical porosity in cases of intracapsular hip fracture.* Bone, 2000. **27**(2): p. 297-304.

66. Bell, K.L., et al., *Super-osteons (remodeling clusters) in the cortex of the femoral shaft: influence of age and gender.* Anat Rec, 2001. **264**(4): p. 378-86.

67. Jordan, G.R., et al., *Spatial clustering of remodeling osteons in the femoral neck cortex: a cause of weakness in hip fracture?* Bone, 2000. **26**(3): p. 305-13.

68. Compston, J.E., M.R. McClung, and W.D. Leslie, *Osteoporosis.* The Lancet, 2019. **393**(10169): p. 364-376.

69. Kanis, J.A., et al., *European guidance for the diagnosis and management of osteoporosis in postmenopausal women.* Osteoporos Int, 2013. **24**(1): p. 23-57.

70. Papaioannou, A., et al., *2010 clinical practice guidelines for the diagnosis and management of osteoporosis in Canada: summary.* CMAJ, 2010. **182**(17): p. 1864-73.

71. Marshall, D., O. Johnell, and H. Wedel, *Meta-analysis of how well measures of bone mineral density predict occurrence of osteoporotic fractures.* British Medical Journal, 1996. **312**(7041): p. 1254-1259.

72. Johnell, O., et al., *Predictive value of BMD for hip and other fractures.* J Bone Miner Res, 2005. **20**(7): p. 1185-94.

73. Stone, K.L., et al., *BMD at multiple sites and risk of fracture of multiple types: Long-term results from the study of osteoporotic fractures.* Journal of Bone and Mineral Research, 2003. **18**(11): p. 1947-1954.

74. Cranney, A., et al., *Low bone mineral density and fracture burden in postmenopausal women.* CMAJ, 2007. **177**(6): p. 575-80.

75. Siris, E.S., et al., *Bone mineral density thresholds for pharmacological intervention to prevent fractures.* Arch Intern Med, 2004. **164**(10): p. 1108-12.

76. Schuit, S.C.E., et al., *Fracture incidence and association with bone mineral density in elderly men and women: the Rotterdam Study.* Bone, 2004. **34**(1): p. 195-202.

77. Kanis, J.A., et al., *The use of clinical risk factors enhances the performance of BMD in the prediction of hip and osteoporotic fractures in men and women.* Osteoporos Int, 2007. **18**(8): p. 1033-46.

78. Kanis, J.A., et al., *FRAX and the assessment of fracture probability in men and women from the UK.* Osteoporos Int, 2008. **19**(4): p. 385-97.

79. Busse, B., et al., *Increased calcium content and inhomogeneity of mineralization render bone toughness in osteoporosis: mineralization, morphology and biomechanics of human single trabeculae.* Bone, 2009. **45**(6): p. 1034-43.

80. Milovanovic, P., et al., *Osteocytic canalicular networks: morphological implications for altered mechanosensitivity.* ACS Nano, 2013. **7**(9): p. 7542-51.

81. Milovanovic, P., et al., *Nano-structural, compositional and micro-architectural signs of cortical bone fragility at the superolateral femoral neck in elderly hip*

fracture patients vs. healthy aged controls. Experimental Gerontology, 2014. **55**: p. 19-28.

82. Mullender, M.G., et al., *Osteocyte density changes in aging and osteoporosis.* Bone, 1996. **18**(2): p. 109-13.

83. Busse, B., et al., *Decrease in the osteocyte lacunar density accompanied by hypermineralized lacunar occlusion reveals failure and delay of remodeling in aged human bone.* Aging Cell, 2010. **9**(6): p. 1065-75.

84. Mori, S., et al., *Trabecular bone volume and microdamage accumulation in the femoral heads of women with and without femoral neck fractures.* Bone, 1997. **21**(6): p. 521-526.

85. Vashishth, D., et al., *Decline in osteocyte lacunar density in human cortical bone is associated with accumulation of microcracks with age.* Bone, 2000. **26**(4): p. 375-380.

86. Martig, S., et al., *Subchondral bone morphology in the metacarpus of racehorses in training changes with distance from the articular surface but not with age.* Journal of Anatomy, 2018. **232**(6): p. 919-930.

87. Ashique, A., et al., *Lacunar-canalicular network in femoral cortical bone is reduced in aged women and is predominantly due to a loss of canalicular porosity*. Bone reports, 2017. **7**: p. 9-16.

88. Bach-Gansmo, F.L., et al., *Osteocyte lacunar properties and cortical microstructure in human iliac crest as a function of age and sex.* Bone, 2016. **91**: p. 11-19.

89. Frost, H.M., *Micropetrosis.* JBJS, 1960. **42**(1): p. 144-150.

90. Milovanovic, P., et al., *The Formation of Calcified Nanospherites during Micropetrosis Represents a Unique Mineralization Mechanism in Aged Human Bone.* Small, 2017. **13**(3).

91. Carpentier, V.T., et al., *Increased proportion of hypermineralized osteocyte lacunae in osteoporotic and osteoarthritic human trabecular bone: implications for bone remodeling.* Bone, 2012. **50**(3): p. 688-94.

92. Tiede-Lewis, L.M. and S.L. Dallas, *Changes in the osteocyte lacunocanalicular network with aging.* Bone, 2019. **122**: p. 101-113.

93. Han, Y., et al., *Mechanotransduction and strain amplification in osteocyte cell processes.* Proc Natl Acad Sci U S A, 2004. **101**(47): p. 16689-94.

94. Thi, M.M., et al., *Mechanosensory responses of osteocytes to physiological forces occur along processes and not cell body and require alphaVbeta3 integrin.* Proc Natl Acad Sci U S A, 2013. **110**(52): p. 21012-7.

95. Burra, S., et al., *Dendritic processes of osteocytes are mechanotransducers that induce the opening of hemichannels.* Proc Natl Acad Sci U S A, 2010. **107**(31): p. 13648-53.

96. Holguin, N., M.D. Brodt, and M.J. Silva, *Activation of Wnt Signaling by Mechanical Loading Is Impaired in the Bone of Old Mice.* J Bone Miner Res, 2016. **31**(12): p. 2215-2226.

97. Kiel, D.P., et al., *Low-Magnitude Mechanical Stimulation to Improve Bone Density in Persons of Advanced Age: A Randomized, Placebo-Controlled Trial.* J Bone Miner Res, 2015. **30**(7): p. 1319-28.

98. Kerschnitzki, M., et al., *Architecture of the osteocyte network correlates with bone material quality.* J Bone Miner Res, 2013. **28**(8): p. 1837-45.

99. Ma, Y.L., et al., *Quantitative associations between osteocyte density and biomechanics, microcrack and microstructure in OVX rats vertebral trabeculae.* J Biomech, 2008. **41**(6): p. 1324-32.

100. Tu, X., et al., *Osteocytes mediate the anabolic actions of canonical Wnt/beta-catenin signaling in bone.* Proc Natl Acad Sci U S A, 2015. **112**(5): p. E478-86.

101. Lin, C., et al., *Sclerostin mediates bone response to mechanical unloading through antagonizing Wnt/beta-catenin signaling.* J Bone Miner Res, 2009. **24**(10): p. 1651-61.

102. Nakashima, T., et al., *Evidence for osteocyte regulation of bone homeostasis through RANKL expression.* Nat Med, 2011. **17**(10): p. 1231-4.

103. Kobayashi, K., et al., *Mitochondrial superoxide in osteocytes perturbs canalicular networks in the setting of age-related osteoporosis.* Sci Rep, 2015. **5**: p. 9148.

104. Sims, N.A., *Senescent Osteocytes: Do They Cause Damage and Can They Be Targeted to Preserve the Skeleton?* J Bone Miner Res, 2016. **31**(11): p. 1917-1919.

105. Almeida, M., et al., *Skeletal involution by age-associated oxidative stress and its acceleration by loss of sex steroids.* J Biol Chem, 2007. **282**(37): p. 27285-97.

106. Qing, H., et al., *Demonstration of osteocytic perilacunar/canalicular remodeling in mice during lactation.* J Bone Miner Res, 2012. **27**(5): p. 1018-29.

107. Wysolmerski, J.J., *Osteocytic osteolysis: time for a second look?* Bonekey Rep, 2012. **1**: p. 229.

108. Bélanger, L.F., *Osteocytic osteolysis.* Calcified tissue research, 1969. **4**(1): p. 1-12.

109. Baud, C. and G. Boivin, *Effects of hormones on osteocyte function and perilacunar wall structure.* Clinical orthopaedics and related research, 1978(136): p. 270-281.

110. Belanger, L. and P. Drouin, *Osteolysis in the frog: the effects of parathormone.* Canadian journal of physiology and pharmacology, 1966. **44**(6): p. 919-922.

111. Bélanger, L.F., L. Jarry, and H.K. Uhthoff, *Osteocytic osteolysis in Paget's disease.* Revue canadienne de biologie, 1968. **27**(1): p. 37-44.

112. Sharma, D., et al., *Alterations in the osteocyte lacunar-canalicular microenvironment due to estrogen deficiency.* Bone, 2012. **51**(3): p. 488-97.

113. van Hove, R.P., et al., *Osteocyte morphology in human tibiae of different bone pathologies with different bone mineral density--is there a role for mechanosensing?* Bone, 2009. **45**(2): p. 321-9.

114. Carter, Y., et al., *Femoral osteocyte lacunar density, volume and morphology in women across the lifespan.* J Struct Biol, 2013. **183**(3): p. 519-526.

115. Bonewald, L.F. and M.L. Johnson, *Osteocytes, mechanosensing and Wnt signaling.* Bone, 2008. **42**(4): p. 606-15.

116. Doty, S.B., *Morphological evidence of gap junctions between bone cells.* Calcified tissue international, 1981. **33**(1): p. 509-512.

117. Salter, D.M., J.E. Robb, and M.O. Wright, *Electrophysiological responses of human bone cells to mechanical stimulation: evidence for specific integrin function in mechanotransduction.* J Bone Miner Res, 1997. **12**(7): p. 1133-41.

118. Tatsumi, S., et al., *Targeted ablation of osteocytes induces osteoporosis with defective mechanotransduction.* Cell Metab, 2007. **5**(6): p. 464-75.

119. Xu, H., et al., *Connexin 43 channels are essential for normal bone structure and osteocyte viability.* J Bone Miner Res, 2015. **30**(3): p. 436-48.

120. Lloyd, S.A., et al., *Connexin 43 deficiency attenuates loss of trabecular bone and prevents suppression of cortical bone formation during unloading.* Journal of Bone and Mineral Research, 2012. **27**(11): p. 2359-2372.

121. Ozcivici, E., et al., *Mechanical signals as anabolic agents in bone.* Nat Rev Rheumatol, 2010. **6**(1): p. 50-9.

122. Britz, H.M., et al., *The effects of immobilization on vascular canal orientation in rat cortical bone.* J Anat, 2012. **220**(1): p. 67-76.

123. Rittweger, J., et al., *Muscle atrophy and bone loss after 90 days' bed rest and the effects of flywheel resistive exercise and pamidronate: results from the LTBR study.* Bone, 2005. **36**(6): p. 1019-29.

124. Rittweger, J., et al., *Prevention of bone loss during 56 days of strict bed rest by side-alternating resistive vibration exercise.* Bone, 2010. **46**(1): p. 137-47.

125. Jones, H.H., et al., *Humeral hypertrophy in response to exercise.* J Bone Joint Surg Am, 1977. **59**(2): p. 204-8.

126. Robinson, J.A., et al., *Wnt/beta-catenin signaling is a normal physiological response to mechanical loading in bone.* J Biol Chem, 2006. **281**(42): p. 31720-8.

127. Sawakami, K., et al., *The Wnt co-receptor LRP5 is essential for skeletal mechanotransduction but not for the anabolic bone response to parathyroid hormone treatment.* J Biol Chem, 2006. **281**(33): p. 23698-711.

128. Kramer, I., et al., *Osteocyte Wnt/beta-catenin signaling is required for normal bone homeostasis.* Mol Cell Biol, 2010. **30**(12): p. 3071-85.

129. Javaheri, B., et al., *β-catenin haploinsufficiency in osteocytes abolishes the osteogenic effect of mechanical loading in vivo.* J Bone Miner Res, 2011. **26**(Suppl 1).

130. Bonnet, N., P. Garnero, and S. Ferrari, *Periostin action in bone.* Mol Cell Endocrinol, 2016. **432**: p. 75-82.

131. Ascenzi, M.G. and A.K. Roe, *The osteon: the micromechanical unit of compact bone.* Front Biosci (Landmark Ed), 2012. **17**(2012 Jan 1;17:1551-81.): p. 1551-81.

132. Kitase, Y., et al., *Mechanical induction of PGE2 in osteocytes blocks glucocorticoid-induced apoptosis through both the beta-catenin and PKA pathways.* J Bone Miner Res, 2010. **25**(12): p. 2657-68.

133. Xia, X., et al., *Prostaglandin promotion of osteocyte gap junction function through transcriptional regulation of connexin 43 by glycogen synthase kinase 3/beta-catenin signaling.* Mol Cell Biol, 2010. **30**(1): p. 206-19.

134. Zhang, K., et al., *E11/gp38 selective expression in osteocytes: regulation by mechanical strain and role in dendrite elongation.* Mol Cell Biol, 2006. **26**(12): p. 4539-52.

135. Gluhak-Heinrich, J., et al., *Mechanical loading stimulates dentin matrix protein 1 (DMP1) expression in osteocytes in vivo.* J Bone Miner Res, 2003. **18**(5): p. 807-17.

136. Quarles, L.D., *FGF23, PHEX, and MEPE regulation of phosphate homeostasis and skeletal mineralization.* Am J Physiol Endocrinol Metab, 2003. **285**(1): p. E1-9.

137. Harris, S.E., et al., *DMP1 and MEPE expression are elevated in osteocytes after mechanical loading in vivo: theoretical role in controlling mineral quality in the perilacunar matrix.* J Musculoskelet Neuronal Interact, 2007. **7**(4): p. 313-5.

138. Kulkarni, R.N., et al., *Inhibition of osteoclastogenesis by mechanically loaded osteocytes: involvement of MEPE.* Calcif Tissue Int, 2010. **87**(5): p. 461-8.

139. Xiong, J., et al., *Matrix-embedded cells control osteoclast formation.* Nat Med, 2011. **17**(10): p. 1235-41.

140. Petrtyl, M., J. Hert, and P. Fiala, *Spatial organization of the haversian bone in man.* J Biomech, 1996. **29**(2): p. 161-9.

141. Pazzaglia, U.E., et al., *A model of the intracortical vascular system of long bones and of its organization: an experimental study in rabbit femur and tibia.* Journal of Anatomy, 2008. **213**(2): p. 183-193.

142. Young, D.R., et al., *Immobilization-associated osteoporosis in primates.* Bone, 1986. **7**(2): p. 109-17.

143. Maes, C. and H.M. Kronenberg, *Bone Development and Remodeling*, in *Endocrinology: Adult and Pediatric*. 2016: (ossification center). p. 1038-1062.e8.

144. Yang, L., et al., *Hypertrophic chondrocytes can become osteoblasts and osteocytes in endochondral bone formation.* Proc Natl Acad Sci U S A, 2014. **111**(33): p. 12097-102.

145. Yang, G., et al., *Osteogenic fate of hypertrophic chondrocytes.* Cell Res, 2014. **24**(10): p. 1266-9.

146. Zhou, X., et al., *Chondrocytes transdifferentiate into osteoblasts in endochondral bone during development, postnatal growth and fracture healing in mice.* PLoS Genet, 2014. **10**(12): p. e1004820.

147. Ono, N., et al., *A subset of chondrogenic cells provides early mesenchymal progenitors in growing bones.* Nat Cell Biol, 2014. **16**(12): p. 1157-67.

148. Jing, Y., et al., *Chondrocytes Directly Transform into Bone Cells in Mandibular Condyle Growth.* J Dent Res, 2015.

149. Ren, Y., et al., *Sclerostin antibody (Scl-Ab) improves osteomalacia phenotype in dentin matrix protein 1 (Dmp1) knockout mice with little impact on serum levels of phosphorus and FGF23.* Matrix Biology, 2016. **52**: p. 151-161.

150. Zhang, H., et al., *Essential role of osterix for tooth root but not crown dentin formation.* J Bone Miner Res, 2015. **30**(4): p. 742-6.

151. Feng Jian, Q., et al., *Dentin Matrix Protein 1, a Target Molecule for Cbfa1 in Bone, Is a Unique Bone Marker Gene.* Journal of Bone and Mineral Research, 2009. **17**(10): p. 1822-1831.

152. Gruber, H.E., *Adaptations of Goldner's Masson trichrome stain for the study of undecalcified plastic embedded bone.* Biotech Histochem, 1992. **67**(1): p. 30-4.

153. Dempster, D.W., et al., *Standardized nomenclature, symbols, and units for bone histomorphometry: a 2012 update of the report of the ASBMR Histomorphometry Nomenclature Committee.* J Bone Miner Res, 2013. **28**(1): p. 2-17.

154. Osborne, D.L. and J. Curtis, *A protocol for the staining of cement lines in adult human bone using toluidine blue.* Journal of Histotechnology, 2005. **28**(2): p. 73-79.

155. Hu, Z., et al., *Immunomodulatory ECM-like Microspheres for Accelerated Bone Regeneration in Diabetes Mellitus.* ACS Appl Mater Interfaces, 2018. **10**(3): p. 2377-2390.

156. Salic, A. and T.J. Mitchison, *A chemical method for fast and sensitive detection of DNA synthesis in vivo.* Proc Natl Acad Sci U S A, 2008. **105**(7): p. 2415-20.

157. Jing, Y., et al., *Vital Roles of beta-catenin in Trans-differentiation of Chondrocytes to Bone Cells.* Int J Biol Sci, 2018. **14**(1): p. 1-9.

158. Ciani, C., S.B. Doty, and S.P. Fritton, *An effective histological staining process to visualize bone interstitial fluid space using confocal microscopy.* Bone, 2009. **44**(5): p. 1015-7.

159. Bouxsein, M.L., et al., *Guidelines for assessment of bone microstructure in rodents using micro-computed tomography.* J Bone Miner Res, 2010. **25**(7): p. 1468-86.

160. Jing, Y., et al., *Chondrogenesis and osteogenesis are one continuous developmental and lineage defined biological process.* Sci Rep, 2017. **7**(1): p. 10020.

161. Risau, W., *Mechanisms of angiogenesis.* nature, 1997. **386**(6626): p. 671.

162. Carmeliet, P., *Mechanisms of angiogenesis and arteriogenesis.* Nature medicine, 2000. **6**(4): p. 389.

163. Maes, C., et al., *Osteoblast precursors, but not mature osteoblasts, move into developing and fractured bones along with invading blood vessels.* Dev Cell, 2010. **19**(2): p. 329-44.

164. Duan, X., et al., *VEGF stimulates intramembranous bone formation during craniofacial skeletal development.* Matrix Biol, 2016. **52-54**: p. 127-140.

165. Duan, X., et al., *Vegfa regulates perichondrial vascularity and osteoblast differentiation in bone development.* Development, 2015. **142**(11): p. 1984-91.

166. Andric, T., A.C. Sampson, and J.W. Freeman, *Fabrication and characterization of electrospun osteon mimicking scaffolds for bone tissue engineering.* Materials Science & Engineering C-Materials for Biological Applications, 2011. **31**(1): p. 2-8.

167. Chen, X., et al., *Shell-core bi-layered scaffolds for engineering of vascularized osteon-like structures.* Biomaterials, 2013. **34**(33): p. 8203-12.

168. Zhong, M., et al., *Vascularization in Engineered Tissue Construct by Assembly of Cellular Patterned Micromodules and Degradable Microspheres.* ACS Appl Mater Interfaces, 2017. **9**(4): p. 3524-3534.

169. Zuo, Y., et al., *Photo-cross-linkable methacrylated gelatin and hydroxyapatite hybrid hydrogel for modularly engineering biomimetic osteon.* ACS Appl Mater Interfaces, 2015. **7**(19): p. 10386-94.

170. Mehrali, M., et al., *Nanoreinforced Hydrogels for Tissue Engineering: Biomaterials that are Compatible with Load-Bearing and Electroactive Tissues.* Adv Mater, 2017. **29**(8).

171. Makihara, T., et al., *Formation of osteon-like structures in unidirectional porous hydroxyapatite substitute.* J Biomed Mater Res B Appl Biomater, 2018.

APPENDIX A

FIGURES

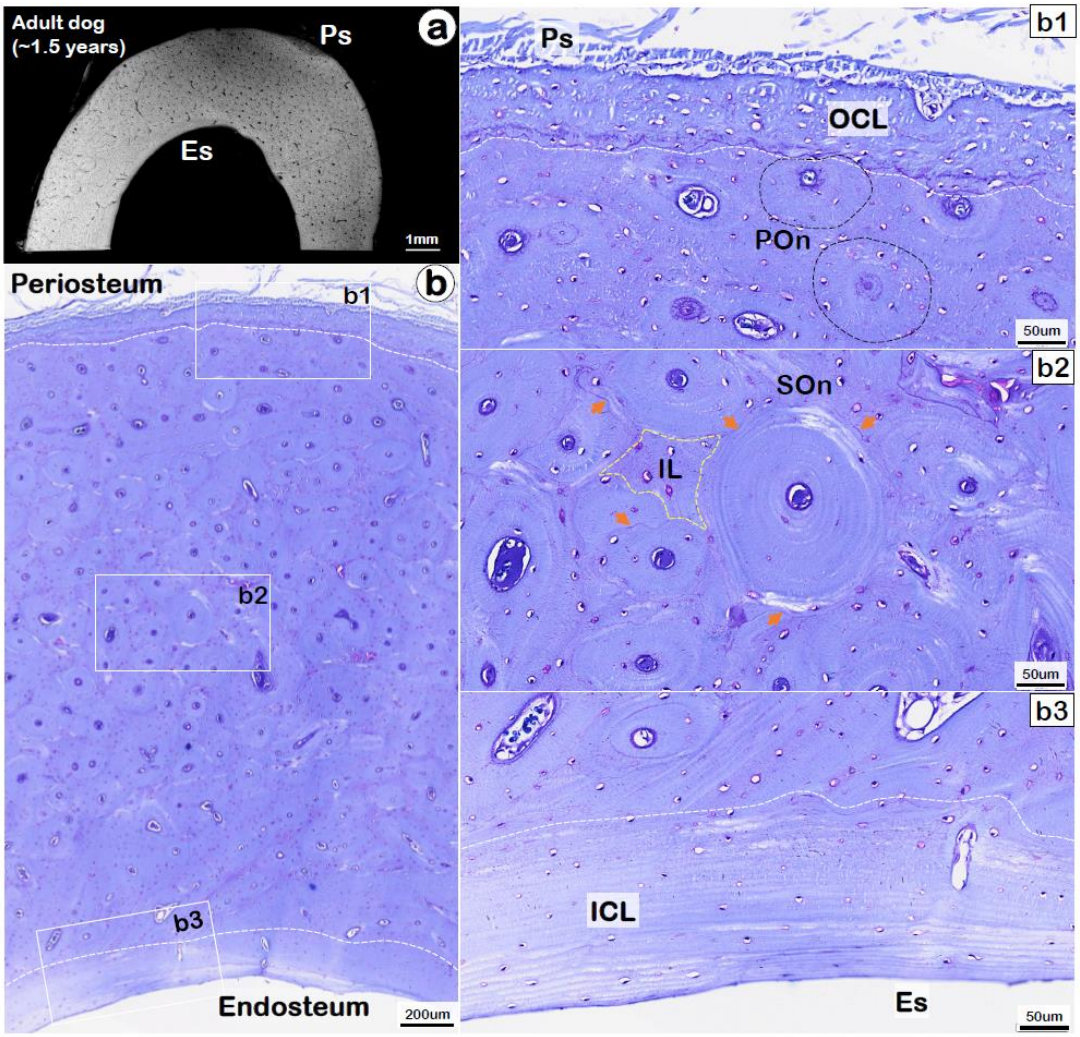

Figure 1 Plain X-ray Radiographs and Toluidine Blue Staining of the Cross Section of the Tibia Midshafts in Adult Dogs.

Shown are the representative Plain X-ray radiograph (a) and toluidine blue staining (b) of the cross section of the tibia midshafts in young adult dogs. B1-b3 are the corresponding magnified areas marked in white boxes. White dashed outlines indicate the boundary between OCL and osteons (b1), or the boundary between osteons and ICL (b3). Black dashed outlines indicate the boundaries of primary osteons (b1). The orange arrows indicate the cement lines of secondary osteons (b2). The yellow dashed outline indicates the boundary of interstitial lamellae (b2). Abbreviations: Ps, periosteum; Es, endosteum; OCL, outer circumferential lamellae; ICL, inner circumferential lamellae; POn, primary osteon; SOn, secondary osteon; IL, interstitial lamellae.

Figure 2 Plain X-ray Radiographs and Toluidine Blue Staining of the Cross Sections of the Tibia Midshafts in Puppies.

Shown are the representative Plain X-ray radiograph (a) and toluidine blue staining (b and c) of the cross section of the tibia midshafts in puppies at postnatal day 1 (P1), P14, P28, and 4 months (4M). C1-c3 are the corresponding magnified areas marked in white boxes. Yellow areas indicate preosteons (b, c, and c1); Orange arrows indicate cement lines of secondary osteons (c2); Black dashed outlines indicate the boundaries of primary osteons (c1); White dashed outlines indicate the boundary between osteons and ICL. Bar = 1mm in (a).

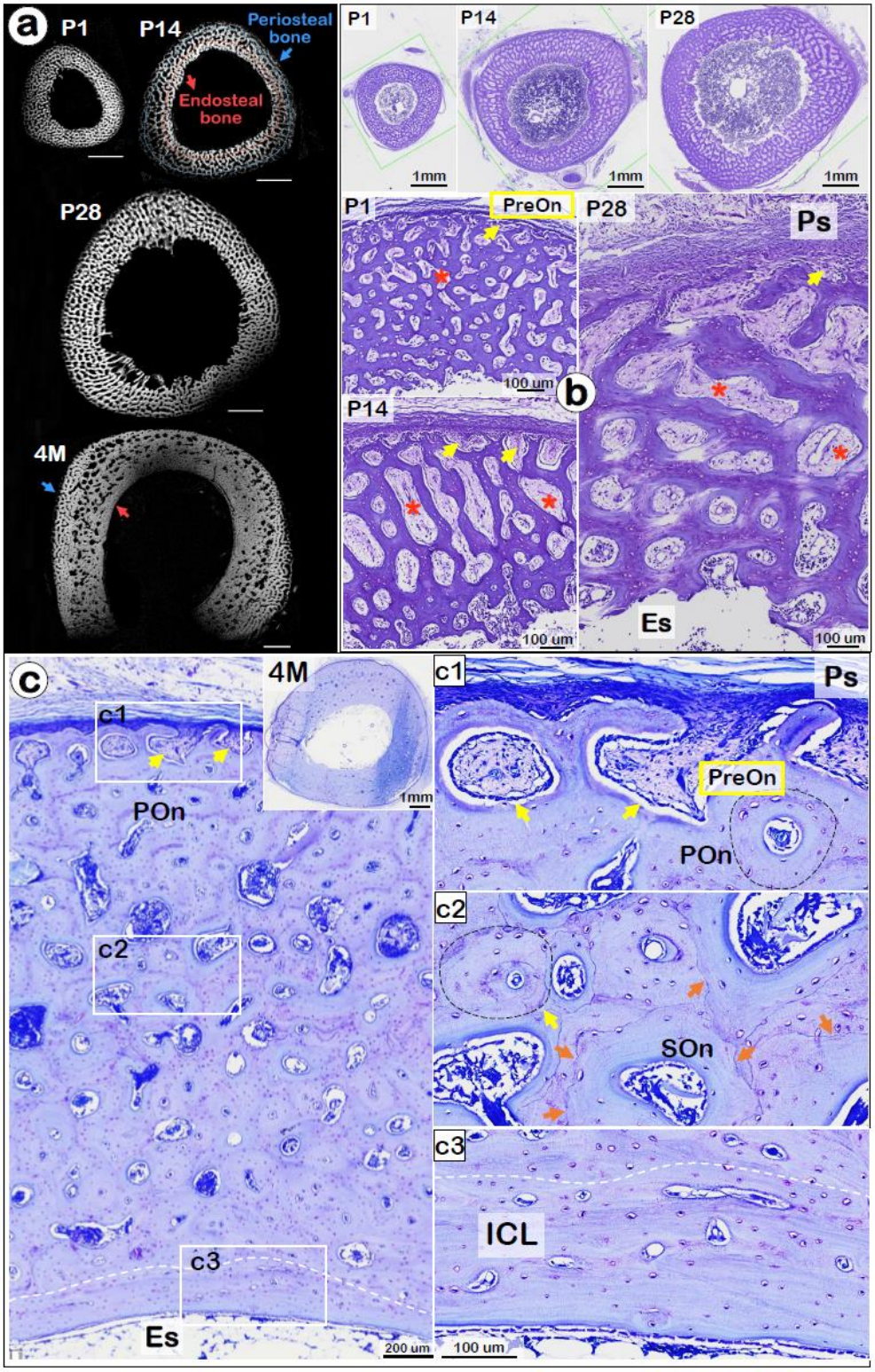

Figure 2 Continued.

Figure 3 μCT Analyses of Young Dog Tibia Midshafts.
(a) Representative images of μCT 3D dimensional reconstruction of young dog tibia midshafts. **(b)** Statistical analyses of the changes in bone microstructure variables with age, including total cross-sectional area (Tt.Ar), cortical bone area (Ct.Ar), cortical area fraction (Ct.Ar/Tt.Ar), bone marrow area (Ma.Ar), cortical porosity (Ct.Po), and Bone Mineral Density (BMD). N=4/group, one-way ANOVA with Bonferroni post-hoc test, *P<0.05, **P<0.01, ***P<0.001. (c) The μCT images of tibia cross sections were diveided into three equal part: periosteal 1/3, middle 1/3, and endosteal 1/3. The Ct.Po and BMD of periosteal 1/3 bone and endosteal 1/3 bone in each individual bone were analyzed and quantified. N=4/group, paired t-test. *P<0.05, **P<0.01, ***P<0.001.

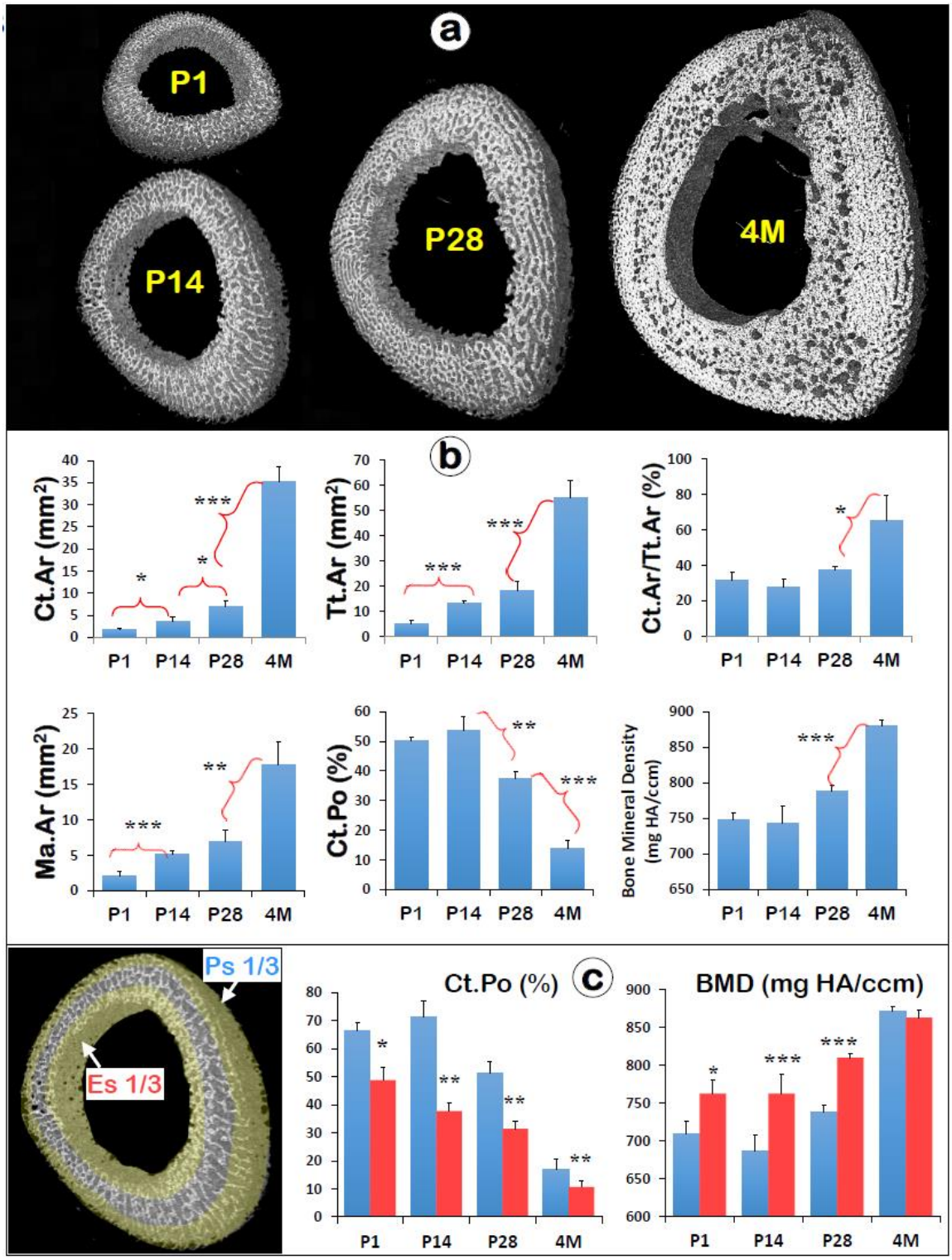

Figure 3 Continued.

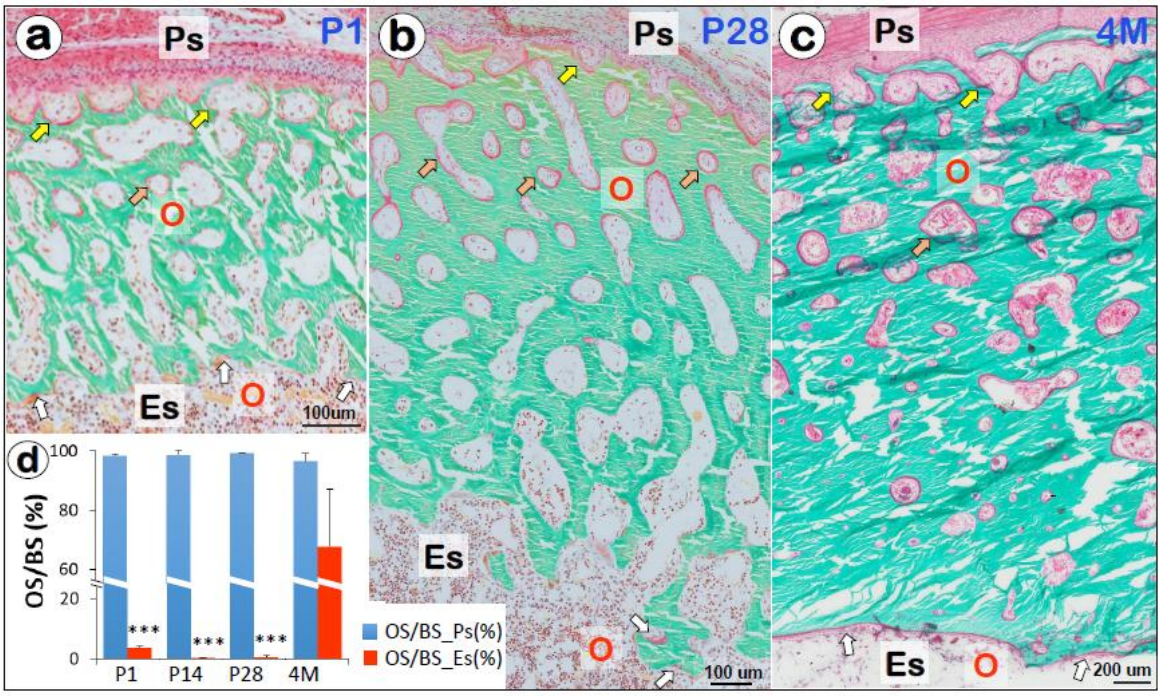

Figure 4 Masson-Goldner Trichrome Staining of Young Dog Tibia Midshafts.
(a-c) Representative Masson-Goldner trichrome staining images of young dog bones at P1 (a), P28 (b) and 4 months (c). Bone matrix stained in red color is osteoid (O), while bone matrix stained in green is fully mineralized. Yellow arrows indicate the osteoid surrounding preosteons; Orange arrows indicate osteoid surrounding immature osteons in periosteal bone; white arrows indicate osteoid on endosteal surface. **(d)** Bone histomorphometric analyses of osteoid surface/bone surface (OS/BS) on periosteal surface (Ps) and endosteal surface (Es). N=4/group, paired t-test, ***P<0.001.

Figure 5 SEM Assays and FITC Staining of Nondecalcified Young Dog Bones.
Shown are representative images of backscattered SEM (a-c), FITC staining (d-f) and acid-etched SEM (g-i) of nondecalcified bone at P1, P14, P28, and 4M. A1-i1 and a2-i2 are the corresponding magnified areas marked in yellow boxes. Abbreviation: SEM, scanning electron microscopy.

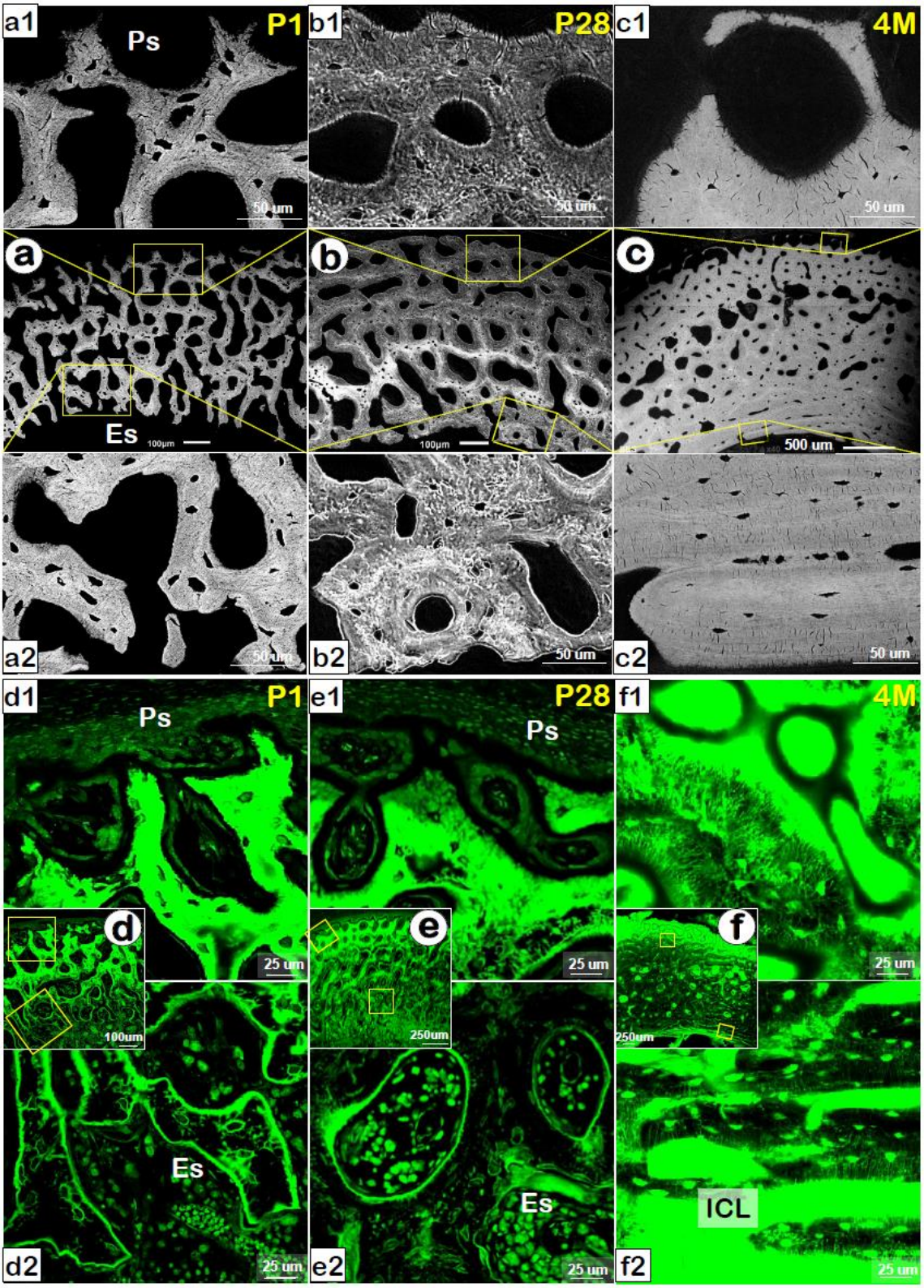

Figure 5 Continued.

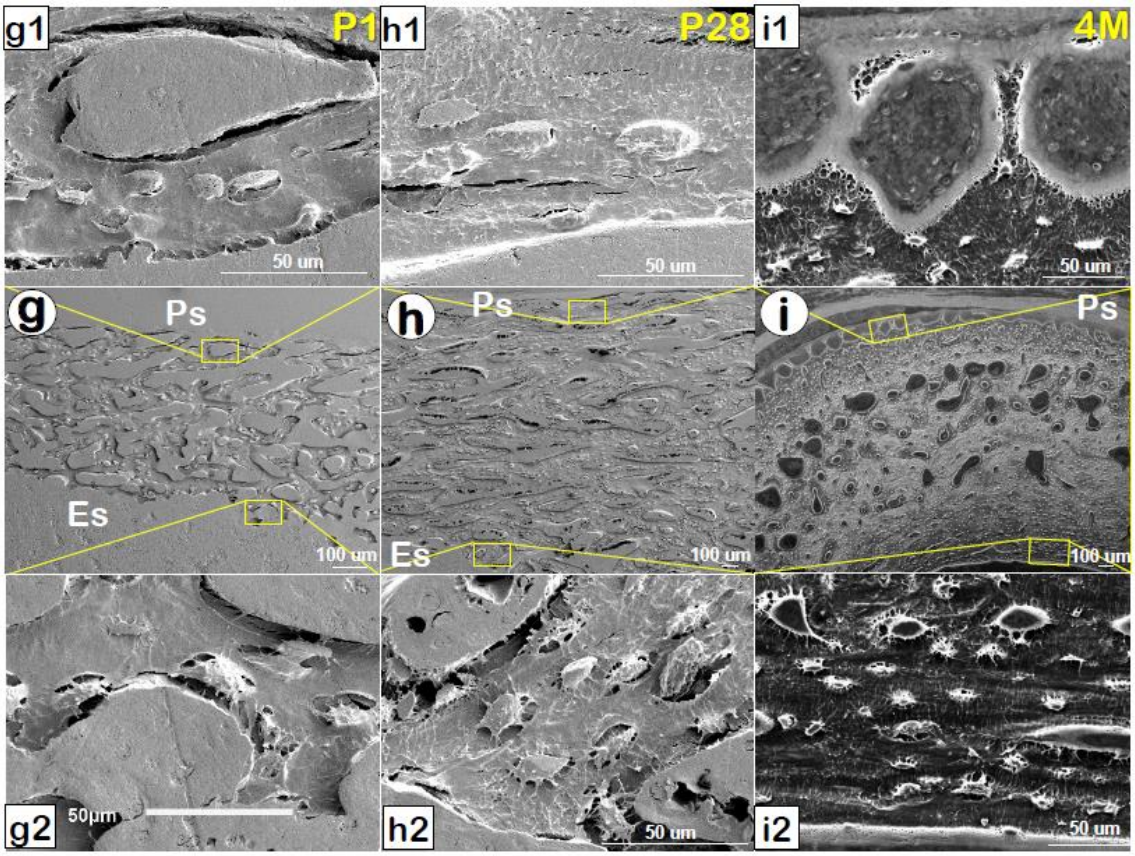

Figure 5 Continued.

Figure 6 Fluorochrome Labeling Assay of Young Dog Bone.
Shown are representative images of fluorochrome labeling on periosteal and endosteal bone at P1, P14, P28, and 4M. White double-headed arrows indicate the bone matrix laid down between the time of first injection and the time of second injection (b and c, b2 and c2). A1-d1, and a2-d2 are the corresponding magnified areas marked in white boxes in a-d. D3 and d4 are the corresponding magnified areas marked in white boxes in d1 and d2, respectively. Yellow arrows indicate the bone matrixes where the second and the third injections overlapped (b1, b2, d, and d1-d4).

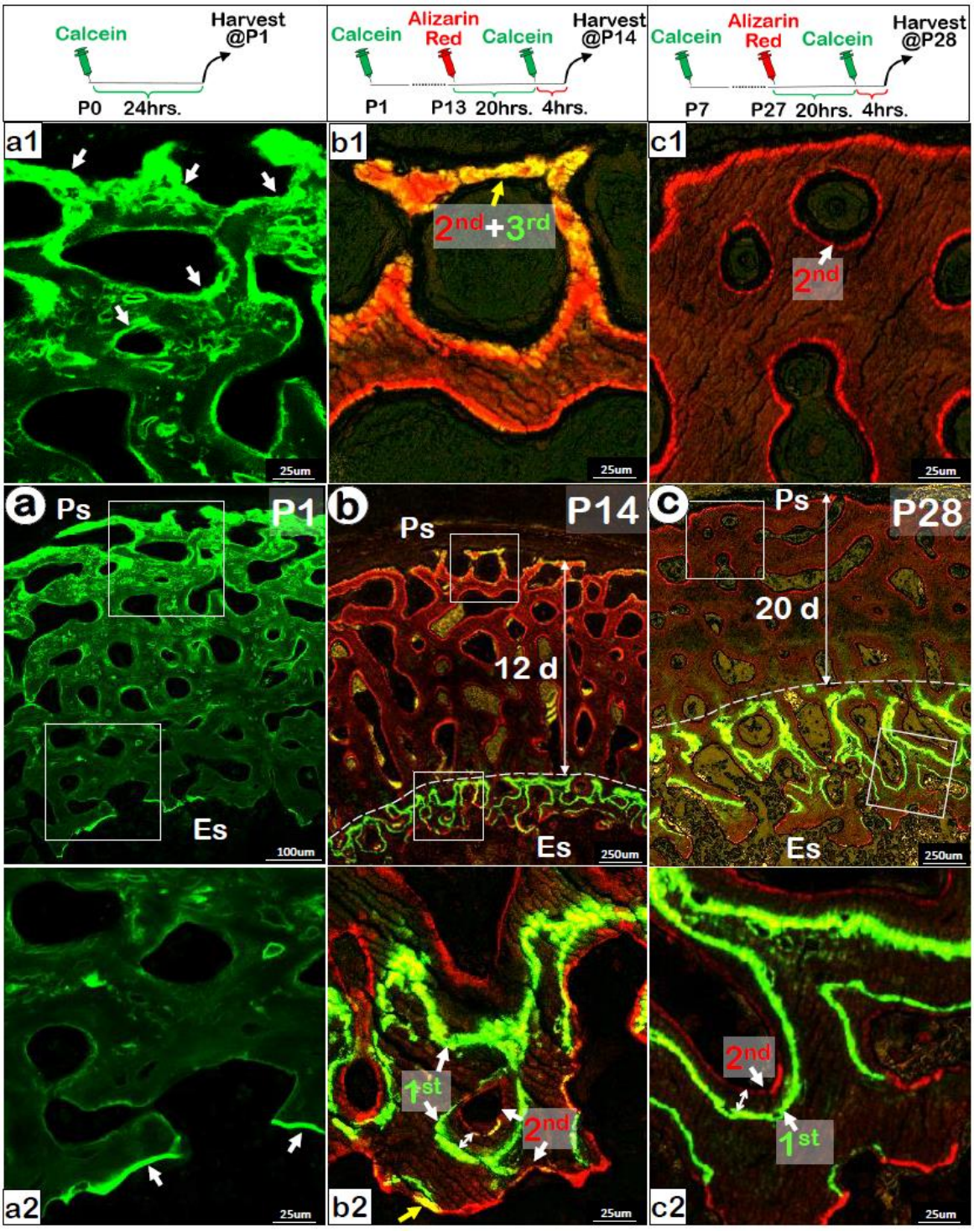

Figure 6 Continued.

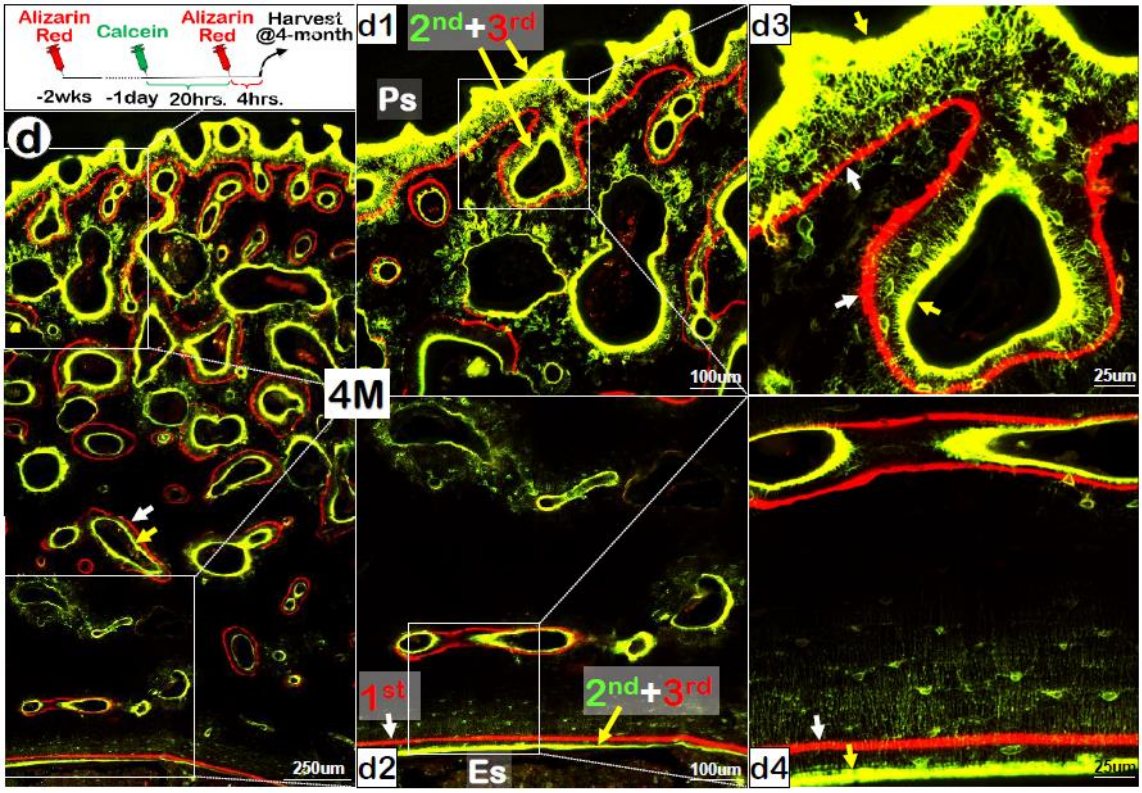

Figure 6 Continued.

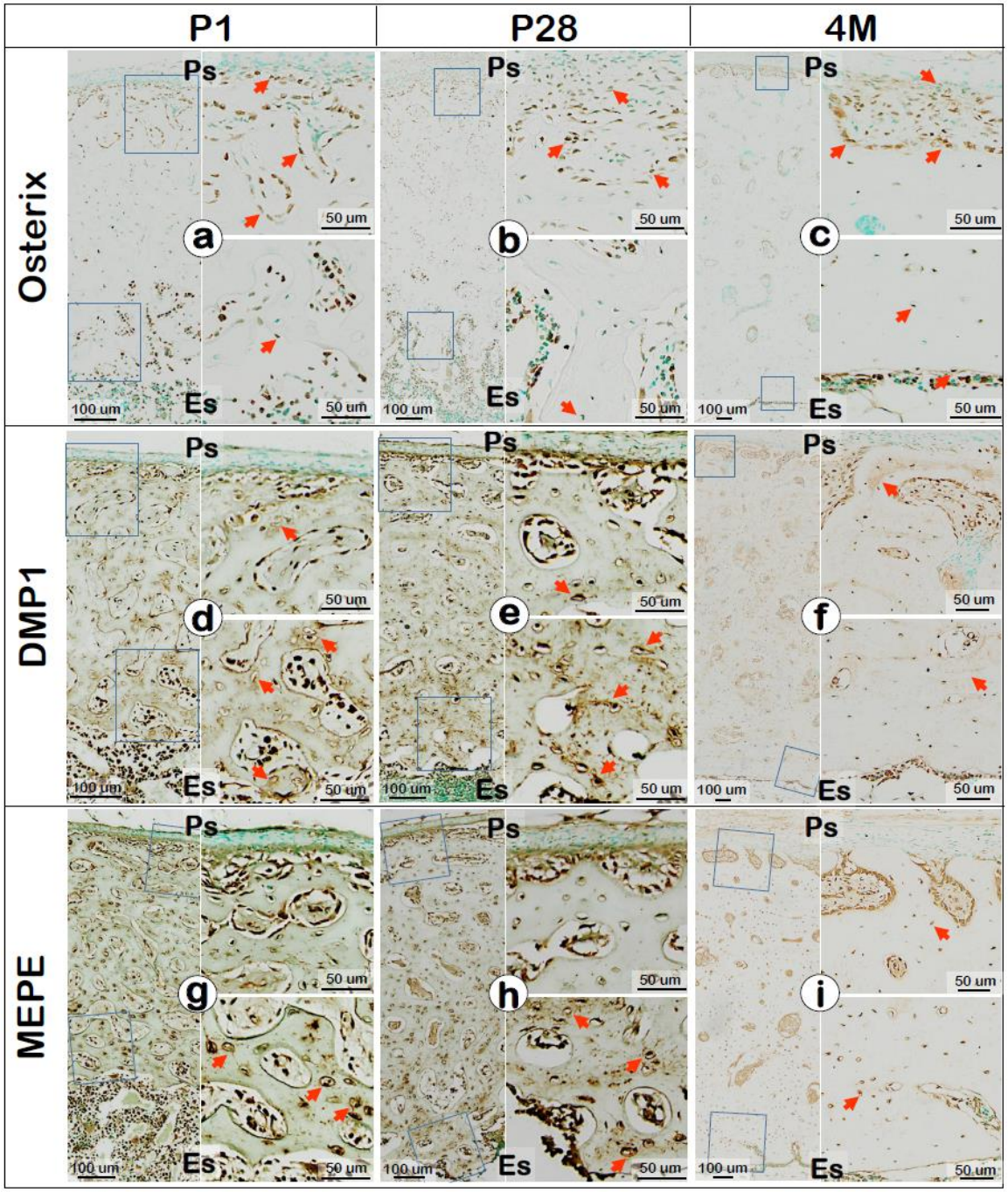

Figure 7 Immunohistochemistry of Young Dog Bones.
Shown are representative images of immunohistochemistry of young dog bones, including osterix (a-c), DMP1 (d-f), MEPE (g-i), slcerostin (j-l), β-catenin (m-o), periostin (p-r). Upper right and lower right panels of each figure are the corresponding magnified areas marked in blue boxes in the left panels.

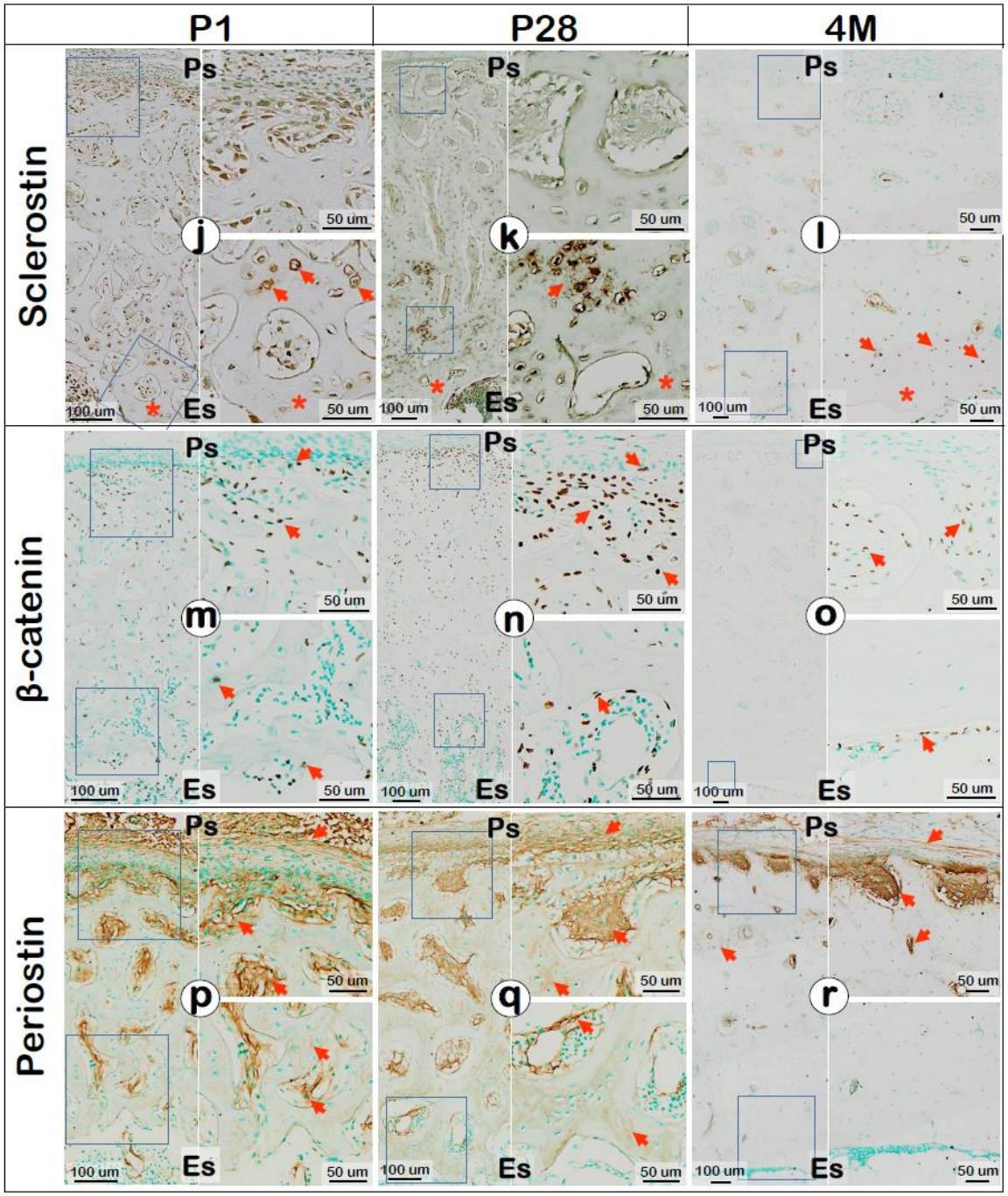

Figure 7 Continued.

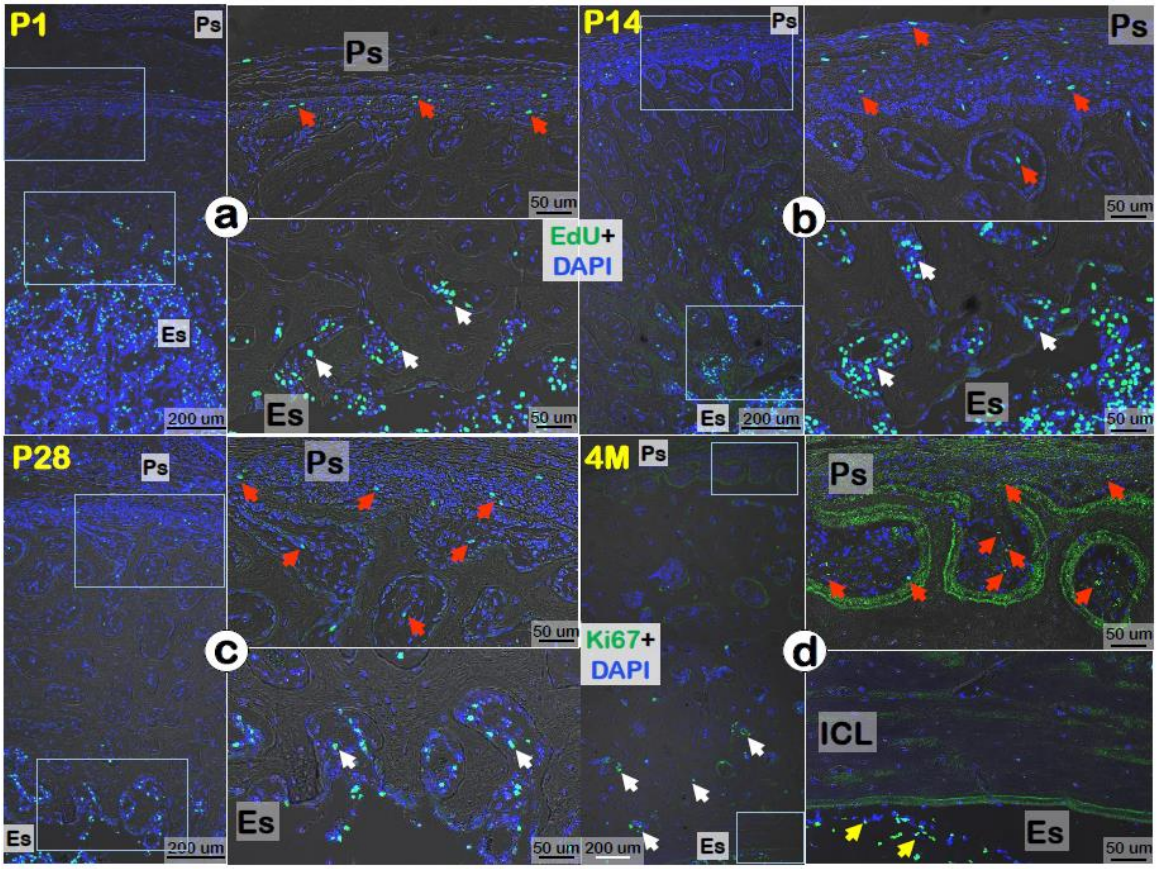

Figure 8 Cell Proliferation Assays of Young Dog Bones.
Shown are representative images of EdU staining for P1, P14, and P28 dog tibias (a-c) and the immunofluorescent staining of Ki67 for 4-month dog tibia (d). Upper right and lower right panels of each figure are the corresponding magnified areas marked in blue boxes in the left panels. Red arrows indicate EdU (+) or Ki67 (+) cells in periosteum and periosteal bone; White arrows indicate EdU (+) or Ki67 (+) cells in endocortical bone; Yellow arrows indicate Ki67 (+) cells in bone marrow close to endosteum at 4 months (d).

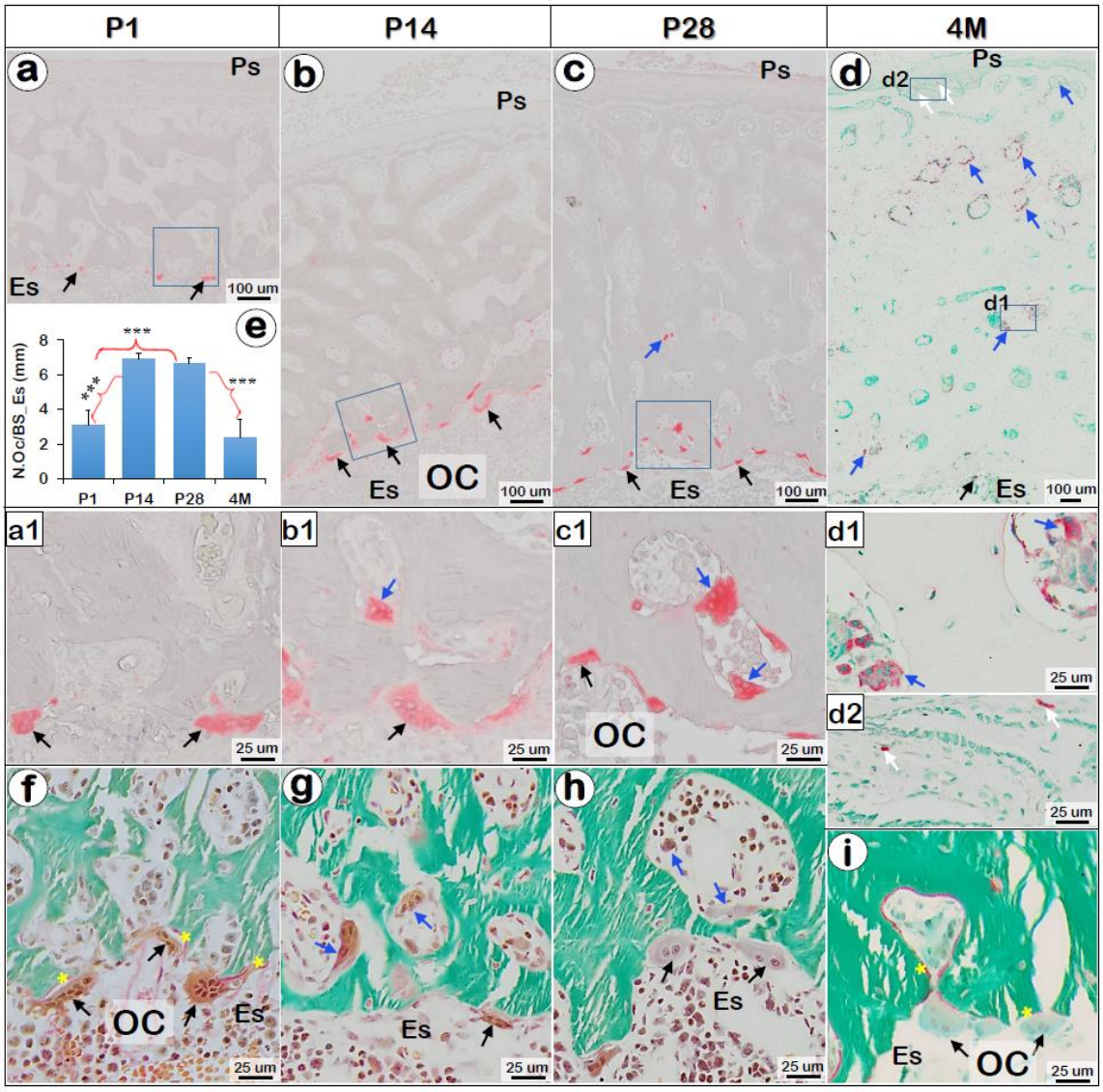

Figure 9 Osteoclast Activities on the Endosteal Surface.

(a-d) TRAP staining of young dog bones at P1, P14, P28, and 4 month. A1-d1, and d2 are the corresponding magnified areas marked in blue boxes. **(e)** Quantitation of osteoclast number per unit of bone surface (N.Oc/BS) at endosteal surface. **(f-i)** Masson-Goldner trichrome staining of young dog bones at P1, P14, P28, and 4 month. Black arrows indicate osteoclasts (OC) on endosteal surfaces; Blue arrows indicate OC in the Haversian canals in endocortical bone; White arrows indicate OC in the periosteum at 4 months (d); Yellow asterisks indicate osteoid on endosteal surfaces (f-i).

Figure 10 Plain X-Ray Radiographs and Toluidine Blue Staining of the Loaded Tibias and Control Tibias.

(a) X-ray radiographs to show the establishment of mechanical loading model in adult dog tibias. For one side of the tibias, two mini-screw implants were placed in the midshaft, with a coil spring in between which constantly generated force of approximately 200 g. The contralateral tibias served as control. Yellow boxed areas indicate the bone tissue used for later analyses after 5-week loading. **(b)** X-ray radiographs of cross sections of dog tibia midshafts. **(c-d)** Representative toluidine blue staining of the cross sections of loaded tibias (with new bone formation only on periosteal surface) and control tibias. C1-c4, and d1-d3 are the corresponding magnified areas marked in black boxes. White dashed outlines indicate the boundary between osteons and ICL (c4 and d3). The yellow arrows indicate preosteons in loaded bone (c1 and c2); The orange arrows indicate the cement lines of secondary osteons (b2); The red and black arrows indicate the outer and inner boundaries of OCL, respectively (c1, c2, and d1). **(e)** Representative toluidine blue staining of the cross sections of loaded tibias (with new bone formation on both periosteal and endosteal surfaces). E1-e4 are the corresponding magnified areas marked in black boxes. In e1 and e2, yellow asterisks indicate the estimated outer boundary of OCL, namely the boundary between new bone and original OCL; black arrows indicate the remained inner boundary of OCL; White dashed outline in e2 indicate the estimated inner boundary of OCL since the actual boundary has become obscure. White dashed outline in e4 indicate the outer boundary of ICL. Yellow arrows indicate newly formed immature osteons on endosteal surface; Red arrows indicate newly formed trabeculae-like bone immersed in bone marrow cavity.

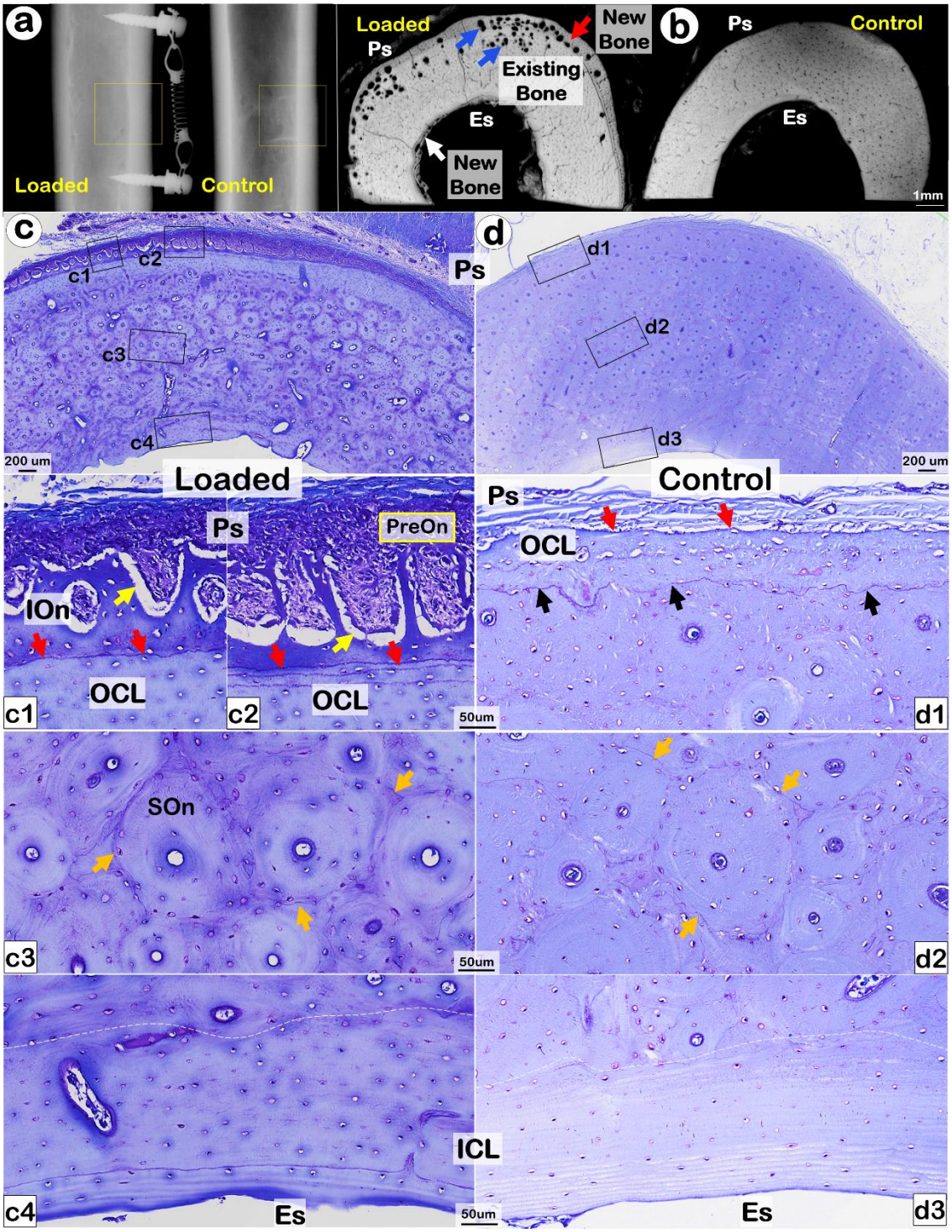

Figure 10 Continued.

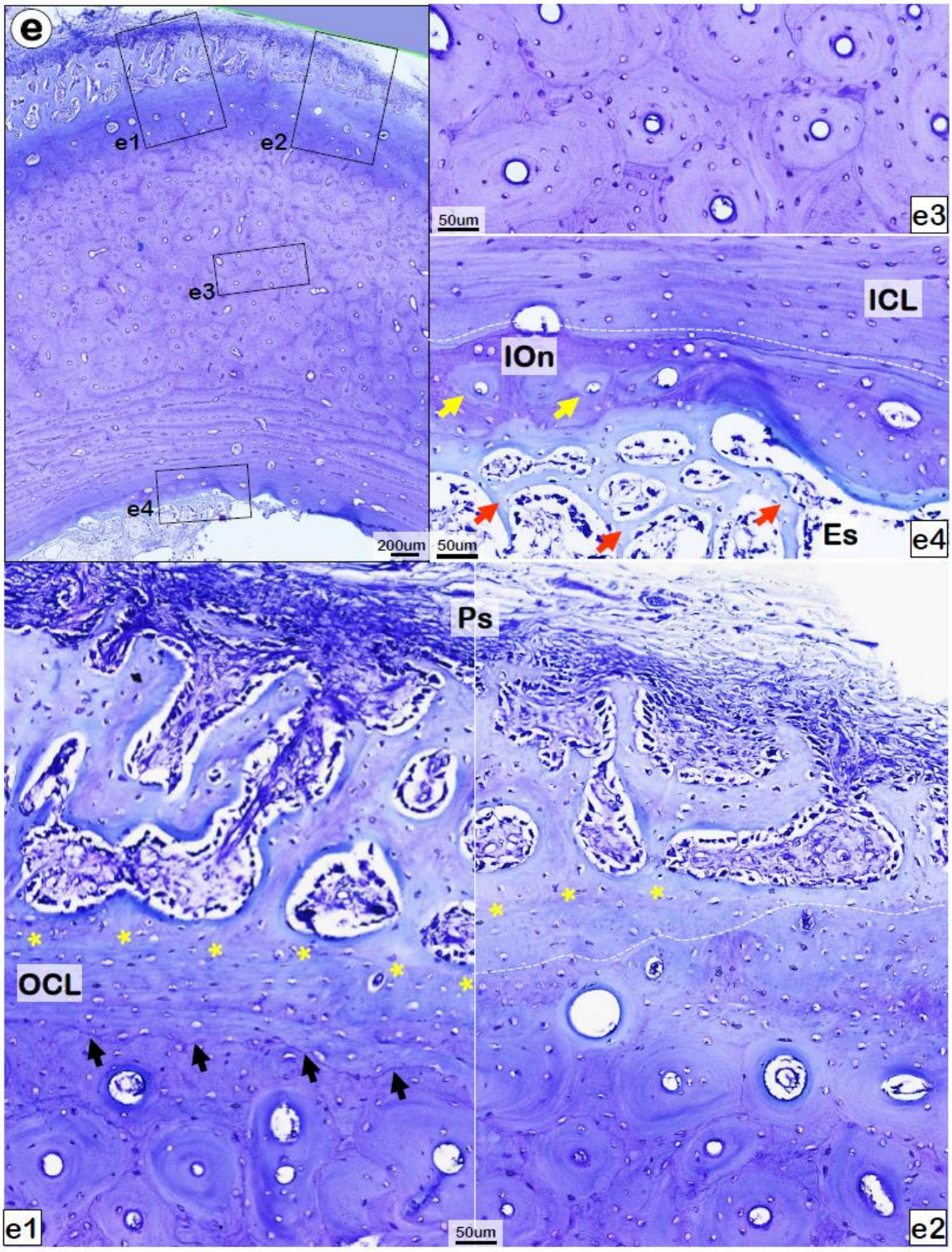

Figure 10 Continued.

Figure 11 Backscattered SEM/EDX Assays and Corresponding Fluorochrome Labeling Images of Loaded Bone and Control Bone.

(a-b) Representative backscattered SEM images of loaded bone (with new bone formation on both periosteal and endosteal surfaces) and control bone. Energy Dispersive X-ray (EDX) analyses to show calcium content in periosteal new bone (blue asterisks) and existing bone area (pink asterisks) of loaded dog, along with the counterparts in control dog (blue and purple asterisks, repectively). N=4/group, paired t-test, *P<0.05. A1, a2, b1, and b2 are the corresponding magnified areas marked in white boxes in a and b. A3, a4, b3, and b4 are the corresponding magnified areas marked in white boxes in a1, a2, b1, and b2. Yellow arrows indicate preosteons newly formed in periosteal (a1) and endosteal (a2) surfaces. White arrows indicate immature osteons (IOn) in periosteal (a1) and endosteal (a2) new bones. White dashed outlines indicate the outer and inner boundaries of OCL. **(c-d)** Corresponding fluorochrome labeling images achieved using the MMA-embedded blocks for SEM in a and b. The first injection of calcein was given one day after the surgery (5 weeks before euthanasia), followed by the second injection of alizarin red two weeks later (3 weeks before euthanasia), and the third injection of calcein another two weeks later (1 weeks before euthanasia). White arrows indicate osteocytes with strong fluorochrome labeling. White dashed outlines indicate the outer and inner boundaries of OCL.

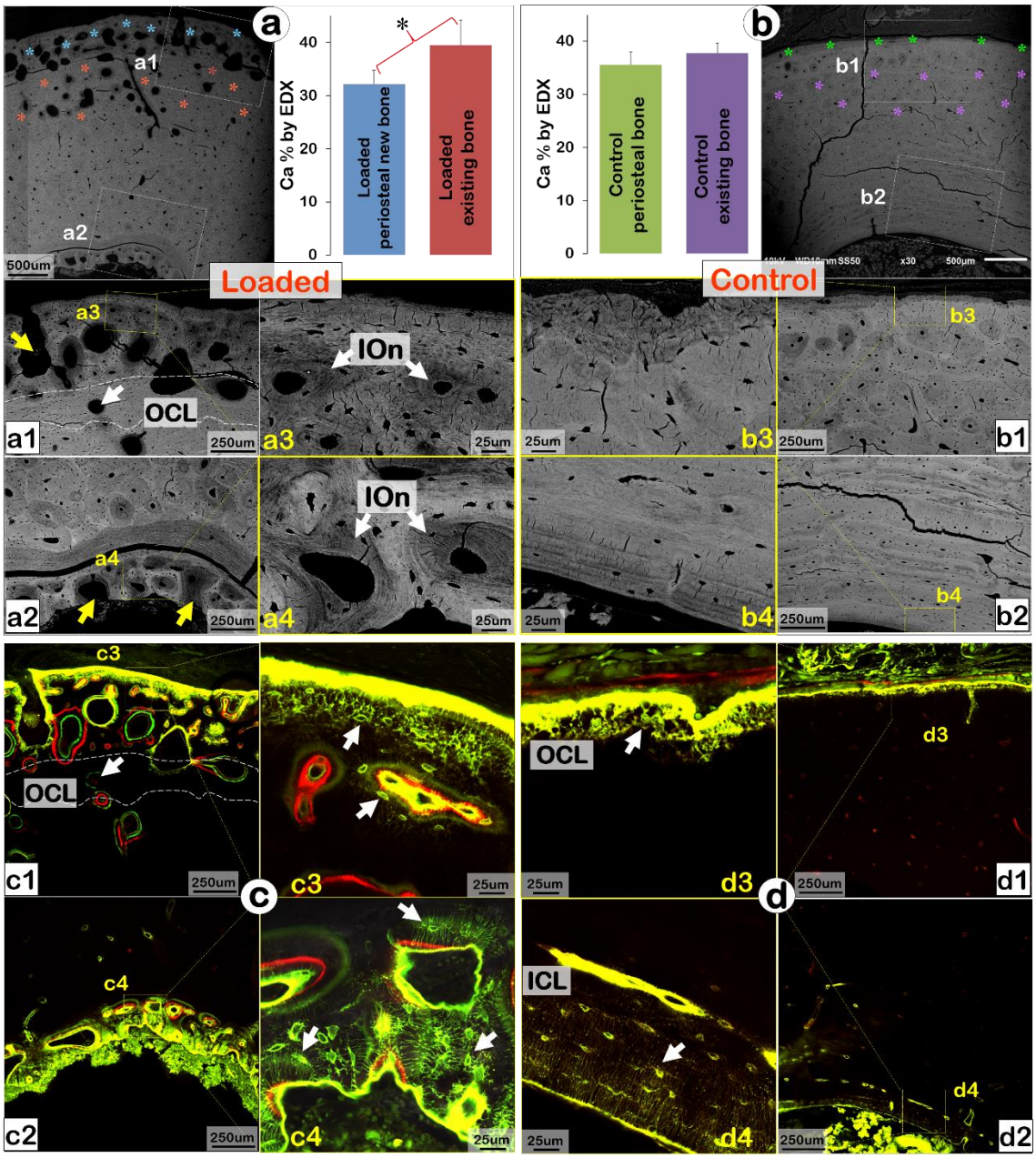

Figure 11 Continued.

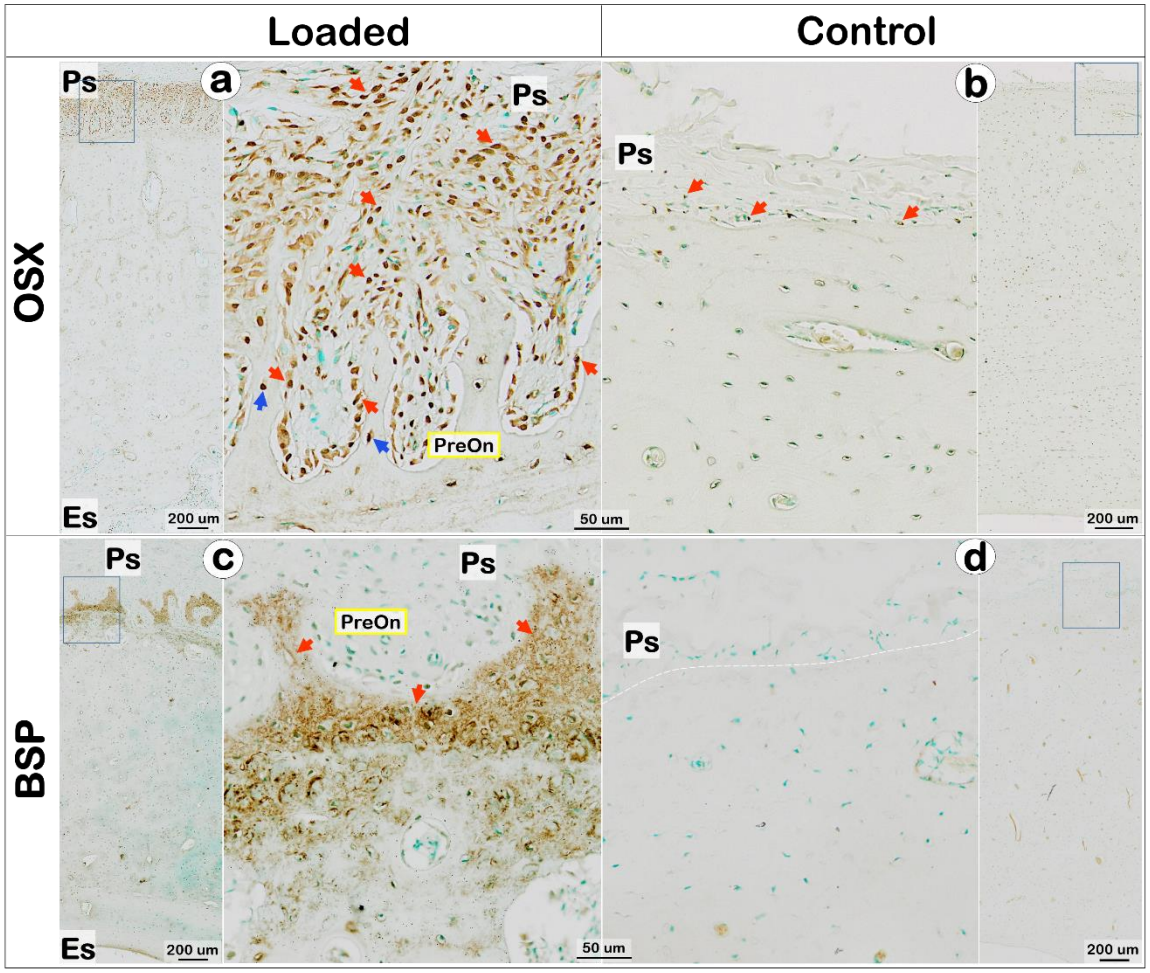

Figure 12 Immunohistochemistry of Loaded Bone and Control Bone.
Shown are representative images of immunohistochemistry of loaded bone and control bone, including osterix (a, and b), BSP (c and d), β-catenin (e-f), periostin (g-h), and Ki67 (i and j). Right panels of each figure are the corresponding magnified areas marked in blue boxes in the left panels. Red and blue arrows indicate positive signals for immunohistochemistry.

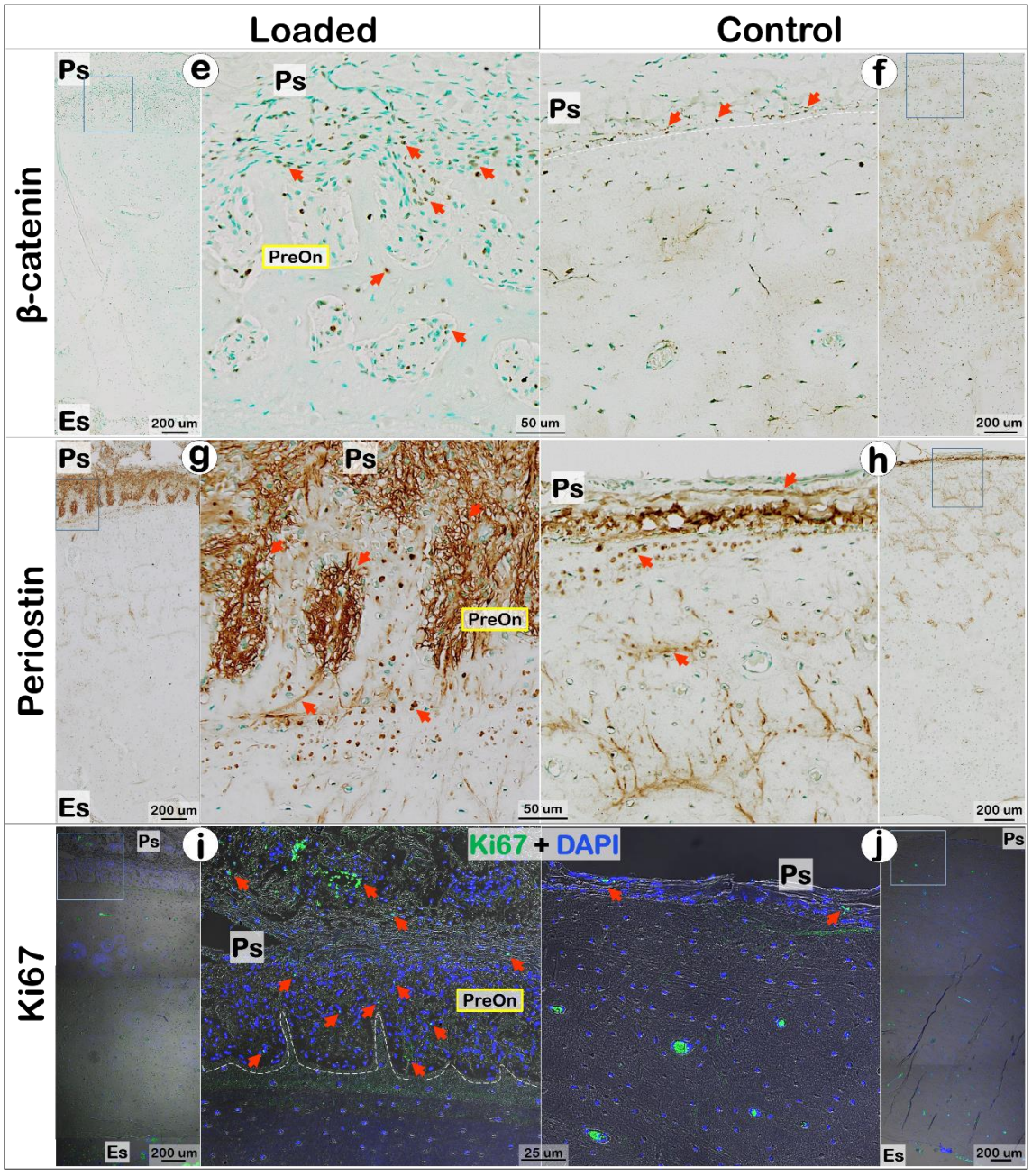

Figure 12 Continued.

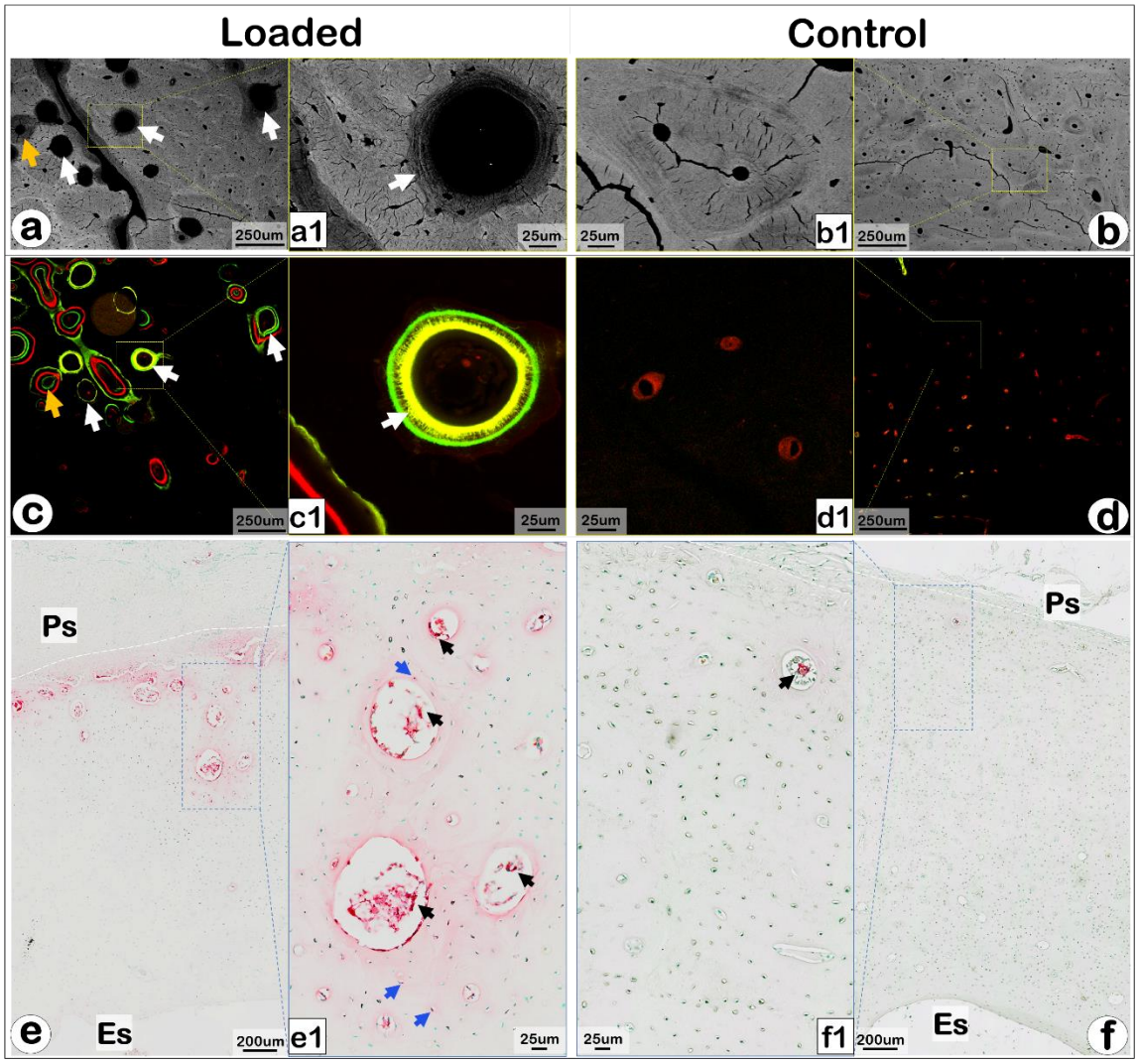

Figure 13 Backscattered SEM Images and TRAP Staining for the Existing Bone Area of Loaded Bone and the Counterpart of Control Bone.
Shown are backscattered SEM images (a-d) and TRAP staining (e and f) for the existing bone area of loaded bone and the counterpart of control bone. A1-f1 are the corresponding magnified areas marked in yellow or blue boxes in a-f. Orange arrows indicate an osteon in existing bone area of loaded dog that is undergoing demineralization (a) and remineralization (c); White arrows indicate newly formed osteons in existing bone area of loaded dog; Black arrows indicate TRAP (+) osteoclasts; Blue arrows indicate TRAP (+) osteocytes.

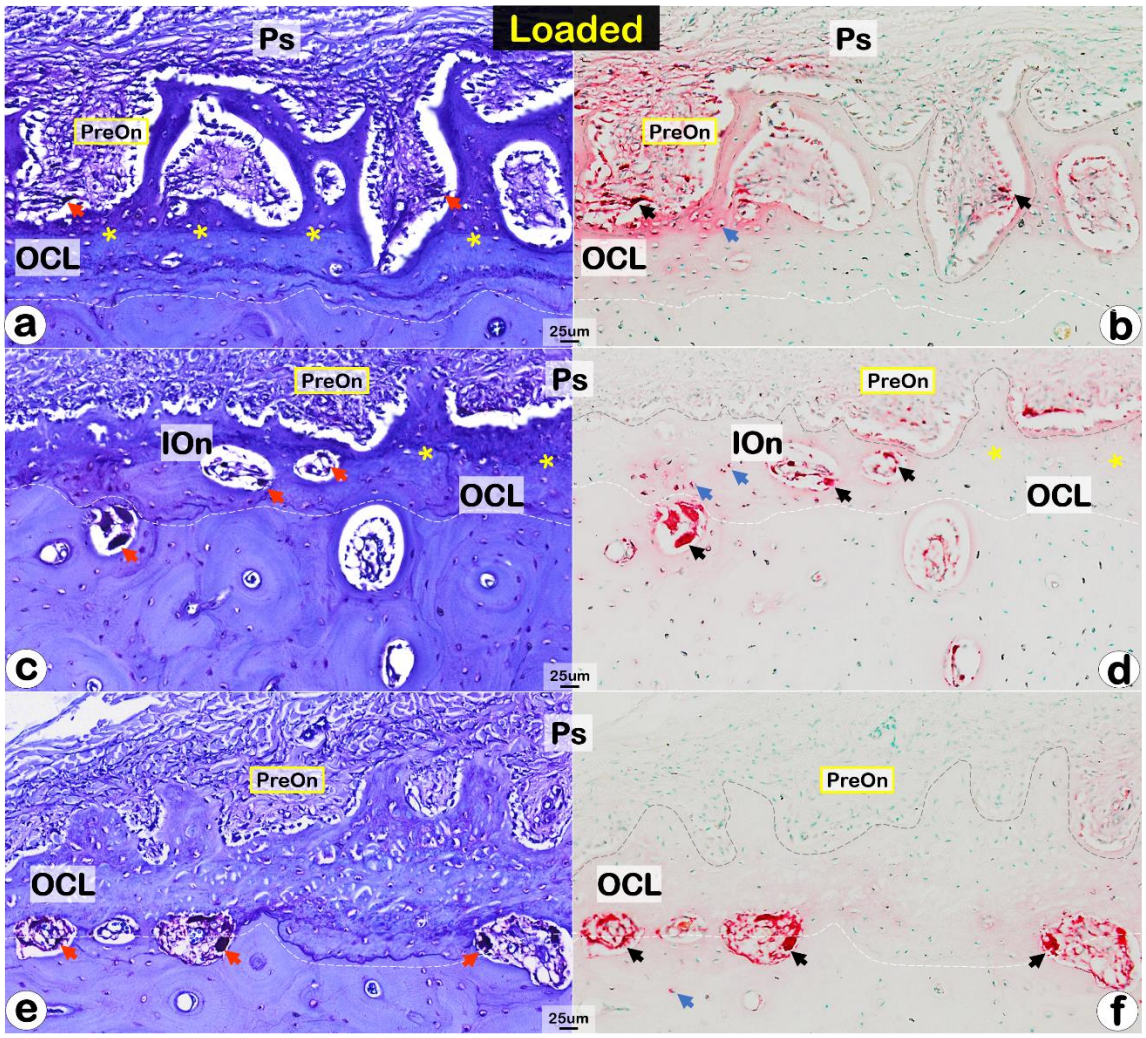

Figure 14 TRAP Staining of Transition Zone in Loaded Tibias and the Corresponding Toluidine Blue Staining.

Shown are the TRAP staining of transition zone of loaded tibias, which ranged from preosteons to the inner boundary of OCL (b, d, and f), along with the corresponding toluidine blue staining (a, c, and e). Control tibias did not have transition zone, as they did not have apparent new bone formation. Therefore, toluidine blue and TRAP stainings of control tibias are not shown here, and can be referred to Fig.10 and Fig.13. White dashed outlines indicate the inner boundaries of OCL; Grey dashed outlines indicate the boundaries of preosteons; Yellow asterisks indicate the outer boundaries of OCL (a and c) or estimated outer boundaries of OCL (d); Black arrows indicate TRAP (+) osteoclasts, and red arrows indicate the corresponding locations in toluidine blue staining; Blue arrows indicate TRAP (+) osteocytes.